USER'S MANUAL FOR THE HYDRATE v1.5 OPTION OF TOUGH+ v1.5: A CODE FOR THE SIMULATION OF SYSTEM BEHAVIOR IN HYDRATE-BEARING GEOLOGIC MEDIA

George J. Moridis

Earth Sciences Division,
Lawrence Berkeley National Laboratory,
Berkeley, CA 94720

August 2014

This work was supported by the Assistant Secretary for Fossil Energy, Office of Natural Gas and Petroleum Technology, through the National Energy Technology Laboratory, under the U.S. Department of Energy, Contracts No. DE-AC03-76SF00098 and DE-AC02-05CH11231.

User's Manual for the HYDRATE v1.5 Option of TOUGH+ v1.5: A Code For The Simulation Of System Behavior In Hydrate-Bearing Geologic Media

George J. Moridis
Earth Sciences Division, Lawrence Berkeley National Laboratory
University of California, Berkeley, California

Abstract

HYDRATE v1.5 is a numerical code that for the simulation of the behavior of hydrate-bearing geologic systems, and represents the third update of the code since its first release [*Moridis et al*., 2008]. It is an option of TOUGH+ v1.5 [*Moridis*, 2014], a successor to the TOUGH2 [*Pruess et al.*, 1999] family of codes for multi-component, multiphase fluid and heat flow developed at the Lawrence Berkeley National Laboratory. HYDRATE v1.5 needs the TOUGH+ v1.5 core code in order to compile and execute. It is written in standard FORTRAN 95/2003, and can be run on any computational platform (workstation, PC, Macintosh) for which such compilers are available.

By solving the coupled equations of mass and heat balance, the fully operational TOUGH+HYDRATE code can model the non-isothermal gas release, phase behavior and flow of fluids and heat under conditions typical of common natural CH_4-hydrate deposits (i.e., in the permafrost and in deep ocean sediments) in complex geological media at any scale (from laboratory to reservoir) at which Darcy's law is valid.

TOUGH+HYDRATE v1.5 includes both an equilibrium and a kinetic model of hydrate formation and dissociation. The model accounts for heat and up to four mass components, i.e., water, CH_4, hydrate, and water-soluble inhibitors such as salts or alcohols. These are partitioned among four possible phases (gas phase, liquid phase, ice phase and hydrate phase). Hydrate dissociation or formation, phase changes and the corresponding thermal effects are fully described, as are the effects of inhibitors. The model can describe all possible hydrate dissociation mechanisms, i.e., depressurization, thermal stimulation, salting-out effects and inhibitor-induced effects.

PAGE LEFT INTENTIONALLY BLANK

TABLE OF CONTENTS

Abstract iii

LIST OF FIGURES vii

LIST OF TABLES ix

1.0. Introduction 1

1.1. Background 1

1.2. The HYDRATE v1.5 Code 3

2.0 Concepts, Underlying Physics, and Governing Equations 11

2.1. Modeled Processes and Underlying Assumptions 11

2.2. Components and Phases 14

2.3. The Mass and Energy Balance Equation 16

2.4. Mass Accumulation Terms 16

2.5. Heat Accumulation Terms 19

2.6. Flux Terms 21

2.7. Source and Sink Terms 25

2.8. Thermophysical Properties 26

2.8.1. Water 26

2.8.2. CH_4-Hydrate 27

2.8.3. CH_4 Gas 28

2.9. Hydrate Phase Relationships 29

2.10. Inhibitor Effects on Hydrate Equilibrium 31

2.11. Other Processes, Properties, Conditions, and Related Numerical Issues 34

3.0. Design and Implementation of TOUGH+HYDRATE 35

3.1. Primary Variables 35

3.2. Compiling the TOUGH+HYDRATE Code 36

4.0. Input Data Requirements 43

4.1. Input Data Blocks 44

4.2. Data Block MEMORY 44

4.3. Data Block ROCKS or MEDIA 49

4.4. Data Block PARAM 49

4.5. Data Block DIFFUSION 53

5. Outputs 59
6.1. The Standard Outputs 60
6.3. Time Series Outputs 62
6.0. Example Problems 65
6.1. Example Files and Naming Conventions 65
6.2. Problem Test_1T: Thermal Stimulation, Equilibrium Dissociation, No Inhibitor 66
6.3. Problem Test_1Tk: Thermal Stimulation, Kinetic Dissociation, No Inhibitor 72
6.4. Problems Test_1P: Depressurization, Equilibrium Dissociation, No Inhibitor 81
6.5. Problem Test_1Pk: Depressurization, Kinetic Dissociation, No Inhibitor 82
6.6. Problem Test_1P_Ice: Thermal Stimulation, Kinetic Dissociation, No Inhibitor, Ice Evolution 84
6.7. Problem Test_1TbS and Test_1TbSk: Hydrate Formation, Equilibrium and Kinetic Hydration Reaction, Inhibitor 92
6.8. Problem Test_2Qp: Equilibrium Hydrate Dissociation, Depressurization, Radial Grid - Single Well 96
6.9. Problem Test_3Qpk: Kinetic Hydrate Dissociation, Depressurization, Radial Grid - Single Well with Wellbore Heating 100
6.10. Problem Test_2D: Equilibrium Hydrate Dissociation, 2-D Areal System 104
7. Acknowledgements 111
8. References 113

LIST OF FIGURES

Figure 2.1. Relationship of the equilibrium hydration pressure *Pe* and temperature *Te* of the CH_4-hydrate [*Moridis,* 2003]. 32

Figure 2.2. Modified *Pe* -*Te* relationship in the vicinity of the quadruple point. 33

Figure 2.3. Pressure-temperature equilibrium relationship in the phase diagram of the water--CH4--hydrate system in T+H. 33

Figure 4.1. The **DIFFUSION** data block, with examples of the `Diffusion_Key_Parameters` and `Component_Diffusivities_in_Phases` namelists. 56

Figure 6.1. Input file for example problem Test_1T (in Section 6.2) involving thermal stimulation, equilibrium dissociation, and no inhibitor. 71

Figure 6.2. Input file for example problem Test_1Tk (in Section 6.3) involving thermal stimulation, kinetic dissociation, and no inhibitor. 76

Figure 6.3. Comparison of the volumetric rates of CH_4 release from hydrate dissociation in problems `Test_1T` and `Test_1Tk`. 77

Figure 6.4. Comparison of the cumulative volumes of CH_4 released from hydrate dissociation in problems `Test_1T` and `Test_1Tk`. 78

Figure 6.5. Comparison of the volumetric production rates of CH_4 (measured as the flux crossing the x = 0 boundary) in problems `Test_1T` and `Test_1Tk`. 79

Figure 6.6. Comparison of the total production volumes of CH_4 (measured as the total volumes crossing the x = 0 boundary) in problems `Test_1T` and `Test_1Tk`. 80

Figure 6.7. Input file for example problem Test_1Pk (in Section 6.4) involving depressurization, equilibrium dissociation, and no inhibitor. 83

Figure 6.8. Comparison of the volumetric rates of CH_4 release from depressurization-induced hydrate dissociation in problems `Test_1P, Test_1Pk` and `Test_1P_ice`. 88

Figure 6.9. Comparison of the cumulative volumes of CH_4 released from depressurization-induced hydrate dissociation in problems `Test_1P, Test_1Pk` and `Test_1P_ice`. 89

Figure 6.10. Comparison of the volumetric production rates of CH_4 (measured as the flux crossing the x = 0 boundary) in problems `Test_1P, Test_1Pk` and `Test_1P_ice`. 90

Figure 6.11. Comparison of the total production volumes of CH_4 (measured as the total volumes crossing the x = 0 boundary) in problems `Test_1P, Test_1Pk` and `Test_1P_ice`. 91

Figure 6.12. Comparison of the volumetric rates of CH_4 consumption during hydrate formation in problems `Test_1TbS, Test_1TbSk` and `Test_1TbS2`. 94

Figure 6.13. Comparison of the cumulative volumes of CH_4 consumed during hydrate formation in problems `Test_1TbS, Test_1TbSk` and `Test_1TbS2`. 95

Figure 6.14. Volumetric rate of CH_4 release during hydrate dissociation in problem `Test_2Qp`. 98

Figure 6.15. Cumulative volume of CH_4 released during hydrate dissociation in problem `Test_2Qp`. 99

Figure 6.16. Volumetric rates of CH_4 (a) release in the reservoir during hydrate dissociation and (b) production from the well in problem `Test_3Qpk`. 102

Figure 6.17. Cumulative volumes of CH_4 (a) released in the reservoir during hydrate dissociation and (b) produced from the well in problem `Test_3Qpk`..... 103

Figure 6.18. Volumetric rates of CH_4 release from the hydrate in the reservoir during gas production in problem `Test_2D`..... 107

Figure 6.19. Pressure distribution in the reservoir at t = 2 days in problem `Test_2D`..... 108

Figure 6.20. Temperature distribution in the reservoir at t = 2 days in problem `Test_2D`. 109

Figure 6.21. Hydrate saturation distribution in the reservoir at t = 2 days in problem `Test_2D`. 110

Figure 6.22. Aqueous phase saturation distribution in the reservoir at t = 2 days in problem `Test_2D`. 111

Figure 6.23. Gas saturation distribution in the reservoir at t = 2 days in problem `Test_2D`. 112

LIST OF TABLES

Table 3.1. Primary Variables in Equilibrium Hydrate Simulations without Inhibitor*. 37

Table 3.2. Primary Variables in Kinetic Hydrate Simulations without Inhibitor*. 38

Table 4.1. TOUGH+ input data blocks. 45

PAGE LEFT INTENTIONALLY BLANK

1.0. Introduction

1.1. Background

Gas hydrates are solid crystalline compounds in which gas molecules are encaged inside the lattices of ice crystals. These gases are referred to as guests, whereas the ice crystals are called hosts. Of particular interest are hydrates in which the gas is a hydrocarbon. Under suitable conditions of low temperature and high pressure, a hydrocarbon gas M will react with water to form hydrates according to

$$M + N_H H_2O = M \cdot N_H H_2O \tag{1.1}$$

where N_H is the hydration number.

Vast amounts of hydrocarbons are trapped in hydrate deposits [*Sloan*, 1998]. Such deposits exist where the thermodynamic conditions allow hydrate formation, and are concentrated in two distinctly different types of geologic formations where the necessary low temperatures and high pressures exist: in the permafrost and in deep ocean

sediments. The lower depth limit of hydrate deposits is controlled by the geothermal gradient.

Current estimates of the worldwide quantity of hydrocarbon gas hydrates range between 10^{15} to 10^{18} m^3. Even the most conservative estimates of the total quantity of gas in hydrates may surpass by a factor of two the energy content of the total fuel fossil reserves recoverable by conventional methods. The magnitude of this resource could make hydrate reservoirs a substantial future energy resource. While current economic realities do not favor gas production from the hydrate accumulations, their potential clearly demands evaluation.

The majority of naturally occurring hydrocarbon gas hydrates contain CH_4 in overwhelming abundance. Simple CH_4-hydrates concentrate methane volumetrically by a factor of 164, and require less than 15% of the recovered energy for dissociation. Natural CH_4-hydrates crystallize mostly in the I structure, which contains 46 H_2O molecules per unit cell. They have a N_H ranging from 5.77 to 7.41, with N_H = 6 being the average hydration number and N_H = 5.75 corresponding to complete hydration [*Sloan*, 1998].

There are three main methods of hydrocarbon recovery from gas hydrates: (a) thermal stimulation [*McGuire*, 1981], in which gas release is effected by heating the hydrate above the dissociation temperature at a given pressure, (b) depressurization [*Holder et al.*, 1982], in which the gas release is achieved by lowering the pressure below that of the hydrate stability, and (c) 'inhibitor' injection [*Kamath and Godbole*, 1987] in which the hydrocarbon is produced after the injection of substances (e.g., brines, alcohols) that destabilize the hydrate. Combinations of these methods can also be used.

Numerical codes and studies on the simulation of gas production from dissociating hydrates are limited. *Drenth and Swinkels* [2000] developed a four-component, three-phase numerical model for the equilibrium dissociation of binary hydrates in marine environments. They provided an in-depth discussion of the challenges facing production from gas hydrates and identified knowledge gaps in numerical simulation of gas production from hydrate dissociation. *Kurihara et al.* [2003] developed a numerical simulator, and used it for the prediction of gas production from gas hydrates from both marine and permafrost hydrate deposits.

Moridis et al. [1998] developed EOSHYDR, a TOUGH2 [*Pruess et al.*, 1999] module for the simulation of dissociating simple methane hydrates under equilibrium conditions in both permafrost and marine accumulations. *Moridis et al*. [2003] enhanced EOSHYDR and developed EOSHYDR2 – also a TOUGH2 module – for the simulation of binary hydrates reacting under both equilibrium and kinetic conditions. TOUGH2/EOSHYDR2 was used for the simulation of gas production from hydrates under a variety of geologic and thermodynamic conditions, and involving various production strategies [*Moridis*, 2003; *Moridis et al*., 2004; *Moridis and Collett*, 2004].

1.2. The HYDRATE v1.5 Code

The HYDRATE v1.5 is a code for the simulation of the behavior of hydrate-bearing geologic systems. It is the third update of the code first released in 2008 [*Moridis et al.*, 2008]. It is a member of the TOUGH+ family of codes, written in standard FORTRAN 95/2003 to take advantage of all the object-oriented capabilities and the enhanced computational features of that language. It is a successor to the TOUGH2 [*Pruess et al.*,

1991] family of codes for multi-component, multiphase fluid and heat flow developed at the Lawrence Berkeley National Laboratory. The current implementation of HYDRATE v1.5 is far more modular than its earlier versions, which involved a more intertwined structure of the hydrate-related part of the model and the code that is common to all members of the TOUGH+ family.

From the present version and onward, the core code of TOUGH+ is completely generic in its design, includes the procedures that are common to all simulations (e.g., reading input data that are universally needed by any study, time advancement, solution of the Jacobian matrix, updating of primary and secondary varisbales, etc.), and is not problem-specific, i.e., it is completely independent of the hydrate-specific aspects or of the specifics of any other type of problem being simulated. It is also distributed as a separate entity and cannot conduct any simulations by itself, but needs an additional code unit – named ***option*** in TOUGH+ and describing a particular type of problem or Equation of State (EOS) – before it can become operational. Note that therm ***option*** – rather the older term ***module*** or ***EOS*** that were used in the TOUGH2 [*Pruess et al*., 1999] nomenclature – is used to avoid confusion, as the term *module* has a particular meaning in the FORTRAN 95/2003 language of TOUGH+.

All hydrate-related physics and the corresponding relationships, as well the corresponding inputs and outputs, are now included in the HYDRATE V1.5 option which, combined with the core TOUGH+ code [*Moridis*, 2014], can solve the problem of hydrate-bearing system behavior in porous geologic media. The combined TOUGH+HYDRATE code (in the current versions of its two constituents) will be hereafter referred to as **T+H** for brevity.

The underlying principles, physics, thermodynamics and computational approach in **T+H** are similar to those used in the earlier versions of the code [*Moridis*, 2003; *Moridis et al*., 2005; 2008], but significant differences also exist because of the introduction of more advanced structures, capabilities and output options. As before, the current **T+H** code employs dynamic memory allocation, thus minimizing storage requirements. It follows the tenets of Object-Oriented Programming (OOP), and involves entirely new data structures that describe the objects upon which the code is based. The basic objects are defined through derived data types, and their properties and processes are described in modules and sub-modules, i.e., entities that incorporate the object attributes and parameters in addition to the procedures (corresponding to the older concepts of "functions" and "subroutines" in FORTRAN 77) that describe its behavior and processes. The TOUGH+ code is based on a completely modular structure that is designed for maximum traceability and ease of expansion.

In addition to improvements in the code structure and data flow, the current version of **T+H** features significant new additions in terms of capabilities, as well as more advanced thermodynamics. Thus, **T+H** allows the definition of *subdomains* that are composed of one or more *regions*, each describing a subset of the grid that can be defined by several methods (e.g., geometry, listing of the included elements), thus allowing the monitoring of the evolution of particular attributes and variables in these subdomains through printing of the outputs in individual external files. Similarly, **T+H** allows the definition of *interfaces* that comprise one or more *surfaces*, each of which can be defined by several methods (e.g., geometry, listing of the included connections), thus allowing the monitoring of the evolution of flow-related attributes and parameters

through printing of the outputs in individual external files. T+H now includes more advanced physics in several areas, e.g., real gas properties, water properties, hydrate density equations, salinity effects, and diffusion, as well as expanded boundary condition options (such as time variable boundary conditions).

By using the capabilities of the FORTRAN95/2003 language, the new OOP architecture involves the use of pointers, lists and trees, data encapsulation, defined operators and assignments, operator extension and overloading, use of generic procedures, and maximum use of the powerful intrinsic vector and matrix processing operations (available in the extended mathematical library of FORTRAN 95/2003). This leads to increased computational efficiency, while allowing seamless applicability of the code to multi-processor parallel computing platforms. The result is a code that is transparent and compact, and frees the developer from the tedium of tracking the disparate attributes that define the objects, thus enabling a quantum jump in the complexity of problem that can be tackled. This is demonstrated in **T+H**, in which 26 different phase combinations can be easily described. An additional feature of the FORTRAN 95/2003 language of TOUGH+ is the near complete interoperability with C/C++, which allows the interchangeable use of procedures written in either FORTRAN 95/2003 or C/C++, and makes possible the seamless interaction with pre- and post-processing graphical environments.

Based on insights provided by extensive experience with earlier versions of the code [*Moridis et al.*, 2008; 2009; 2012], numerical 'bottlenecks' were removed, more efficient primary variables and state-changing criteria were selected, and more powerful linearization techniques were employed in **T+H**, resulting in significant improvements in

execution speed and numerical performance. Note that **T+H** v1.5 still uses most of the inputs (and the input formats) used by the conventional TOUGH2 code [*Pruess et al.* 1999] in order to fulfill the functional requirement (part of the code design) of backward compatibility of the TOUGH+ family codes [*Moridis*, 2014] with older input data files used in earlier simulations. However, more advanced input data structures and formats are introduced in this version to support and describe capabilities unavailable in earlier code versions. More powerful input data file structures will be available in future releases of TOUGH+.

By solving the coupled equations of mass and heat balance, **T+H** can model the non-isothermal gas release, phase behavior and flow of fluids and heat in complex geologic media. The code can simulate formation of, or production from, natural CH_4-hydrate deposits in the subsurface (i.e., in the permafrost and in deep ocean sediments), as well as laboratory experiments of hydrate formation/dissociation in porous/fractured media. The only limitations on the size of the domain to be simulated are imposed by the underlying physics. Thus, if the volume of the domain and its subdivision are such that (a) a representative volume can be defined and (b) Darcy's law applies, then **T+H** can be used for the prediction of the behavior of a hydrate-bearing geological system. Note that hydrate problems involving very large grids and an accordingly large number of equations (>300,000) are more appropriately addressed with a parallel version of the code [*Reagan et al.*, 2014].

T+H v1.5 includes both an equilibrium and a kinetic model of hydrate formation and dissociation. Assming an equilibrium hydration model, the model accounts for heat and up to four mass components, i.e., H_2O, CH_4, and water-soluble inhibitors such as

salts or alcohols; the kinetic model introduces an additional component, the CH_4-hydrate, which is now treated as an individual component and not just a state of the H_2O-CH_4 system. These components are partitioned among four possible phases (gas phase, liquid phase, ice phase and hydrate phase). Hydrate dissociation or formation, phase changes and the corresponding thermal effects are fully described, as are the effects of inhibitors. The model can describe all possible hydrate dissociation mechanisms, i.e., depressurization, thermal stimulation, salting-out effects and inhibitor-induced effects, both singly and in any combination.

While the capabilities to describe binary hydrates, and the properties and behavior of all hydrate forming gases are fully implemented, only methane hydrates can be simulated by this version of the **T+H** code. The reason for this stems from the fact that our ability to mathematically describe the problem exceeds the supporting fundamental knowledge on the subject, as large knowledge gaps exist. Treating the component hydrates as individual entities unaffected by each other or as segregated macroscopic quantities of hydrocarbon within the hydrate is incorrect because binary hydrates behave in a manner akin to solid solutions [*Sloan*, 1998]. Thus, changes in the composition of the hydrate and in the gas phase are functions not only of pressure and temperature, but also of concentration. Currently, there are no readily available P-T-X diagrams for such hydrates. In our studies, the empirical distribution coefficient K_{vsi} method of *Carson and Katz* [1942] have been shown to be difficult, and often impossible, to converge (the highest convergence rate was 65%, and was observed in rather simple problems), and lead to long execution times. The most physically and mathematically robust approach is to incorporate fast regression relationships based on the computationally intensive but

conceptually sound statistical thermodynamics approach of *Sloan* [1998], full implementation of which is impractical in simulators. This option is currently being explored for incorporation into later version of the code if such a need arises.

This report provides a detailed presentation of the features and capabilities of **T+H**, and includes a thorough discussion of the underlying physical, thermodynamic and mathematical principles of the model in addition to the main governing equations. The various phase regimes and the corresponding primary variables are discussed in detail, as well as the reasons for their selection. Examples of input data files (and of the corresponding output files) are included as an aide to the **T+H** user. Results from simulations of gas production from realistic hydrate-bearing geologic systems are also included.

PAGE LEFT INTENTIONALLY BLANK

2.0 Concepts, Underlying Physics, and Governing Equations

2.1. Modeled Processes and Underlying Assumptions

T+H can model the following processes and phenomena in hydrate-bearing geologic systems:

(1) The flow of gases and liquids in the geologic system

(2) The corresponding heat flow and transport

(3) The partitioning of the mass components among the possible phases

(4) Heat exchanges due to

   a. Conduction

   b. Advection/convection

   c. Radiation

   d. Hydrate reaction (dissociation or formation)

   e. Latent heat related to phase changes (ice melting or water fusion, water evaporation or vapor condensation)

f. Gas dissolution

g. Inhibitor dissolution

(5) Equilibrium or kinetic hydration reaction (dissociation or formation),

(6) The transport of water-soluble gases and inhibitors (such as salts and alcohols), accounting for advection and molecular diffusion

(7) The effects of water-soluble inhibitors on the hydrate behavior

(8) Any method of hydrate dissociation (i.e., depressurization, thermal stimulation and inhibitor effects), and combinations thereof

A deliberate effort was made to keep the simplifying assumptions involved in the development of the underlying physical, thermodynamic and mathematical model to a minimum. These include:

(1) Darcy's law is valid in the simulated domain under the conditions of the study.

(2) In the transport of dissolved gases and inhibitors, mechanical dispersion is small compared to advection (by neglecting mechanical dispersion, memory requirements and execution times are substantially reduced).

(3) The movement of the geologic medium (soil heaving) while freezing is not described, and the effects on pressure (caused by density differences between the liquid and ice phases) are accommodated through a relatively high pore compressibility of the geologic medium.

(4) Dissolved salts do not precipitate as their concentration increases during water freezing. Consequently, the aqueous phase is not allowed to disappear when salts are present. This simplification was necessitated by (a) the marginal practical aspects of such a scenario, (b) the lack of fundamental knowledge and

quantitative relationships describing the hydrate-salt interaction under these conditions, and (c) the computationally intensive requirements of describing the thermodynamics of dense brines and halite precipitation.

(5) The concentration of the dissolved inhibitors is such that it does not affect the thermophysical properties of the aqueous phase. Although the thermodynamics of inhibitor-water systems are well known and are already available within **T+H**, they are not invoked in this version – but will be considered as an option in future code releases – because their effect may not very important, they are computationally intensive (as they may affect a wide range of thermophysical properties such as density, vapor pressure, enthalpy, etc., all of which have to be computed regardless of even minimal inhibitor effect), and inhibitor-induced dissociation is not considered an attractive first option for gas production from hydrate deposits [*Moridis and Reagan*, 2007].

(6) The inhibitor is non-volatile in the temperature-pressure range of the study. This simplification was introduced because of the limited practical possibility for such a scenario, and of the significant computational requirements to account for the inhibitor vapor pressure and diffusion in the gas phase.

(7) The pressure P < 100 MPa (14,504 psi). The pressure-dependent equations describing the hydrate properties and behavior in **T+H** provide accurate solutions for a P over nine times larger than the largest pressure at which natural gas hydrates are known to exist (i.e., about 11 MPa). Thus, the existing capabilities can easily accommodate any natural or laboratory hydrate system. Although equations for an accurate description of the thermophysical properties

of hydrate systems for P as high as 1000 MPa are available in the code, this option is disabled because it involves an iterative process that increases the execution time by a factor of 3 or 4 even for $P < 100$ MPa.

2.2. Components and Phases

Depending on the thermodynamic state of the system, the amount of CH_4-hydrate created or CH_4 gas released is determined from the reaction

$$CH_4 + N_H H_2O = CH_4 \cdot N_H H_2O \,, \tag{2.1}$$

where N_H is the hydration number, and the subscript m denotes methane. In addition to simple CH_4-hydrates, natural hydrates may include one or more additional gasses. Such hydrate-forming gases exist practically in all natural hydrates and can play a significant role in their nucleation and behavior.

The reaction describing the formation/hydration of a composite (binary) hydrate is

$$\chi_m \left[CH_4 \cdot N_H H_2O\right] + \chi_G \left[G \cdot N_G H_2O\right] = \chi_m CH_4 + \chi_G G + \left(\chi_m N_H + \chi_G N_G\right) H_2O \,, \tag{2.2}$$

where G is the second hydrate-forming gas, N_G is the hydration number of the G-hydrate, χ is the mole fraction in the binary hydrate, and the subscripts m and G denote the methane and the second gas, respectively. Obviously, $\chi_m + \chi_G = 1$. The gas G can be one of CO_2, H_2S, N_2, or another gaseous alkane $C_n H_{2n+2} (m = 2,3,4)$. In permafrost hydrate accumulations, χ_m routinely exceeds 95% [*Collett et al.*, 1999].

A non-isothermal hydrate system can be fully described by the appropriate mass balance equations and an energy balance equation. The following components κ (and the

corresponding indicators used in the subsequent equations), corresponding to the number of equations, are considered in **T+H**:

$\kappa \equiv$	h	hydrate
	w	water
	m	CH_4
	i	water-soluble inhibitor (salt or organic substance)
	θ	heat

Note that heat is included in this list as a pseudo-component (as the heat balance is tracked similarly to the mass balance of the individual mass components) for the purpose of defining the maximum number of simultaneous equations to be solved. Thus, the list indicates that the maximum number of mass components that may be considered in a problem involving kinetic hydrate formation/dissociation is 4, and the corresponding number of equation is 5 because there is no possibility to treat hydrate dissociation or formation as an isothermal process. For an equilibrium hydration reaction, hydrate is not treated as an individual component, but simply as a state of the H_2O-CH_4 system. In that case, the maximum number of mass components is 3, and the maximum possible number of equations is 4.

These mass and energy components are partitioned among four possible phases β, which are listed below along with the corresponding indicators (used in the subsequent equations):

$\beta \equiv$	H	solid-hydrate (components: m,w – equilibrium; h - kinetic)
	A	aqueous (components: dissolved m, dissolved i)
	G	gaseous (components: m, vapor w)

I solid-ice (component: w)

Note that hydrate is both a component and a phase under kinetic hydration reaction conditions. Under equilibrium conditions, hydrate is treated only as a phase.

2.3. The Mass and Energy Balance Equation

Following *Pruess et al.* [1999], mass and heat balance considerations in every subdomain (gridblock) into which the simulation domain is been subdivided by the integral finite difference method dictates that

$$\frac{d}{dt}\int_{V_n} M^{\kappa}\, dV = \int_{\Gamma_n} \mathbf{F}^{\kappa} \cdot \mathbf{n}\, d\tilde{A} + \int_{V_n} q^{\kappa}\, dV \ , \tag{2.3}$$

where:

V, V_n volume, volume of subdomain n [L^3];

M^{κ} mass accumulation term of component κ [kg m^{-3}];

A, Γ_n surface area, surface area of subdomain n [L^2];

$\mathbf{F}^{\kappa}$ Darcy flux vector of component κ [kg m^{-2}s^{-1}];

$\mathbf{n}$ inward unit normal vector;

q^{κ} source/sink term of component κ [kg m^{-3}s^{-1}];

t time [T].

2.4. Mass Accumulation Terms

Under equilibrium conditions, the mass accumulation terms M^{κ} for the mass components in equation (2.3) are given by

$$M^{\kappa} = \sum_{\beta \equiv A,G,I,H} \phi S_{\beta} \rho_{\beta} X_{\beta}^{\kappa}, \quad \kappa \equiv w,m,i \tag{2.4}$$

where

ϕ porosity [*dimensionless*];

ρ_{β} density of phase β [kg m^{-3}];

S_{β} saturation of phase β [*dimensionless*];

X_{β}^{κ} mass fraction of component $\kappa \equiv w,m,i$ in phase β [kg/kg]

In the equilibrium model, different cases of β give the following relations:

$$\beta \equiv G: \; X_G^i = 0$$
$$\beta \equiv H: \; X_H^w = \frac{W^m}{W^h}, \; X_M^m = 1 - X_H^w, \; X_H^i = 0$$
$$\beta \equiv I: \; X_I^m = X_I^i = 0, \; X_I^w = 1$$

The terms W^m and W^h denote the molecular weights of the CH_4 and of the hydrate, respectively. Thus, the values of X_H^w and X_M^m reflect the stoichiometry in Equation (2.1).

Under kinetic conditions, the mass accumulation terms M^{κ} in Equation (2.3) are given by

$$M^{\kappa} = \sum_{\beta \equiv A,G,H,I} \phi S_{\beta} \rho_{\beta} X_{\beta}^{\kappa}, \quad \kappa \equiv w,m,h,i \tag{2.5}$$

In the kinetic model, different cases of β give the following relations

$$\beta \equiv A: \; X_A^h = 0$$
$$\beta \equiv G: \; X_G^h = X_G^i = 0$$
$$\beta \equiv H: \; X_H^w = X_H^m = X_H^i = 0, \quad X_H^h = 1$$
$$\beta \equiv I: \; X_I^m = X_I^h = X_I^i = 0, \quad X_I^w = 1$$

Under kinetic conditions, the equation describing the behavior of the hydrate mass component and phase is provided by the model of [*Kim et al.*, 1987] as

$$Q_H = \frac{\partial M}{\partial t} = -K_0 \exp\left(\frac{\Delta E_a}{RT}\right) F_A A\left(f_{eq} - f_v\right), \tag{2.6}$$

where

K_0 intrinsic hydration reaction constant [kg m^{-2} Pa^{-1} s^{-1}];

ΔE_a hydration activation energy [J mol^{-1}];

R universal gas constant [8.314 J mol^{-1} K^{-1}];

T temperature [^{o}K];

F_A area adjustment factor [dimensionless];

A surface area participating in the reaction [m^2];

f_{eq} fugacity at equilibrium at temperature T (Pa)

f_v fugacity in the gas phase at temperature T (Pa)

The surface area is computed by assigning the hydrate saturation uniformly to the interstitial spaces of the porous medium. To accomplish this, the original solid grain volume (considered to be composed of spherical particles) is determined as $V_p = \frac{4}{3}\pi r_p^3$, where r_p is the solid grain radius [m]. Then, the number of voids N_V (pore spaces) is assumed to be equal to the number of solid grains (a valid approach for spherical particles), and the corresponding void volume V_V is computed from

$$N_V = \frac{(1-\phi)}{V_p}, \quad V_V = \frac{\phi}{N_V}, \tag{2.7}$$

At the interface of pores and voids, the grain surface area is the same for both the grains and the voids, and is computed as $A_p = 4\pi r_p^2$, resulting in a total area (per unit volume) of $A_{TV} = N_V A_p$. Then the volume of the void is assumed to vary linearly with the r_V^3, where $r_V = 0.1547\ r_p$, is a representative radius describing the radius of the sphere fitting in the

interstitial space between the spherical grains. Then, at any time t, a representative hydrate particle radius r_H and volume V_H are computed as

$$V_H = \frac{\phi S_H}{N_V}, \qquad r_h = r_V \left(\frac{V_H}{V_V} \right)^{1/3} = r_V S_H^{1/3} \tag{2.8}$$

and the hydrate reactive area is computed as

$$A = f_A A_{TV} \left(\frac{r_H}{r_V} \right)^2 = f_A N_V \left(4\pi r_p^2 \right) S_H^{2/3} . \tag{2.9}$$

The area adjustment factor f_A accounts for the deviation of the interstitial volume from that based on the assumption of grain sphericity, and can incorporate heterogeneity effects related to the hydrate "particle" size and saturation distribution. Given the intrinsic permeability k of a porous medium, the Kozeny-Carman equation can provide an estimate of the average (effective) radius r_p of the porous medium grains as [*Bear*, 1972]

$$r_p = \left[45k \frac{(1-\phi)^2}{\phi^3} \right]^{1/2} .$$

Alternatively, an estimate of r_p can be obtained from sieve analysis (if such data are available).

2.5. Heat Accumulation Terms

The heat accumulation term includes contributions from the rock matrix and all the phases, and, in the kinetic model, is given by the equation

$$M^\theta = (1-\phi)\rho_R C_R T + \sum_{\beta=A,G,H,I} \phi S_\beta \rho_\beta U_\beta + Q_{diss} , \tag{2.10}$$

where

$$Q_{diss} = \begin{cases} \Delta\left(\phi\rho_H S_H \Delta H^0\right) & \text{for equilibrium dissociation} \\ Q_H \Delta H^0 & \text{for kinetic dissociation} \end{cases} \tag{2.11}$$

ρ_R rock density [kg m^{-3}];

C_R heat capacity of the dry rock [J kg^{-1} K^{-1}];

U_β specific internal energy of phase β [J kg^{-1}];

$\Delta()$ change in the quantity in parentheses over the current time step;

ΔU_H specific enthalpy of hydrate dissociation/formation [J kg^{-1}]

The specific internal energy of the gaseous phase is a very strong function of composition, is related to the specific enthalpy of the gas phase H_G, and is given by

$$U_G = \sum_{\kappa=w,m} X_G^\kappa u_G^\kappa + U_{dep} \quad \left(= H_G - \frac{P}{\rho_G}\right), \tag{2.12}$$

where u_G^κ is the specific internal energy of component κ in the gaseous phase, and U_{dep} is the specific internal energy departure of the gas mixture [J kg^{-1}].

The internal energy of the aqueous phase accounts for the effects of gas and inhibitor solution, and is estimated from

$$U_A = X_A^w u_A^w + X_A^m\left(u_A^m + U_{sol}^m\right) + X_A^i\left(u_A^i + U_{sol}^i\right), \tag{2.13}$$

where u_A^w, u_A^m and u_A^i are the specific internal energies of H_2O, CH_4 and the inhibitor at the conditions prevailing in the aqueous phase, respectively, and U_{sol}^m and U_{sol}^i are the specific internal energies corresponding to the dissolution of CH_4 and of the inhibitor in water, respectively. The terms u_A^i and U_H are determined from

$$u_A^i = h_A^i - \frac{P}{\rho_i} = \int_{T_0}^{T} C_i dT - \frac{P}{\rho_i} \quad \text{and} \quad U_H = H_H - \frac{P}{\rho_H} = \int_{T_0}^{T} C_H dT - \frac{P}{\rho_H} \tag{2.14}$$

where T_0 is a reference temperature, h_A^i and H_H are the specific enthalpies of H_2O and hydrate (phase or component), respectively, and C_i and C_H are the temperature-dependent heat capacities of the inhibitor and the gas hydrate, respectively [J kg^{-1} K^{-1}].

2.6. Flux Terms

The mass fluxes of water, CH_4 and inhibitor include contributions from the aqueous and gaseous phases, i.e.,

$$\mathbf{F}^{\kappa} = \sum_{\kappa \equiv A,G} \mathbf{F}_{\beta}^{\kappa}, \quad \kappa \equiv w,m,i \tag{2.15}$$

Because they are immobile, the contributions of the two solid phases ($\beta \equiv H,I$) to the fluid fluxes are zero. Therefore, in the kinetic model the mass flux of the hydrate component ($\kappa \equiv h$) across all subdomain boundaries is

$$\mathbf{F}^{h} = 0 \tag{2.16}$$

For the aqueous phase, $\mathbf{F}_A^w = X_A^w \mathbf{F}_A$, and the phase flux $\mathbf{F}_A$ is described by Darcy's law as

$$\mathbf{F}_A = -k \frac{k_{rA}\rho_A}{\mu_A}\left(\nabla P_A - \rho_A \mathbf{g}\right), \tag{2.17}$$

where

k rock intrinsic permeability [m^2];

k_{rA} relative permeability of the aqueous phase [dimensionless];

μ_A viscosity of the aqueous phase [Pa s];

P_A pressure of the aqueous phase [Pa];

$\mathbf{g}$ gravitational acceleration vector [m s^{-2}].

The aqueous pressure P_A is given by

$$P_A = P_G + P_{cGW} \,, \tag{2.18}$$

where $P_G = P_G^m + P_G^w$ is the gas pressure [Pa], P_{cGW} is the gas-water capillary pressure [Pa], and P_G^m, P_G^w are the CH_4 and water vapor partial pressures [Pa] in the gas phase, respectively. The CH_4 solubility in the aqueous phase is related to P_G^m through Henry's law,

$$P_G^m = H^m X_A^m \,, \tag{2.19}$$

where $H^m = H^m(T)$ [Pa] is the temperature-dependent Henry's coefficient, as opposed to its original/classical definition as Henry's constant. Note that it is possible to determine the CH_4 from the equality of fugacities in the aqueous and the gas phase. Although this approach provides a more accurate solution, the difference does not exceed 2-3% for the vast majority of CH_4-hydrate problems in reservoir or laboratory settings, but the execution time can increase as much as 30%.

The mass flux of the gaseous phase ($\beta \equiv G$) incorporates advection and diffusion contributions, and is given by

$$\mathbf{F}_G^\kappa = -k_0 \left(1 + \frac{b}{P_G}\right) \frac{k_{rG}\rho_G}{\mu_G} X_G^\kappa \left(\nabla P_G - \rho_G \mathbf{g}\right) + \mathbf{J}_G^\kappa \,, \quad \kappa \equiv w, m \tag{2.20}$$

where

k_0 absolute permeability at large gas pressures (= k) [m^2];

b *Klinkenberg* [1941] b-factor accounting for gas slippage effects [Pa];

k_{rG} relative permeability of the gaseous phase [*dimensionless*];

μ_G viscosity of the gaseous phase [Pa s].

Methods to estimate the *b*-factor are discussed in *Moridis* [2014].

The term $\mathbf{J}_G^\kappa$ is the diffusive mass flux of component κ in the gas phase [kg/m^2/s], and is described by

$$\mathbf{J}_G^\kappa = -\phi S_G \underbrace{\left(\phi^{1/3} S_G^{7/3}\right)}_{\tau_G} D_G^\kappa \rho_G \nabla X_G^\kappa = -\phi\left(\tau_G\right) D_G^\kappa \rho_G \nabla X_G^\kappa, \quad \kappa \equiv w, m \tag{2.21}$$

where D_G^κ is the multicomponent molecular diffusion coefficient of component κ in the gas phase in the absence of a porous medium [m^2 s^{-1}], and τ_G is the gas tortuosity [dimensionless]. Several methods to compute τ_G are discussed by *Moridis* [2014]. The diffusive mass fluxes of the water vapor and CH_4 gas are related through the relationship of *Bird et al.* [1960]

$$\mathbf{J}_G^w + \mathbf{J}_G^m = 0, \tag{2.22}$$

which ensures that the total diffusive mass flux of the gas phase is zero with respect to the mass average velocity when summed over the two components ($\kappa \equiv w, m$). Then the total gas phase mass flux is the product of the Darcy velocity and density of the gas phase.

The flux of the dissolved inhibitor is described by

$$\mathbf{F}_A^i = X_A^i \mathbf{F}_A + \mathbf{J}_W^i, \tag{2.23}$$

where

$$\mathbf{J}_W^i = -\phi S_W \left(\phi^{1/3} S_A^{7/3}\right) D_A^i \rho_A \nabla X_A^i = -\phi S_W\left(\tau_A\right) D_A^i \rho_A \nabla X_A^i, \tag{2.24}$$

D_A^i is the molecular diffusion coefficient of the inhibitor in water, and τ_A is the medium tortuosity of the aqueous phase.

The heat flux accounts for conduction, advection and radiative heat transfer, and is given by

$$\mathbf{F}^{\theta} = -\bar{k}_{\theta}\nabla T + f_{\sigma}\sigma_0\nabla T^4 + \sum_{\beta\equiv A,G} h_{\beta}\mathbf{F}_{\beta}\,, \tag{2.25}$$

where

$\bar{k}_{\theta}$ composite thermal conductivity of the medium/fluid ensemble [W m^{-1} K^{-1}];

h_{β} specific enthalpy of phase $\beta \equiv A,G$ [J kg^{-1}];

f_{σ} radiance emittance factor [dimensionless];

σ_0 Stefan-Boltzmann constant [5.6687×10^{-8} J m^{-2} K^{-4}].

Several options to estimate $\bar{k}_{\theta}$ are discussed in *Moridis* [2014].

The specific enthalpy of the gas phase is computed as

$$H_G = \sum_{\kappa\equiv w,m} X_G^{\kappa} h_G^{\kappa} + H_{dep}\,, \tag{2.26}$$

where h_G^{κ} is the specific enthalpy of component κ in the gaseous phase, and H_{dep} is the specific enthalpy departure of the gas mixture [J kg^{-1}]. The specific enthalpy of the aqueous phase is estimated from

$$H_W = X_A^w h_A^w + X_A^m\left(h_A^m + H_{sol}^m\right) + X_A^i\left(h_A^i + H_{sol}^i\right), \tag{2.27}$$

where h_A^w, h_A^m and h_A^i are the specific enthalpies of H_2O, CH_4 and the inhibitor at the conditions prevailing in the aqueous phase, respectively, and H_{sol}^m and H_{sol}^i are the specific enthalpy of dissolution [J kg^{-1}] of CH_4 and of the inhibitor in the aqueous phase, respectively.

2.7. Source and Sink Terms

In sinks with specified mass production rate, withdrawal of the mass component κ is described by

$$\hat{q}^{\kappa} = \sum_{\kappa \equiv A,G} X_{\beta}^{\kappa} q_{\beta} \ , \quad \kappa \equiv w,m \tag{2.28}$$

where q_{β} is the production rate of the phase β [kg m^{-3}]. For a prescribed production rate, the phase flow rates q_{β} are determined internally according to the general different options available in the TOUGH+ code (see *Moridis* [2014]). For source terms (well injection), the addition of a mass component κ occurs at desired rates $\hat{q}^{\kappa}$ ($\kappa \equiv w,m$). Inhibitor injection can occur either as a rate as an individual mass component ($\hat{q}^{i}$) or as a fraction of the aqueous phase injection rate, i.e., $\hat{q}^{i} = X_{A}^{i}\hat{q}_{A}$, where X_{A}^{i} is the inhibitor mass fraction in the injection stream.

In the kinetic model, the additional sink/source terms corresponding to hydrate dissociation and release of CH_4 and H_2O must be accounted for. The source term for CH_4 thus becomes $\hat{q}^{m} = Q^{m}$, where the production rate Q^{m} [kg m^{-3} s^{-1}] of CH_4 is computed from Equation (2.6) as

$$Q^{m} = -\frac{W^{m}}{W^{c}} Q_{H} \ , \tag{2.29}$$

Similarly, the source term for water (liquid or ice) becomes $\hat{q}^{m} + Q^{m}$, where the hydrate-related release of water Q^{w} is determined from the stoichiometry of Equation (2.1) as

$$Q^{w} = -\frac{N_{m} W^{w}}{W^{c}} Q_{H} \ , \tag{2.30}$$

Under equilibrium conditions, the rate of heat removal or addition includes contributions of (a) the heat associated with fluid removal or addition, as well as (b) direct heat inputs or withdrawals (e.g., microwave heating), and is described by

$$\hat{q}^{\theta} = q_d + \sum_{\kappa=A,G} h_\beta q_\beta \tag{2.31}$$

Under kinetic conditions, the rate of heat removal or addition is determined from

$$\hat{q}^{\theta} = q_d + \sum_{\kappa=A,G} h_\beta q_\beta + Q_H \Delta H^0 , \tag{2.32}$$

2.8. Thermophysical Properties

2.8.1. Water

The properties and parameters of liquid water and steam in **T+H** are provided by (a) fast regression equations based on data from *NIST* [2000] and (b) steam table equations from the IAPWS97 formulation [*Wagner et al*., 2000]. These equations are accurate up to 700 ^{o}C and 100 MPa, and computationally more efficient that those in the earlier versions of T+H (i.e., those in *Moridis et al*. [2008; 2009; 2012]). The code also incorporates additional capabilities extending the temperature and range to 3000 ^{o}C and 1000 MPa, but these are based on an iterative approach, are computationally very demanding, and, thus, are not invoked in the current version.

The enthalpy, sublimation pressure and fusion/melting pressure of ice (on the ice-vapor and ice-liquid water equilibrium lines of the water phase diagram) are computed using fast regression equations from data obtained using *NIST* [2000]. Within the solid ice phase (to T = 50 K and $P \approx$ 200 MPa), ice densities are determined using the ice

compressibility model of *Marion and Jakubowski* [2004] and the thermal expansivity data from *Dantle* [1962]. The ice enthalpy was computed using the heat capacity polynomial equation with the coefficients reported in *Yaws* [1999].

2.8.2. CH_4-Hydrate

The hydration number N_m and the thermal properties of the CH_4-hydrate (the specific heat C_H and the themal conductivity $k_{\theta H}$) are input functions of temperature in **T+H**. The specific enthalpy of the solid hydrate H_H (in J/kg) is estimated from the general equation $H_H = \int_{T_{0H}}^{T} C_H dT$, where T_{0H} = 273.15 K is the reference temperature for all enthalpy computation in **T+H** v1.5.

What is different from earlier T+H versions is that, in addition to the earlier option, the hydrate density ρ_H can now be computed also from the following equation proposed by *Ballard* [2002]:

$$\rho_H = \left[v_0 \exp\left(\alpha_1 \Delta T + \alpha_2 \Delta T^2 + \alpha_3 \Delta T^3 + \alpha_4 \Delta P \right) \right]^{-1}, \tag{2.30}$$

where is, $\Delta T = T - T_0$, $\Delta P = P - P_0$, the subscript *0* denotes a reference state, α_1 = 3.38496x10^{-4} K^{-1}, α_2 = 5.40099x10^{-7} K^{-2}, α_3 = -4.76946x10^{-11} K^{-3}, α_4 = 10^{-10} Pa^{-1}, the specific volume $v_0 = 1000 M_H/(22.712\ N_H)$, and M_H is the molecular weight of the hydrate [g/mol]. The reference temperature and pressure for Equation (2.30) are T_0 = 298.15 K and $P_0 = 10^5$ Pa, respectively *Ballard* [2002].

The parameters of kinetic dissociation of the hydrate are also inputs to **T+H**. The hydration equilibrium pressure-temperature relationship and the dependence of the heat of dissociation on temperature are discussed in Section 2.9.

2.8.3. CH_4 Gas

The properties of the gas phase are provided by the Peng-Robinson equation of state [*Peng and Robinson*, 1976], one of several options available in the real-gas property package (code unit **`T_RealGas_Properties.f95`**, see Section 3.4) included in **T+H**. This package computes the compressibility, density, fugacity, specific enthalpy and internal energy (ideal and departure) of pure gases and gas mixtures over a very wide range of pressure and temperature conditions. Additionally, the package computes the gas viscosity and thermal conductivity using the method of *Chung et al.* [1988], and binary diffusivities from the method of *Fuller et al.* [1969] and *Riazi and Whitson* [1993].

The package also allows determination of gas solubility in water either by using a set of temperature-dependent Henry's coefficients, or by equating fugacities in the gas and aqueous phases through a process that involves the computation of the activity coefficients (in the aqueous phase) and of the fugacities. For the case of CH_4, scoping calculations indicated that, for pressures P<100 MPa, accurate estimates can be obtained from the temperature-dependent Henry's coefficient H^m, and hence this is the one used by **T+H**. Determination of gas solubility through fugacities and activity coefficients provides accurate estimates for pressures as high as 1000 MPa, but is also very computationally demanding, while providing little (if any) benefit for any pressure

regime expected in CH_4-hydrate studies. Thus, this option is available but deactivated in the current code version.

2.9. Hydrate Phase Relationships

Of particular interest are the pressures and temperatures of the Lw-H-V and I-H-V three-phase lines in the H_2O-CH_4 diagram, which delineate the limits to hydrate formation/dissociation. The relationship between the equilibrium hydration pressure P_e and the corresponding equilibrium hydration temperature T_e in **T+H** can be obtained from two sources. The first is the regression equation of *Kamath* [1984]

$$P = \exp\left(e_1 + \frac{e_2}{T}\right), \tag{2.33}$$

where P is in KPa, T is in K,

$$e_1 = \begin{cases} 38.980 \\ 14.717 \end{cases}, \quad e_2 = \begin{cases} -8533.80 & \text{for} \quad 0°\text{C} > T_c \geq 25°\text{C} \\ -1886.79 & \text{for} \quad -25°\text{C} \geq T_c > 0°\text{C} \end{cases} \quad \text{and } T = T_c + 273.15 \tag{2.34}$$

The second source is a general regression expression derived by *Moridis* [2003] based on data from several researchers reported by *Sloan* [1998]. The two relationships and their range are shown in **Figure 2.1**. Limited smoothing in the vicinity of the quadruple point Q_1 (**Figure 2.2**) was implemented to allow continuity of the derivatives and smooth phase changes. This is a necessity in the Newton-Raphson iterations implemented in TOUGH+ (see Section 3.4). Because of its limited range, and the discontinuity at the quadruple point, the parametric equations in **Figures 2.1** and **2.2** are the default option in **T+H**. Use of the *Kamath* [1984] equation is advisable only when (a)

T is within the temperature range defined in Equation (2.34), and (b) no phase boundaries are crossed in the system.

In **T+H**, ΔH^0 under three-phase conditions (Lw-H-V and I-H-V) is computed from the simple equation of *Kamath* [1984] as

$$\Delta H^0 = C_f \left(C_1 + C_2 / T \right), \tag{2.35}$$

where ΔH^0 is in J/kg, T is in K, the conversion factor C_f = 33.72995 (J/kg)/(cal/gmol),

$$C_1 = \begin{cases} 13{,}521 \\ 6{,}534 \end{cases}, \text{ and } C_2 = \begin{cases} -4.02 & \text{for} \quad 0\ ^\circ\text{C} > T_c \geq 25\ ^\circ\text{C} \\ -11.97 & \text{for} \quad -25\ ^\circ\text{C} \geq T_c > 0\ ^\circ\text{C} \end{cases} \tag{2.36}$$

Equation (2.35) is a very weak function of temperature, and there is more recent evidence that ΔH^0 is practically constant over a wide range of temperatures [*Gupta*, 2007], so extension past the temperature range defined by Equation (2.36) is acceptable. Additionally, ΔH^0 for T_c < 0.01 ^{o}C is also obtained by subtracting the absolute value of the heat of fusion of ice ΔH^f from the ΔH^0 estimate for T_c > 0.01 ^{o}C.

There are no specific measurements of the equilibrium P -T relationship along the I-H-L$_w$ and the I-V-L$_w$ phase lines of a H_2O-CH_4O system, but is generally considered to follow the solidus line (melting/fusion equilibrium) of the water-ice system [*NIST*, 2000]. Thus, the equilibrium P-T relationship along the I-Lw-H phase line is computed as

$$P = P_Q - 6.26 \times 10^5\ (1.0 - T_d^{-3}) + 1.97135 \times 10^5 (1.0 - T_d^{21}) \tag{2.37}$$

where P is in Pa, T_d = T/273.16 (T in K), P_Q (in Pa) is the pressure at the hydrate quadruple point (see **Figures 2.1** and **2.2**). Finally, temperature was considered invariable (and equal to 0 ^{o}C along the I-V-L$_w$ phase line). The complete phase diagram of the water--CH_4--hydrate system is shown in **Figure 2.3**.

2.10. Inhibitor Effects on Hydrate Equilibrium

The effect of salinity on the dissociation equilibrium pressure-temperature relationship is described by the equation of *Dickens and Quinby-Hunt* [1997]

$$T_S = \left[\frac{1}{T_e} - \frac{N_H \Delta H^f}{\Delta H^0} \left(\frac{1}{273.15} - \frac{1}{T_f} \right) \right]^{-1}, \tag{2.39}$$

In this equation, T_s is the equilibrium dissociation temperature in the salt solution (K), ΔH^f is the heat of fusion of ice (J/kg), T_e is the equilibrium dissociation temperature in the presence of pure water (K), and T_f is the freezing point of the salt solution (K). The predictions of this equation are in broad agreement with the measurements of *Wright et al*. (1999). Further analysis allowed the above complex equation to be replaced with the simpler and equally accurate relationship, which has the additional benefits of applying to both salts and inhibitors such as alcohols. In the simplified equation, the temperature depression (shift) induced by the inhibitors is computed as

$$\Delta T_D = \Delta T_{D,r} \frac{\ln\left(1 - Y_A^i\right)}{\ln\left(1 - Y_{A,r}^i\right)}, \tag{2.40}$$

where

Y_A^i mole fraction of the inhibitor in the aqueous phase;

$Y_{A,r}^i$ reference mole fraction of the inhibitor in the aqueous phase [K];

ΔT_D inhibitor-induced temperature depression [K];

$\Delta T_{D,r}$ temperature depression at the reference mole fraction $x_{A,r}^i$.

This approach is entirely consistent with the equation of *Makogon* [1981] for alcohols. Exploratory calculations have shown this equation to be within 1-3% of the estimates of the far more computationally intensive method of Equation (2.39).

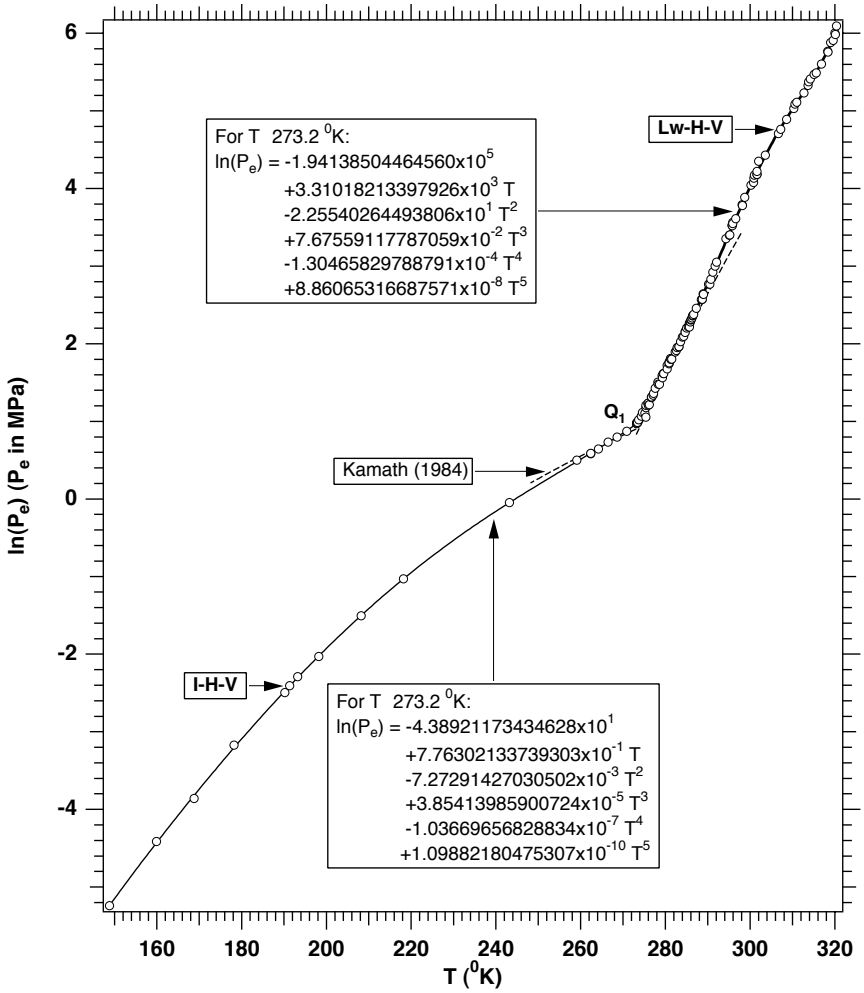

Figure 2.1. Relationship of the equilibrium hydration pressure *Pe* at a temperature *T* of the CH_4-hydrate [*Moridis,* 2003].

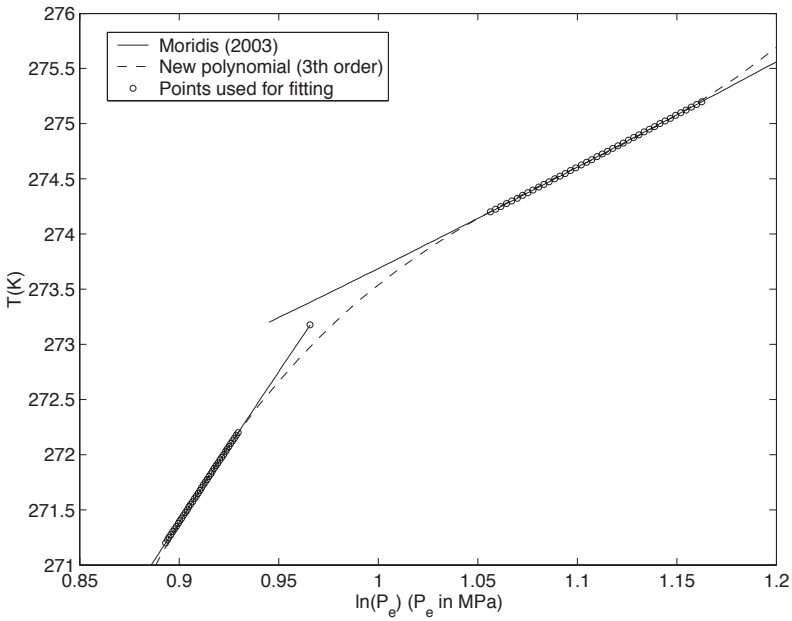

Figure 2.2. Modified *Pe -Te* relationship in the vicinity of the quadruple point.

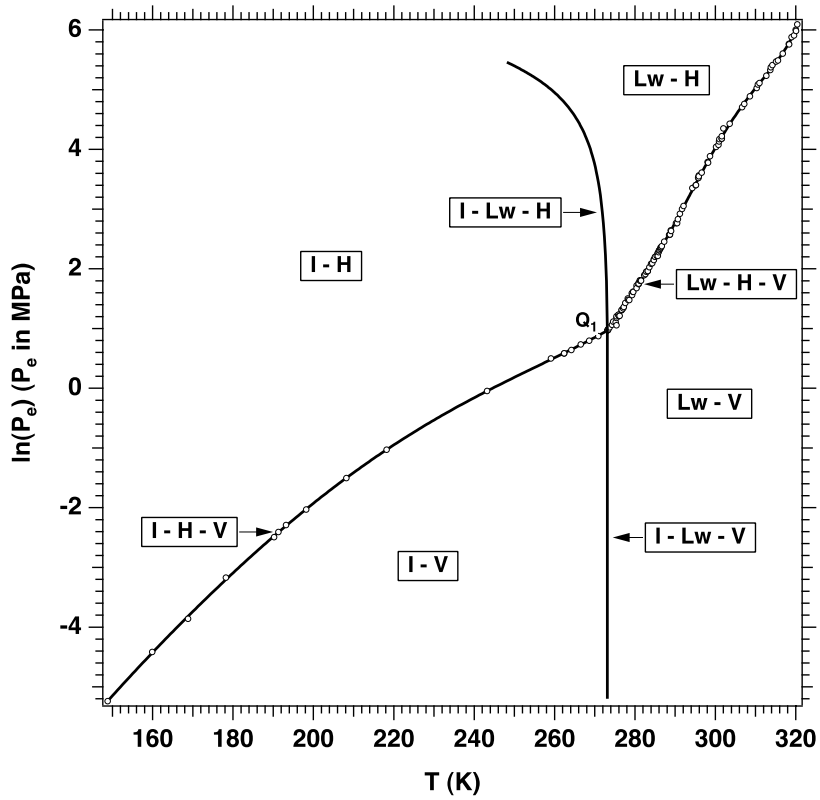

Figure 2.3. Pressure-temperature equilibrium relationship in the phase diagram of the H_2O-CH_4-hydrate system in T+H.

2.11. Other Processes, Properties, Conditions, and Related Numerical Issues

All other processes needed to complete the description of the fluid flows and system behavior in hydrate-bearing geologic media are common to most problems of flow and heat flow through porous/fractured media, are fully covered in the description of the core TOUGH+ code [*Moridis*, 2014], and will not be repeated here. These include issues related to relative permeability, capillary pressure, hydrate-dependent medium compressibility, treatment of fractured media, as well as the space and time discretization, the Newton-Raphson method and the use of the Jacobian in the fully implicit solution of these problems (the standard approach in all TOUGH+ applications). The interested reader is directed to *Moridis* [2014] for a detailed discussion of all these subjects.

3.0. Design and Implementation of TOUGH+HYDRATE v1.5

3.1. Primary Variables

The thermodynamic state and the distribution of the mass components among the four possible phases are determined from the hydrate equation of state. Following the standard approach employed in the TOUGH2 [*Pruess et al.*, 1999] family of codes, in **T+H** v1.5 the system is defined uniquely by a set of N_κ primary variables (where κ denotes the number of mass and heat components under consideration, see Section 2.2) that completely specifies the thermodynamic state of the system.

Although the number N_k of the primary variables is initially set at the maximum expected in the course of the simulation and does not change during the simulation, the thermodynamic quantities used as primary variables can change in the process of

simulation to allow for the seamless consideration of emerging or disappearing phases and components.

A total of 26 states (phase combinations) covering the entire phase diagram in **Figure 2.5** are described in **T+H**. Of those, 13 correspond to the equilibrium hydration reaction option, and 13 to the kinetic hydration reaction option. The primary variables used for the various phase states without inhibitor are listed in **Tables 3.1** and **3.2**, respectively. For systems with an inhibitor, the additional primary variable is *X_i_A*, (corresponding to X_A^i, i.e., the mass fraction of the inhibitor in the aqueous phase). The option set for either equilibrium or kinetic hydration reactions is complete, although some of the phase states are only possible under laboratory conditions and difficult to reach under any conditions of gas production from dissociating natural hydrate deposits.

The primary variables in **Tables 3.1** and **3.2** are necessary and sufficient to uniquely define the H_2O-CH_4 system. Note that the lack of equilibrium in the kinetic model introduces an additional degree of freedom, and consequently necessitates an additional equation. This requires special care to ensure that the resulting system is not over-defined when the hydrate and/or gas phases are not present.

3.2. Compiling the TOUGH+HYDRATE Code

T+H v1.5 is written in standard FORTRAN 95/2003. It has been designed for maximum portability, and runs on any computational platform (Unix and Linux workstations, PC, Macintosh) for which such compilers are available. Running **T+H** involves compilation and linking of the following code units and in the following order:

Table 3.1. Primary Variables in Equilibrium Hydrate Simulations without Inhibitor*.

Phase	State Identifier	Primary Variable 1	Primary Variable 2	Primary Variable 3
1-Phase: G	**Gas**	*P_gas*	*Y_m_G*	*T*
1-Phase: A	**Aqu**	*P*	*X_m_A*	*T*
2-Phase: A+G	**AqG**	*P_gas*	*S_aqu*	*T*
2-Phase I+G	**IcG**	*P_gas*	*S_ice*	*T*
2-Phase H+G	**GsH**	*P_gas*	*S_gas*	*T*
2-Phase: A+H	**AqH**	*P*	*S_aqu*	*T*
2-Phase: A+I	**AqI**	*P*	*S_aqu*	*X_m_A*
2-Phase: I+H	**IcH**	*P*	*S_ice*	*T*
3-Phase: A+H+G	**AGH**	*S_gas*	*S_aqu*	*T*
3-Phase: A+I+G	**AIG**	*P_gas*	*S_aqu*	*S_gas*
3-Phase: A+I+H	**AIH**	*P*	*S_aqu*	*S_ice*
3-Phase: I+H+G	**IGH**	*S_gas*	*S_ice*	*T*
Quadruple Point: I+H+A+G	**QuP**	*S_gas*	*S_aqu*	*S_ice*

Where the possible primary variables are: *P*, pressure [Pa]; *P_gas*, gas pressure [Pa]; *T*, temperature [C]; *X_m_A*, mass fraction of CH_4 dissolved in the aqueous phase [-]; *Y_m_G*, mass fraction of CH_4 dissolved in the gas phase [-]; *S_aqu*, liquid saturation [-]; *S_gas*, gas saturation [-]; *S_ice*, ice saturation [-]; *X_i_A*, mass fraction of inhibitor dissolved in the aqueous phase [-].

*For inhibitor: *X_i_A* becomes the 3rd primary variable, and the 3rd primary variable (as listed in this table) becomes the 4th primary variable.

Table 3.2. Primary Variables in Kinetic Hydrate Simulations Without Inhibitor*.

Phase	State Identifier	Primary Variable 1	Primary Variable 2	Primary Variable 3	Primary Variable 4
1-Phase: G	**Gas**	*P_gas*	*Y_m_G*	*S_hyd*	*T*
1-Phase: A	**Aqu**	*P*	*X_m_A*	*S_hyd*	*T*
2-Phase: A+G	**AqG**	*P_gas*	*S_aqu*	*S_hyd*	*T*
2-Phase I+G	**IcG**	*P_gas*	*S_ice*	*S_hyd*	*T*
2-Phase H+G	**GsH**	*P_gas*	*S_gas*	*S_ice*	*T*
2-Phase: A+H	**AqH**	*P*	*S_aqu*	*X_m_A*	*T*
2-Phase: A+I	**AqI**	*P*	*S_aqu*	*X_m_A*	*T*
2-Phase: I+H	**IcH**	*P*	*S_ice*	*S_gas*	*T*
3-Phase: A+H+G	**AGH**	*P_gas*	*S_aqu*	*S_gas*	*T*
3-Phase: A+I+G	**AIG**	*P_gas*	*S_aqu*	*S_hyd*	*S_gas*
3-Phase: A+I+H	**AIH**	*P*	*S_aqu*	*S_ice*	*T*
3-Phase: I+H+G	**IGH**	*P_gas*	*S_gas*	*S_ice*	*T*
Quadruple Point: I+H+A+G	**QuP**	*P_gas*	*S_aqu*	*S_gas*	*S_ice*

Where the possible primary variables are: *P*, pressure [Pa]; *P_gas*, gas pressure [Pa]; *T*, temperature [C]; *X_m_A*, mass fraction of CH_4 dissolved in the aqueous phase [-]; *Y_m_G*, mass fraction of CH_4 dissolved in the gas phase [-]; *S_aqu*, liquid saturation [-]; *S_gas*, gas saturation [-]; *S_hyd*, hydrate saturation [-]; *S_ice*, ice saturation [-]; *X_i_A*, mass fraction of inhibitor dissolved in the aqueous phase [-].

*For inhibitor: *X_I_A* becomes the 4th primary variable, and the 4th primary variable (as listed in this table) becomes the 5th primary variable.

(1) T_Hydrate_Definitions.f95 (*)

Code unit providing default parameter values describing the basic attributes of the equation of state (i.e., number of components, number of phases, etc.)

(2) T_Allocate_Memory.f95

Code unit responsible for the dynamic memory allocation (following input describing the size of the problem) and dimensioning of most arrays needed by the code, in addition to memory deallocation of unnecessary arrays.

(3) T_Utility_Functions.f95

Code unit that includes utility functions, i.e., a wide variety of mathematical functions, table interpolation routines, sorting algorithms, etc.).

(4) T_H2O_Properties.f95 (#)

Code unit that includes (a) all the water-related constants (parameters), and (b) procedures describing the water behavior and thermophysical properties/processes in its entire thermodynamic phase diagram.

(5) T_Media_Properties.f95

Code unit that describes the hydraulic and thermal behavior of the geologic medium (porous or fractured), i.e., capillary pressure and relative permeability under multiphase conditions, interface permeability and mobility, and interface thermal conductivity.

(6) T_RealGas_Properties.f95 (#)

Code unit that includes (a) the important constants (parameters) that are needed for the estimation of the properties of all hydrate-forming gases (see below), and (b) procedures describing the equation of state (EOS) of real gases (pure or mixtures) using any of the Peng-Robinson, Redlich-

Kwong, or Soave-Redlich-Kwong cubic EOS model. The procedures in this code unit compute the following parameters and processes: compressibility, density, fugacity, enthalpy (ideal and departure), internal energy (ideal and departure), entropy (ideal and departure), thermal conductivity, viscosity, binary diffusion coefficients, solubility in water, and heat of dissolution in water.

(7) `T_Hydrate_Properties.f95 (*)`

Code unit that describes the properties and processes of the CH_4-hydrate. It includes procedures that describe the *P-T* relationship along the three-phase equilibrium regimes of the CH_4-hydrate phase diagram (see **Figure 2.3**) and compute the heat of the hydration reaction, the hydrate density and enthalpy, and the reaction rate when kinetic formation/dissociation are invoked.

(8) `T_Geomechanics.f95`

Code unit that describes the geomechanically-induced changes on the flow properties of the porous media. These include porosity ϕ changes caused by pressure and/or temperature variations, intrinsic permeability k changes caused by porosity changes, and scaling of capillary pressures P_{cap} to reflect changes in ϕ and k. The ϕ and k changes are computed using either simplified of full geomechanical models. When the simplified model is invoked, ϕ is a function of (a) P and the pore compressibility α_P and (b) of T and the pore thermal expansivity α_T, while (c) k changes are estimated using emprirical relationships (see Section 8). Changes in ϕ and k can also be computed by using a full geomechanical model, which can be optionally coupled with TOUGH+.

(9) `T_Hydrate_Specifics.f95 (*)`

Code unit that includes procedures specific to the hydrate simulation, such as the reading of hydrate-specific inputs, the preparation of hydrate-

specific output files, and the computation of the thermal conductivity in hydrate-bearing media. Generic procedures and operator extension -- which override (*overload*) the standard procedures used by TOUGH+ for the simulation of non-hydrate problems – are defined in this code unit, which does not include any procedures describing the hydrate equation of state.

(10) T_Main.f95

Main program that organizes the calling sequence of the high-level events in the simulation process, and includes the writing of important general comments in the standard output files, timing procedures, and handling of files needed by the code and/or created during the code execution.

(11) T_Hydrate_EOS.f95 (*)

Code unit that describes the equation of state of the CH_4-hydrate, assigns initial conditions, computes the thermophysical properties of the hydrate-bearing medium, and determines phase changes and the state of the system from the 22 possible options (see Section 3.1). This code unit also includes the procedure that computes the elements of the Jacobian matrix for the Netwon-Raphson iteration.

(12) T_Matrix_Solvers.f95

A linear algebra package that includes all the direct and iterative solvers available in TOUGH+ (see *Moridis* [2014]).

(13) T_Executive.f95

The executive code unit of TOUGH+. It includes the procedures that advance the time in the simulation process, estimate the time-step size for optimum performance, populate the matrix arrays and invoke the solvers of the Jacobian, invoke special linear algebra for matrix pre-processing in cases of very demanding linear algebra problems, compute rates in sources

and sinks, compute binary diffusion coefficients, write special output files, and conduct other miscellaneous operations.

(14) `T_Inputs.f95`

This code unit includes the procedures involved in the reading of the general input files needed for TOUGH+ simulations. It does not include any procedure reading hydrate-related data (this is accomplished in the **`T_Hydrate_Specifics.f95`** code unit).

The code units denoted by (*) are specific to the hydrate problem, and are needed by **T+H**. The code unit denoted by (#) is not part of core TOUGH+ code but of the wider TOUGH+ code ensemble [*Moridis*, 2014], and is invoked to carry out the computations related to the behavior of CH_4 needed by the HYDRATE v1.5 application option. All other code units are common to all TOUGH+ simulations.

Additionally, **T+H** is distributed with the **`Meshmaker.f95`** FORTRAN code, which used to be part of the main code in the TOUGH and TOUGH2 simulators, but is a separate entity in the TOUGH+ family of codes. **`Meshmaker.f95`** is used for the space discretization (gridding) of the domain of the problem under study (see *Moridis* [2014]).

NOTE: In compiling **T+H** v1.5, *it is important that the free-format source code option be invoked for proper compilation*.

4.0. Input Data Requirements

In this section, we discuss in detail mainly the input requirements that are specific to the needs of the HYDRATE v1.5 option. All inputs that are generic in type and common to any simulation of flow and transport through porous media are fully described in *Moridis* [2014] and will not be repeated here. The reader is directed to the *Moridis* [2014] report for details on the description of all such inputs and on the structure of the input files. Note that, to ensure backward compatibility with input files for older **T+H** versions, some input data for **T+H** v1.5 conform to older formats. The data inputs to activate the new capabilities in **T+H** v1.5 follow more advanced formats such as namelists.

Some of these non-hydrate specific data are also discussed here (in essence, repeating the information in *Moridis* [2014]) for additional emphasis, as these *may* play an important role in hydrate simulations. Unless otherwise indicated, all input data are in standard metric (SI) units, such as meters, seconds, kilograms, ˚C and in the corresponding derived units, such as Newtons, Joules, Pascal (= N/m^2 for pressure), etc.

4.1. Input Data Blocks

In the **T+H** v1.5 input file data are organized in standard TOUGH2 and TOUGH+ structure that involves data blocks that are defined by keywords. **Table 4.1** provides a listing and a short description of all the data blocks (mandatory and optional) in a **T+H** v1.5 input file. Note that, as a result of the modular structure of the TOUGH+ architecture [*Moridis*, 2014], only a single data block (**`HYDRATE`**) is specific to the hydrate problem, and all other ones are generic and common to any TOUGH+ simulation.

4.2. Data Block `MEMORY`

This block is a mandatory component of the generic TOUGH+ input file, and is discussed here only in order to provide a list of values for the parameters needed for an appropriate allocation of the dynamic memory. Thus, the following options are possible:

`binary_diffusion` `=.TRUE.` if diffusion is considered
`=.FALSE.` if diffusion is ignored

The following combinations are possible for hydrate simulations in **T+H** v1.5:

(1) `(NumCom, NumEq, NumPhases) = (2,3,4)`:
Equilibrium hydrate reaction, no inhibitor

(2) `(NumCom, NumEq, NumPhases) = (3,4,4)`:
Equilibrium hydrate reaction with inhibitor

(3) `(NumCom, NumEq, NumPhases) = (3,4,4)`:
Kinetic hydrate reaction, no inhibitor

Table 4.1. Input data blocks for TOUGH+HYDRATE v1.5.

Keyword (+)	***Sec.* (#)**	***Function***
TITLE (1st record)	4.1.1	Data record (single line) with simulation title
MEMORY (2nd record)	5.1	Dynamic memory allocation
HYDRATE	4.2(^)	Parameters describing hydrate properties and behavior
ROCKS or **MEDIA**	6.2	Hydrogeologic parameters for various reservoir domains
RPCAP or **WETTA**BILITY	6.3	Optional; parameters for relative permeability and capillary pressure functions
DIFFUSION	6.4	Optional; diffusivities of mass components
***ELEME**	7.1	List of grid blocks (volume elements)
***CONNE**	7.2	List of flow connections between grid blocks
INDOM	8.1	Optional; initial conditions for specific reservoir domains
***INCON**	8.2	Optional; list of initial conditions for specific grid blocks
EXT-INCON	8.3	Optional; list of initial conditions for specific grid blocks
BOUNDARIES	8.6	Optional; provides time-variable conditions at specific boundaries
***GENER**	9.1	Optional; list of mass or heat sinks and sources
PARAM	10.1	Computational parameters; time stepping and convergence parameters; program options
SOLVR	10.2	Optional; specifies parameters used by linear equation solvers.
TIMES	11.2	Optional; specification of times for generating printout
SUBDOMAINS	11.3	Optional; specifies grid subdomains for desired time series data
INTERFACES	11.4	Optional; specifies grid interfaces for desired time series data
SS_GROUPS	11.5	Optional; specifies sink/source groups for desired time series data
ENDCY (last record)	4.1.3	Record closes TOUGH+ input file and initiates simulation
ENDFI (last record)	4.1.4	Alternative for closing TOUGH+ input file which causes flow simulation to be skipped.

#: Denotes the section number in the *Moridis* [2014] report
^: Denotes the section number in this report
*: Data can be provided as separate disk files and omitted from input file.
+: The bold face part of the keyword (left column) suffices for data block recognition

`(NumCom, NumEq, NumPhases) = (4,5,4)`:
Kinetic hydrate reaction with inhibitor

Any value of the `NumCom, NumEq, NumPhases` parameters other than those described here results in an error message and the cessation of the simulation. The selection of appropriate values for all other variables in this data block is left to the user.

4.2. Data Block `HYDRATE`

The parameters describing the hydrate properties and behavior are provided here. Note that free format is used to read the data in this data block.

Record `HYDRATE.1`

The number of component hydrates `NCom` is read in this card. Because of the dearth of quantitative information on the behavior of complex hydrates (as explained in Section 1.2), `NCom = 1` in this version of **T+H**.

Record `HYDRATE.2`

This card reads the following data:

`nameG`	The name of the hydrate-forming gas
`hydrN`	The corresponding hydration number – see Equation (2.1)
`moleF`	The mole fraction in the composite hydrate (for pure hydrates, `moleF = 1`)

Record `HYDRATE.3`

This record includes `N_ThC`, which is the number of coefficients of the polynomial describing the dependence of the thermal conductivity K_H of the hydrate on temperature T.

Record `HYDRATE.4`

This card includes the coefficients A_i ($i = 0,...,n$, n = `N_ThC-1`) of the thermal conductivity polynomial (T in K)

$$K_H = A_0 + A_1T + A_2T^2 + \ldots + A_nT^n \tag{6.1}$$

Record `HYDRATE.5`

This record includes `N_SpH`, which is the number of coefficients of the polynomial describing the dependence of the specific heat C_H of the hydrate on temperature T.

Record `HYDRATE.6`

This card provides the coefficients B_i (i = 0,...,n, n = `N_SpH-1`) of the specific heat polynomial (T in K)

$$C_H = B_0 + B_1T + B_2T^2 + \ldots + B_nT^n \tag{6.2}$$

Possible options are the equations of *Gupta* [2007], according to which:
Option 1: $n = 1$, B_0 = 1.20053978E3 J/kg/K, B_1 = 1.196404E1 J/kg/K^2
Option 2: $n = 3$, B_0 = -3.4270565E5 J/kg/K, B_1 = 3.9553876E3 J/kg/K^2,
B_2 = -1.515176E1 J/kg/K^4, B_3 = 1.9370547E-2 J/kg/K^4

Record `HYDRATE.7`

This record includes `N_Rho`, which is the number of coefficients of the polynomial describing the dependence of the hydrate density ρ_H on temperature T.

Record `HYDRATE.8`

This card provides the coefficients D_i (i = 0,...,n, n = `N_Rho - 1`) of the hydrate density polynomial.

$$\rho_H = D_0 + D_1T + D_2T^2 + \ldots + D_nT^n \tag{6.3}$$

Note that, if `N_Rho=0`, the equation of Ballard [2002] is used to compute ρ_H – see Equation (2.30).

Record `HYDRATE.9`

This card reads the following inhibitor-related data:

`inhibitor_flag`
Logical variable, (flag) indicating presence of an inhibitor when `inhibitor_flag = .TRUE.`. Note that no additional variable values are read past this point if `inhibitor_flag = .FALSE.`.

`Max_TShift`

Real variable describing the inhibitor-induced reference temperature depression – see Equation (2.40). When salt (NaCl) is the inhibitor in question, `Max_Tshift = 2.0E0`.

`Y_atMax_TShift`

Real variable describing the reference inhibitor mole fraction in the aqueous phase, corresponding to `Max_TShift` – see Equation (2.40). For NaCl, `Y_atMax_Tshift = 1.335E-2`.

`InhibitorMW`

Real variable describing the molecular weight of the inhibitor [g mol^{-1}]. For NaCl, `InhibitorMW = 5.8448E1` g mol^{-1}.

`InhibitorDens`

Real variable describinig the inhibitor density [in kg/m^3]. For NaCl, `InhibitorDens = 2.6E3` kg/m^3.

`InhibitorEnthSol`

Real variable describinig the specific enthalpy of the inhibitor dissolution in water [J/kg]. For NaCl, `InhibitorEnthSol = 6.6479E4` J/kg.

`InhibitorCpCoeff`

Real array of dimension 3, containing the coefficients of the inhibitor specific heat C_i vs. T quadratic equation $C_i = C_0 + C_1T + C_2T^2$. For NaCl, `InhibitorCpCoeff(1,2,3) = 41.293E0` J/kg/K, `3.3607E-2` $J/kg/K^2$, and `-1.3927E-5` $J/kg/K^3$.

Record `HYDRATE.10`

The integer variable `EquationOption` in Card `HYDRATE.10` is an option for the selection of the equation describing the *Pe* vs. *Te* and ΔH^0 vs. *Te* relationships (see discussion in Section 2.9). For `EquationOption = 0`, the modified equation of *Moridis* [2003] is used for the *Pe* vs. *T* relationship and ΔH^0 is constant [Gupta, 2007]. For `EquationOption = 1`, the equations of *Kamath* [1984] are employed. For `EquationOption = 2`, the *Pe* vs. *T* relationship is computed using the equation of *Moridis* [2003] and the ΔH^0 vs. *T* relationship is obtained from the *Kamath* [1984] equation. A value of `EquationOption` = 0 is the preferred option (default), with `EquationOption` = 2 being the next best choice.

Record `HYDRATE.11`

The character variable `Reaction_Type (LEN = 5)` in Card `HYDRATE.11` describes the type of hydrate reaction, and can take one of two values. For simulations under equilibrium conditions, `Reaction_Type = 'EQUILIBRIUM'`. Kinetic hydrate reactions are considered when `Reaction_Type = 'KINETIC'`.

Record `HYDRATE.12`

The card `HYDRATE.12` is read only if `Reaction_Type = 'KINETIC'`, and includes the following kinetic dissociation parameters:

`ActivationEnergy`
: Real variable describing the activation energy ΔE_a [J mol^{-1}] of the hydrate dissociation kinetic reaction – see Equation (2.6). A standard value for dissociation is `ActivationEnergy` = 8.1E4 J/mol [*Clarke and Bishnoi*, 2001].

`IntrinsicRateConstant`
: Real variable describing the intrinsic hydration reaction constant K_0 [kg/m^2/Pa/s]. A standard value for a CH_4-hydrate dissociation reaction is `IntrinsicRateConstant` = 3.6E4 kg/m^2/Pa/s [*Clarke and Bishnoi*, 2001].

`Area_Factor`
: Real variable describing the area adjustment factor [dimensionless] – see Equation (2.6). A value of 1 may be used as a starting point, and is then adjusted to match observations (mainly of laboratory data) in history-matching (inverse modeling) simulations.

4.3. Data Block `ROCKS` or `MEDIA`

The discussion here is limited to the specific parameters that *may be* needed in a **T+H** v1.5 simulation. Although all this information can be found in *Moridis* [2014], it is repeated here for additional emphasis. Information on all the other parameters in the specified records is found in *Moridis* [2014].

Record `ROCKS.1`

`NAD`

= `5`: In addition to the standard four records read for NAD > 2, an additional (fifth) record will be read with the coefficients of the porosity polynomial $\phi/\phi_0 = F_0 + F_1\Delta P + F_2\Delta P^2 + \ldots + F_n\Delta P^n$, where ϕ_0 is the reference (initial) default porosity and $\Delta P = P\text{-}P_0$ is the deviation from the initial pressure P_0. This equation will be used instead of Equation (2.23) of *Moridis* [2014] to estimate the effect of pressure on the medium porosity.

= `6`: In addition to the standard four records read for NAD > 2, an additional (fifth) record will be read with the coefficients of Equations (2.44) and (2.45) of *Moridis* [2014] that describe the compressibility of an unconsolidated porous medium in the presence of cementing solid phases (such as ice and/or hydrates).

`PoMedRGrain`

Rock grain radius [m]. This is needed for the estimation of the hydrate surface reaction area when kinetic hydrate reactions are invoked. If `PoMedRGrain = 0.0E0` (e.g., when no value is provided), the TOUGH+ code provides a grain radius estimate using the Kozeny-Carman approximation (see Section 2.4).

Record `ROCKS.1.1` (optional, when `NAD` ≥ 1 only)

`mediaCritSat`

Critical total mobile phase saturation (= S_A+S_G) at which the permeability of hydrate and/or ice-bearing medium becomes equal to zero; it is equal to the critical "open" porosity ϕ_c of a porous medium at which its permeability becomes zero – needed only when the EPM model is invoked (see Sections 2.11 and 2.12 of *Moridis* [2014]).

`mediaPermExpon`

Permeability reduction exponent for solid phase-bearing systems – See Equations (2.26) or (2.43) in *Moridis* [2014].

`mediaGama`

The parameter γ used for the computation of intrinsic permeability k as an empirical function of variations in the porosity ϕ – See Equation (2.24) in *Moridis* [2014].

Record `ROCKS.1.4`

Optional, for NAD = 5 only, to be used when the media porosity is described as a polynomial function of the pressure change ΔP)

Format (I5, 5X, 7E20.13)

```
PhiPolyOrder, (PhiCoeff (i),i=0,…,6)
```

`PhiPolyOrder`

Order n of the polynomial $\phi/\phi_0 = F_0 + F_1\Delta P + F_2\Delta P^2 + \ldots + F_n\Delta P^n$. For a constant ϕ, `PhiPolyOrder = 0.`

`PhiCoeff(i),i=0,…,6`

Coefficients F_n (n = 0,…,`PhiPolyOrder`) of the $\phi = \phi(\Delta P)$ polynomial.

Record `ROCKS.1.4`

Optional, NAD = 6 only, to be used when cementing solid phases such as ice and/or hydrates are present in the pores of unconsolidated media – see Section 2.11.3 in *Moridis* [2014].

Format (10E10.4)

```
LoComp, SatAtLoComp,
HiComp, SatAtHiComp, DeltaSat
```

`LoComp`

The lower limit of the medium compressibility α_{PL} [Pa^{-1}], corresponding to the full stiffening/strengthening effect of the presence of cementing solid phases such as ice and/or hydrates – see Equation (2.56) in *Moridis* [2014].

`SatAtLoComp`

= S_{Smax}, i.e., the lowest S_S saturation at which $\alpha_P = \alpha_{PL}$ – see Equations (2.56) and (2.57) in *Moridis* [2014].

`HiComp`

The upper limit of the medium compressibility α_{PU} [Pa^{-1}], corresponding to the absence of cementing solid phases– see Equation (2.56) in *Moridis* [2014].

`SatAtHiComp`

= S_{Smin}, i.e., the largest S_S saturation at which $\alpha_P = \alpha_{PU}$ – see Equations (2.56) and (2.57) in *Moridis* [2014].

`DeltaSat`

The smoothing factor δ – see Equation (2.57) in *Moridis* [2014]. A value of $\delta = 0.015$ is suggested.

The following capillary pressure curve (which eliminates the discontinuity of the standard Brooks-Corey equation at $S_A = 0$) that is available in standard TOUGH+ v1.5 core code (see *Moridis* [2014]) may be considered as an option for T+H v1.5 simulations:

`PcapEquationNum = 8:` **Brooks-Corey equation modified to account for effect of hydrate on capillary pressure**

$$P_{cap} = -F \cdot G \cdot P_{GE}(S^*)^v, \; S^* = \frac{(S_A - S_{irA})}{(1 - S_{irA})}, \; F = 1 + A \cdot Bx(a, b, S_H)$$

where

v = exponent with the following restrictions: v< 0 and |v| ≤ 1;
P_{GE} = gas entry pressure;
G = error function equation that smoothes curve near S=0;
F = factor that describes effect of hydrate on capillary pressure;
A = parameter > 0;
B_x = incomplete beta function;
a,b = input arguments for B_x;
S_S = $(S_H + S_I)$, saturation of solid phases

Parameters: `CP(1)` = P_{GE}, `CP(2)` = v, `CP(3)` = S_{irA},
`CP(4)` = $P_{cap,max}$, `CP(5)` = A, `CP(6)` = a, `CP(7)` = b

The various parameters are determined from curve fitting of available laboratory data.

4.4. Data Block `PARAM`

The discussion here is limited to the specific parameters that *may be* needed in a **T+H** v1.5 simulation. Although all this information can be found in *Moridis* [2014], it is

repeated here for additional emphasis. Information on all the other parameters in the specified records is found in *Moridis* [2014].

`MOP(10)`

It controls the selection of the interpolation formula for the composite heat conductivity as a function of the various phase saturations. The following options are available

`= 0:` $\bar{k}_\theta = k_{\theta d} + (\sqrt{S_A} + \sqrt{S_H})(k_{\theta w} - k_{\theta d}) + \phi S_I k_{\theta I}$

`= 1:` $\bar{k}_\theta = k_{\theta d} + (S_A + S_H)(k_{\theta w} - k_{\theta d}) + \phi S_I k_{\theta I}$

`= 2:` $\bar{k}_\theta = k_{\theta d} + \phi\left(S_A k_{\theta A} + S_H k_{\theta H} + S_I k_{\theta I}\right)$ – based on the linear model of *Bejan* [1984], gas contribution ignored

`= 3:` $\bar{k}_\theta = k_{\theta d} + \phi\left(S_A k_{\theta A} + S_H k_{\theta H} + S_I k_{\theta I} + S_G k_{\theta G}\right)$ – based on the linear model of *Bejan* [1984], including gas contribution

Here $k_{\theta\beta}$ are the thermal conductivities of the phases β (=*A,G,H,I*), and $k_{\theta w}$ and $k_{\theta d}$ are the wet and dry thermal conductivities of the porous medium.

Options `MOP(10) = 0` and `MOP(10) = 1` are based on extensions of an earlier model of *Somerton et al*. [2003; 2004] based on the analysis of *Moridis et al*. [2005] of the thermal properties of hydrates from laboratory studies [*Kneafsey et al*., 2005].

It is not known under what conditions (if any) the linear model of *Bejan* [1984] – invoked for `MOP(10)= 2` and `MOP(10) = 3` – is applicable, but it is included for completeness. The last option `MOP(10) = 3` is discouraged because of (a) doubts about the validity of the *Bejan* [1984] linear model, (b) the very demanding computations for the estimation of the gas thermal conductivity from the real gas property package in **T+H** v1.5, and (c) the small overall gas contribution to the composite thermal conductivity $\bar{k}_\theta$.

4.5. Data Block `DIFFUSION`

This block reads multicomponent diffusion coefficients using a `NAMELIST` format. This is a very powerful format that allows maximum clarity and flexibility, accepting free

formats, arbitrary ordering of variables, insertions of comments anywhere in the input fields, and providing the option of ignoring any of the `NAMELIST` parameters by not assigning a value to it. For more information, the reader is directed to a textbook on FORTRAN 95/2003.

In **T+H** v1.5 applications, this capability may be invoked in long-term studies (covering multi-year periods) of hydrate formation. Diffusion is not expected to play a significant role during dissociation in the course of gas production from hydrate-bearing geologic media because, in such a case, advective effects constistently overwhelm diffusive transport.

Record `DIFFUSION.1`

This record includes general data describing key diffusion parameters. The namelist in this record is named `Diffusion_Key_Parameters`, and has the following general form.

```
&Diffusion_Key_Parameters
     gas_diffusivity_equation_exponent  = x.xEx,
     P_at_RefDiffusivity                = x.xEx,
     Tk_at_RefDiffusivity               = x.xEx
     full_multiphase_diffusion          = .x
     /
```

The parameters in the namelist `Diffusion_Key_Parameters` are defined as follows:

`gas_diffusivity_equation_exponent`
: A double precision variable describing the dependence of gas diffusivity on temperature (see Equation 6.4 in *Moridis* [2014]). The default value is 1.80.

`P_at_RefDiffusivity`
: Pressure at the reference diffusivity (in Pa). If `P_at_RefDiffusivity <= 0`, the default value is 10^5 Pa.

`Tk_at_RefDiffusivity`
: Temperature at the reference diffusivity (in K). If `T_at_RefDiffusivity <= 0`, the default value is 273.15 K.

`Option_gas_diffusivity_CompuMethod`

A character variable describing the method of estimation of the binary **gas** diffusivities. The following options are available:

`='Standard'`: This option involves the application of Equation (6.4) in *Moridis* [2014], and requires non-zero multicomponent gas diffusivity values read from the standard input file.

`='Real_Gas_EOS'`: In this case, the binary gas diffusivities are computed from the cubic equation of state used to determine all the real gas properties. The diffusivities in the aqueous phase still need to be provided.

`='Constant'`: When this option is invoked, the constant multicomponent diffusivity values provided in the input file are used.

`full_multiphase_diffusion`

A logical variable describing the method of estimation of the method of estimation of multiphase diffusive fluxes. The following options are available:

`=.TRUE.`: With this option, harmonic weighting to the full multiphase effective diffusion strength is applied. This includes contributions from gas and aqueous phases, accounts for coupling of diffusion with phase partitioning effects, and can describe the most general cases of diffusion across phase boundaries.

`=.FALSE.`: In this case, harmonic weighting is performed separately for the diffusive fluxes in the mobile phases.

Records `DIFFUSION.2.1`, `DIFFUSION.2.2`, etc.

Record `DIFFUSION.2.1` is followed by `DIFFUSION.2.x` records, with `x = 1,…,NubMobPhases` (i.e., the number of mobile phases in the system under study). These records describe component diffusivities in the various phases. The same namelist is used in each one of these records. It is named `Component_Diffusivities_in_Phases`, and has the following general form:

```
&Component_Diffusivities_in_Phases
     phase        = x,
     phase_number = x,
     component(1) = x,
          component_number(1)      = x,
          component_diffusivity(1) = x.xEx,
     component(2) = x,
```

```
        component_number(2)       = x,
        component_diffusivity(2) = x.xEx,
…
…
…
/
```

The parameters in the namelist `Diffusion_Key_Parameters` are defined as follows:

`phase`

A character variable identifying the mobile phase for which the diffusivities of the various components are reported. The possible options in the **T+H** code are '`Aqueous`' and '`Gas`'.

`phase_number`

An integer variable providing the number of the phase in the phase numbering sequence used in the code. The possible options in the **T+H** code are:
`= 2` for `phase` = '`Aqueous`', and
`= 1` for `phase` = '`Gas`'.

`component`

A character array of dimension `NumCom` (see Section 5.1) identifying the various mass components partioned in the phase in question (denoted by `phase`). The possible options in the **T+H** v1.5 code are '`CH4`', '`H2O`' and '`NaCl`' (if salinity is considered).

`component_number`

An integer array providing the number of the component in the numbering sequence used in the code. The possible options in the **T+H** code are:
`= 1` for `component` = '`CH4`'
`= 2` for `component` = '`H2O`'
`= 3` for `component` = '`NaCl`' (if present)

`component_diffusivity`

A double precision array of dimension `NumCom` (see Section 5.1) describing the value of the multicomponent diffusivities D_β^κ (see Equations (2.59) and (6.4)) of the various components κ in the phase β under consideration (indentified by `phase` and `phase_number`, respectively).

NOTE: *The records* `DIFFUSION.2.x` *must provide data for all mobile phases and all components, even if the gas diffusivities may be overridden internally when* `Option_gas_diffusivity_CompuMethod = 'Real_Gas_EOS'`.

The structure of the namelists `Diffusion_Key_Parameters` and `Component_Diffusivities_in_Phases` (and their use as input formats in the data block **`DIFFUSION`**) are best illustrated in the example of **Figure 4.1**.

```
DIFFUSION-----*----2----*----3----*----4----*----5----*----6----*----7----*----8
&Diffusion_Key_Parameters  gas_diffusivity_equation_exponent  = 1.8d0
                           P_at_RefDiffusivity                = 1.0d5,    ! in Pa
                           Tk_at_RefDiffusivity               = 273.15d0, ! in K
                           Option_gas_diffusivity_CompuMethod = 'Real_Gas_EOS',
                           full_multiphase_diffusion          = .TRUE.
                           /
&Component_Diffusivities_in_Phases
        phase        = 'Aqueous',  phase_number = 2,
        component(1) = 'CH4',      component_number(1) = 1,
        component_diffusivity(1) = 1.0d-10,  ! (m2/s) ! Diffusivity of component 1 in phase 2
        component(2) = 'H2O',      component_number(2) = 2,
        component_diffusivity(2) = 1.0d-10,  ! (m2/s) ! Diffusivity of component 2 in phase 2
        component(3) = 'NaCl',     component_number(3) = 3,
        component_diffusivity(3) = 1.0d-10   ! (m2/s) ! Diffusivity of component 3 in phase 2
        /
&Component_Diffusivities_in_Phases
        phase        = 'Gas',      phase_number = 1,
        component(1) = 'CH4',      component_number(1) = 1,
        component_diffusivity(1) = 1.0d-05,  ! (m2/s) ! Diffusivity of component 1 in phase 1
        component(2) = 'H2O',      component_number(2) = 2,
        component_diffusivity(2) = 1.0d-05,  ! (m2/s) ! Diffusivity of component 2 in phase 1
        component(3) = 'NaCl',     component_number(3) = 3,
        component_diffusivity(3) = 0.0d-00   ! (m2/s) ! Diffusivity of component 3 in phase 1
        /
```

Figure 4.1. The **`DIFFUSION`** data block, with examples of the `Diffusion_Key_Parameters` and `Component_Diffusivities_in_Phases` namelists

PAGE LEFT INTENTIONALLY BLANK

5. Outputs

In this section, the various primary and secondary variables that may be provided as outputs from **T+H** v1.5 simulations are discussed. Such outputs are provided in the following cases:

- In the standard **T+H** v1.5 output as an ASCII file either at selected times (defined in the data blocks `TIMES`), or at a given timestep frequency (defined by the variable `PRINT_frequency` in the data block `PARAM`, see *Moridis* [2014]). The standard output provides information on all elements and connections in the grid of the system.
- In an output file named **`Plot_Data_Elem`**, which stores the element-specific properties and parameters in a format that conforms to the requirements of the TecPlot package [*TecPlot*, 2003], and is suitable for most other plotting and graphing packages. This file is printed when the variable `MOP(19)=8` for `9` in

the data block `PARAM` and provides information on all elements of the domain (see *Moridis* [2014]). Note that for `MOP(19)=9`, the plotting file and a truncated standard output file are produced (listing only mass balances at the prescribed printout times).

- In output files named after each of the subdomains, interfaces or groups of sinks and sources (wells) defined in the data blocks `SUBDOMAINS`, `INTERFACES` and `SS_GROUPS`, respectively. These files provide time series of relevant data at a frequency determined by the input parameter `TimeSeries_frequency` in the in the data block `PARAM` (see *Moridis* [2014]).

5.1. The Standard Outputs

The standard output of the **T+H** v1.5 code provides the following output:

1. The pressure, temperature, phase saturations, CH_4 partial pressure, H_2O vapor pressure, hydration equilibrium pressure and inhibitor mass fraction in all elements of the domain.

2. The mass fractions of CH_4 in the gas and aqueous phases, phase densities and viscosities, porosities, capillary pressure and relative permeabilities to the mobile phases.

3. The flows and velocities of the phases through the element interfaces (connections) of the domain; the corresponding flows of CH_4 in the mobile phases (i.e., aqueous and gas), and the heat flow; the diffusive flows (if accounting for diffusion).

4. The primary variables and their changes in the elements of the domain.

5. The phase enthalpies, the dissociation reaction rates and the corresponding heat of dissociation, the temperature shift (when inhibitors are involved), the intrinsic permeabilities and the permeability-reduction factor in the presence of solid phases (if the EPM model is used, see *Moridis* [2014]) in all elements of the domain.

6. Source and sink (well) information, including: mass and enthalpy rates, mobile phase mass fractions in the injection/production stream, CH_4 and H_2O mass flow rates in the mobile phases.

7. Volume and mass balances of the phases and components in the domain.

All the units of the various parameters are listed in the standard output file. Of the possible outputs, (1), (2), (6) and (7) are always printed in the standard **T+H** output. The amount of the additional output is controlled by the parameter `OutputOption` in the data block `PARAM`. Thus, (3) is printed in addition when `OutputOption = 2`, and a complete data set (items 1 to 7) is printed when `OutputOption = 3`. In keeping with the TOUGH2 [Pruess et al., 1999] and TOUGH + convention [*Moridis*, 2014], printouts occur after each iteration (not just after convergence) if the `OutputOption` values are increased by 10.

For `MOP(19)>7`, the **`Plot_Data_Elem`** file includes the following information: the coordinates of each element center in the domain, and the corresponding pressure, temperature, phase saturations, relative permeability of the mobile (aqueous and gas) phases, the capillary pressure, the inhibitor mass fraction, permeability, porosity and the permeability-reduction factor in the presence of solid phases (meaningful only if the EPM model is invoked, see *Moridis* [2014]).

T+H v1.5 also provides as a standard output a time series describing the evolution of the gas hydrate mass and its formation/dissociation reaction in the entire domain during the simulation. The data are written at a frequency defined by the parameter `TimeSeries_frequency` to a file named **`Hydrate_Status`**, and include (a) time, (b) mass rate of gas release or reaction, (c) volumetric rate of gas release or reaction, (d) cumulative mass of the released gas, (e) cumulative volume of the released gas, (f)

cumulative volume of the free gas in the domain, and (g) remaining mass of hydrate in the reservoir. All the units of the various listed parameters are listed in the headings of the output file.

5.2. Time Series Outputs

Time series outputs are obtained when the data blocks `SUBDOMAINS`, `INTERFACES` and `SS_GROUPS` are included in the **T+H** v1.5 input files. Thus, individual output files are created for each one of the subdomains identified in `SUBDOMAINS` (see detailed discussion in *Moridis* [2014]), and there the following data are written with a frequency defined by the parameter `TimeSeries_frequency`:

- The subdomain pore volume, and pore-volume averaged pressure, temperature, and gas saturation in the subdomain.
- The mass of each of the phases and of the inhibitor (if present).
- The mass of CH4 in the aqueous and the gas phase.

Similarly, individual output files are created for each one of (a) the interfaces identified in `SUBDOMAINS` and (b) the source/sink (well) groups identified in `SS_GROUPS` (see detailed discussion in *Moridis* [2014]), and there the following data are written with a frequency defined by the parameter `TimeSeries_frequency`:

- The mass flow rate of the mobile (aqueous and gas) phases across the interface or through the source/sink group, as well as the corresponding CH_4 and H_2O flows in each of the mobile phases, the inhibitor flow and the heat flow.

- The cumulative mass of each of the mobile (aqueous and gas) phases that flowed across the interface or through the source/sink group since the beginning of the simulation, as well as the corresponding mass of CH_4 and H_2O in each of the mobile phases and the inhibitor mass.

All the units (SI) of the various listed parameters are listed in the headings of the output file.

PAGE LEFT INTENTIONALLY BLANK

6.0. Example Problems

6.1. Example Files and Naming Conventions

The files corresponding to the examples discussed in this manual can be found in the directory **`T+H_V1.5`** on the USB memory stick accompanying this manual. The input files of the example problems have the general name `Test_XXX` (where `XXX` is an identifier) and are the following:

1. `Test_1T`
2. `Test_1Tk`
3. `Test_1P`
4. `Test_1Pk`
5. `Test_1P_ice`
6. `Test_1TbS`
7. `Test_1TbSk`
8. `Test_1TSk`
9. `Test_2Qp`
10. `Test_3T`
11. `Test_3Qp`
12. `Test_3Qpk`
13. `Test_RadH1`

14. `Test_2D`

The corresponding output files are also included in the directory **`T+H_V1.5`** on the accompanyingUSB memory stick. The naming convention of the generic TOUGH+ output files involves the suffix **`".out"`** at the end of the input file name. The hydrate-specific output files have the general name **`Hydrate_Status_XXX`**, where **`XXX`** is the identifier of the input file name.

For some examples in which the hydration reaction (dissociation or formation) is induced by boundary conditions, the additional output files of the time series at the boundary connection are included under the general name **`Int_1_Series_XXX`**. Similarly, if the hydration reaction is induced by sources or sinks, the corresponding additional output file of the time series of the conditions at the sinks and/or sources is included in the directory **`T+H_V1.5`** under the name **`Wells_Series_XXX`**.

6.2. Problem Test_1T: Thermal Stimulation, Equilibrium Dissociation, No Inhibitor

This 1-D problem is designed to demonstrate the basic concepts of hydrate dissociation by means of thermal stimulation. Note that it is practically impossible to separate the thermal and pressure processes in the course of dissociation, regardless of the dissociation method. As hydrate dissociates in thermal stimulation, gas evolves and accumulates in porous media, leading to pressure increases immediately ahead of the hydrate interface that shift the hydrate toward the stability zone. Conversely, depressurization is a very effective method of hydrate dissociation, the endothermic

nature of which results in rapid temperature drop and enhanced stability of the remaining hydrate.

For convenience, the input file is listed in **Figure 6.1**. As an exercise, a novice user is urged to identify the various variables and parameters in the input file.

The 1-m long domain (represented by 10 active cells of uniform Δx = 0.1 m size) is a pressurized and thermally insulated column of a porous medium, in which hydrate and water coexist at a pressure of 4.0×10^6 Pa and T = 1.2 ^{o}C, i.e., well within the hydrate stability zone. At a time t = 0, the boundary at x = 0 becomes permeable and the column comes in contact with warm water at a temperature of T_b = 45 ^{o}C. As the temperature in the column increases, hydrate dissociation is expected to occur, leading to the evolution of gas, which will then escape the column by flowing through the high-temperature boundary. Note that the pressure in the high-temperature boundary is equal to the initial one in the column, thus allowing escape of the pressurized gas. In this simulation, the hydrate dissociation reaction is assumed to occur at equilibrium. Under these conditions, dissociation is limited and controlled by heat transfer issues.

The porous medium has a porosity ϕ = 0.3, and a permeability $k = 2.96 \times 10^{-13}$ m^2 (= 30 mD in oilfield units). In the presence of the ice and hydrate solid phases, the critical mobile porosity (i.e., the "free" porosity - not occupied by solids - below which the medium becomes impermeable) is 0.05, and the porosity reduction exponent is 3.

Note that a non-zero (and relatively significant) pore compressibility (=10^{-8} 1/Pa) is assigned to the porous medium. This is necessary in hydrate simulations, in which evolution of solid phases of lower density (such as ice and hydrate) can lead to extraordinarily high pressures as the aqueous phase disappears if pore compressibility is

small. In this illustrative example, the thermal conductivity (=3.1 W/m/K) is relatively large, but was given this value to enhance heat conduction (the main heat transfer mechanism from the high-temperature boundary).

The hydrate properties and the type of the reaction are listed in the `HYDRATE` data block. The thermal conductivity, specific heat and density of the CH_4 hydrate are from data in *Sloan* [1998], and are constants because no information is available on their dependence on temperature and/or pressure. However, **T+H** assumes that the constant input density of the CH_4 hydrate is that at the quadruple point, and the hydrate density in the simulations is internally adjusted by assuming that its compressibility and thermal expansivity are the same as those of ice (as calculated within TOUGH+). The inhibitor data correspond to the properties of NaCl.

`Test_1T.out`, the standard TOUGH+ output corresponding to the input file **`Test_1T`**, can be found in the directory **`T+H_V1.5`** on the USB memory stick accompanying this manual. Because `MOP(5) = 3`, the output includes detailed messages about the evolution of the residuals during the Newtonian iterations at each time step, as well as about phase changes occurring during the course of the simulations. Because `OutputOption = 3`, a full output is obtained that provides a very detailed list of the conditions, parameters and thermophysical properties of the system at each cell and at each connection. Thus, the output describes the pressure, temperature, phase saturation, partial CH_4, H_2O-vapor pressure, equilibrium hydration pressure, inhibitor mass fraction in the aqueous phase, CH_4 concentrations in the aqueous and gas phases, phase densities, porosity, capillary pressure, relative permeability of the gas and aqueous phases, heat and fluid fluxes, mobile phase velocities, CH_4 fluxes in the aqueous and gas

phases, primary variables and their changes, phase enthalpies, rate of the hydration reaction, heat of the hydration reaction, and the temperature shift in the hydrate P-T equilibrium caused by the presence of the inhibitor. Additionally, the output provides mass and volume balances of the phases, component mass balances, and component distribution into the phases.

The results in the portion of the output in the **`Test_1T.out`** file (see directory **`T+H_V1.5`**) are consistent with the expected system response. The hydrate dissociation front is observed to move deeper into the column with time, and is in the eighth cell at the end of the simulation period (55th timestep). As temperature increases, hydrate begins to dissociate (see the gradual hydrate saturation decline and eventual disappearance in the warming cells, along with an emerging and then increasing gas saturation). The maximum pressure is observed at the dissociation front, indicated by the first incidence of coexistence of aqueous, gas and hydrate phases in a cell (and immediately ahead of a cell from which all hydrate has disappeared). This higher pressure is caused by the gas evolution in response to hydrate dissociation, and leads to formation of additional hydrate (indicated by higher hydrate saturations and a positive hydrate reaction rate) in the cell immediately in front of the one that contains the dissociation front. As expected, the gas fluxes indicate gas flow toward the high-temperature permeable boundary. Note that, because the maximum pressure occurs at the hydrate dissociation front, gas flows in both directions from the cells that contain the hydrate interface. Comparison of the partial pressure of CH_4 to the hydrate equilibrium pressure confirms that dissociation occurs at equilibrium.

The additional output file **`Hydrate_Status_1T`** (also listed in the directory **`T+H_V1.5`**) provides a measure of the cumulative dissociation behavior in the entire system, as opposed to that in individual cells (described in the standard TOUGH+ output). This output file features self-explanatory headings, and includes the instantaneous cumulative rates of CH_4 gas evolution from hydrate (expressed as mass rates or standard volume rates), as well as the corresponding cumulative amount (in terms of total mass and total standard volume) of hydrate-originating CH4. Thus, it provides a measure of the overall performance of the hydrate-bearing system as a gas production source. Negative rates and masses/volumes indicate hydrate generation. Note that the results in any **`Hydrate_Status`** output indicate conditions and response within the accumulations, and do not necessarily reflect behavior and performance at the production well. Thus, for successful exploitation of a hydrate accumulation, significant CH4 volumes must be released through dissociation within the deposit, but the gas must also be able to be removed from the system through an appropriate collection (i.e., well) facility.

```
"Test1" ... Hydrate dissociation, thermal stimulation
MEMORY
'HYDRATE-EQUILIBRIUM'
   2     3    4    .FALSE.                    ! NumCom, NumEqu, NumPhases, binary_diffusion
'Cartesian'   15   30    5  .FALSE.  .FALSE.
   2                                           ! MaxNum_SS
   2                                           ! MaxNum_Media
.FALSE.  .FALSE.  .FALSE.  'Saturation'
.FALSE.  'Continuous'
.FALSE.  ' '  'Continuous'  0   ! coupled_geomechanics, geomechanical_code_name, property_update, num_geomech_param
ROCKS----1----*----2----*----3----*----4----*----5----*----6----*----7----*----8
DIRT1    1     2.6e3       .30  2.96E-13  2.96E-13  2.96E-13       3.1     1000.
     1.e-8               0.5e0                                  5.0e-2     3.0e0
BOUND    0     2.6e3     0.0e0  0.00E-13  0.00E-13  0.00E-13     1.0e2     1000.

HYDRATE--1----*----2----*----3----*----4----*----5----*----6----*----7----*----8
     1                        ! HCom%NCom
'CH4'  6.0d0 1.00d00          ! Name, hydration number, mole fraction in composite hydrate
     1                        ! Number of coefficients in thermal conductivity polynomial
  4.5e-1                      ! Coefficients in the thermal conductivity polynomial
     1                        ! Number of coefficients in the specific heat polynomial
  2.1e03                      ! Coefficients in the specific heat polynomial
     1                        ! Number of coefficients in density polynomial
  9.2e02                      ! Coefficients in the density polynomial
.FALSE.                       ! inhibitor_present,T_MaxOff,C_MaxOff,MW_Inhib,D_Inhib,H_InhSol,DifCo_Inh
2                             ! F_EqOption
'EQUILIBRIUM'                 ! Type of dissociation
START----1----*----2----*----3----*----4----*----5----*----6----*----7----*----8
----*----1 MOP: 123456789*123456789*1234 ---*----5----*----6----*----7----*----8
PARAM----1----*----2----*----3----*----4----*----5----*----6----*----7----*----8
   3 080     01010003004002000400003111   0.00E-5
            2.200E+5     1.0e2   8.64E+4              9.8060
     1.E-5     1.E00                                  1.0e-8            AqH
            4.000e6               0.5e0                1.20
ELEME
A00 1              10.1000E+000.4000E+00          0.5100E-01-.5000E+00-.5000E+00
A00 2              10.1000E+000.4000E+00          0.1510E+00-.5000E+00-.5000E+00
A00 3              10.1000E+000.4000E+00          0.2510E+00-.5000E+00-.5000E+00
A00 4              10.1000E+000.4000E+00          0.3510E+00-.5000E+00-.5000E+00
A00 5              10.1000E+000.4000E+00          0.4510E+00-.5000E+00-.5000E+00
A00 6              10.1000E+000.4000E+00          0.5510E+00-.5000E+00-.5000E+00
A00 7              10.1000E+000.4000E+00          0.6510E+00-.5000E+00-.5000E+00
A00 8              10.1000E+000.4000E+00          0.7510E+00-.5000E+00-.5000E+00
A00 9              10.1000E+000.4000E+00          0.8510E+00-.5000E+00-.5000E+00
A0010              10.1000E+000.4000E+00          0.9510E+00-.5000E+00-.5000E+00
ina
A00 0              10.1000E-020.4000E-02          0.5000E-03-.5000E+00-.5000E+00

CONNE
A00 0A00 1                   10.5000E-030.5000E-010.1000E+01
A00 1A00 2                   10.5000E-010.5000E-010.1000E+01
A00 2A00 3                   10.5000E-010.5000E-010.1000E+01
A00 3A00 4                   10.5000E-010.5000E-010.1000E+01
A00 4A00 5                   10.5000E-010.5000E-010.1000E+01
A00 5A00 6                   10.5000E-010.5000E-010.1000E+01
A00 6A00 7                   10.5000E-010.5000E-010.1000E+01
A00 7A00 8                   10.5000E-010.5000E-010.1000E+01
A00 8A00 9                   10.5000E-010.5000E-010.1000E+01
A00 9A0010                   10.5000E-010.5000E-010.1000E+01
A0010A0011                   10.5000E-010.5000E-030.1000E+01

RPCAP----1----*----2----*----3----*----4----*----5----*----6----*----7----*----8
    9           .120       .02        3.
    7        0.45000   1.10e-1   8.0E-05      1.E6     1.0e0

INTERFACES----*----2----*----3----*----4----*----5----*----6----*----7----*----8
&Interface_General_Info  number_of_interfaces = 1 /
   &Individual_Interface_Specifics  interface_name         = 'Int_1',
                                    number_of_surfaces     = 1,
                                    sign_of_flow_direction = 'DIR'
                                    /
      &Surface_Specifics  definition_mode       = 'NameList',
                          number_of_connections = 1,    ! Range (min and max) along the first coordinate axis
                          format_to_read_data = '*',
                          /
'A00 0A00 1'


GENER


INCON----1----*----2----*----3----*----4----*----5----*----6----*----7----*----8
A00 0           0.30000000E+00  Aqu
            4.000e6              00.0e0               45.00

ENDCY----1----*----2----*----3----*----4----*----5----*----6----*----7----*----8
```

Figure 6.1. Input file for example problem Test_1T (in Section 6.2) involving thermal stimulation, equilibrium dissociation, and no inhibitor.

6.3. Problem Test_1Tk: Thermal Stimulation, Kinetic Dissociation, No Inhibitor

This 1-D problem is entirely analogous to that discussed in `Test_1T`, from which it differs only in that hydrate dissociation is not treated as an equilibrium reaction but as a kinetic reaction. For convenience, the input file **`Test_1Tk`** is listed in **Figure 6.2**. It can be seen that the inputs are identical, with the exception of parameters and values describing the kinetic nature of the reaction.

Because a kinetic reaction confers an additional degree of freedom, the number of mass components `NumCom` increases by one to `NumCom = 3` (the hydrate is now a mass component in addition to being a solid phase, see discussion in Section 2.2). Consequently, the number of equations per cell increases by one to `NumEqu = 4`, the number of primary variables describing initial conditions (in data blocks `PARAM` and **`INCON`**) increases by one, and the corresponding Jacobian matrix is larger than the one in problem **`Test_1T`**. As an exercise, a novice user is urged to identify the primary variables in this input file, and to differentiate them from those in the input file **`Test_1T`**.

Both the `EOS_Name` heading in the `MEMORY` block (record `MEMORY.2)`, and in the `Reaction_Type` variable in the `HYDRATE` data block (record `HYDRATE.11)` indicate that this is kinetic system. The values of the kinetic parameters of the hydration reaction (i.e., intrinsic reaction rate and the activation energy) were obtained from *Kim et al.* (1987), and *Clarke and Bishnoi* [2002]. The area adjustment factor (variable `Area_Factor` in record `HYDRATE.12` (also see equation 2.6) was assumed to be equal to one.

The interested user is directed to the directory **T+H_V1.5** for review of the standard TOUGH+ output, as well as of the additional **Hydrate_Status_1Tk** and **Int_1_Series_1Tk** output files. Upon inspection, a general observation that can be made is that this is a more difficult problem to solve, and that it takes more timesteps to cover the simulation period than in problem **Test_1T**. A reason for the slower time advance is the kinetic hydrate dissociation, which imposes limits on the time step size.

The results of the illustrative problems in **Test_1T** and **Test_1Tk** are compared in **Figures 6.3** to **6.6**. It should be noted that the results of these two simulations are affected by the relatively coarse discretization in the two simple systems, but conclusions drawn from the relative performance are valid and provide a robust perspective in the evaluation of such simulation results.

Figure 6.3 shows the cumulative rates of CH_4 release from the dissociation of hydrate in the columns of problems **Test_1T** and **Test_1Tk**. The effect of the relatively coarse discretization is evident in the oscillatory nature of the curves of rate evolution over time. An increase in the rate of CH_4 release is a direct consequence of faster dissociation, which leads to a localized increase in pressure (caused by the evolving gas and the resistance to flow posed by the porous medium) and a drop in temperature (caused by the endothermic nature of the hydrate reaction). The increase in pressure and temperature drop result in a subsequent reduction in the rate of dissociation until conduction and convection (of the advancing warm water) can raise the temperature and accelerate dissociation. The result of this sequence of events is the (roughly) periodic nature of the rate curve (involving the repetition of a similar pattern), which is substantially affected by the size of the cells. Thus, each of the four distinct patterns in

Figure 6.3 corresponds to a different cell, and represents the advance of the hydrate dissociation front through that cell at the time of observation.

A significant observation that can be drawn from **Figure 6.3** is that the equilibrium and kinetic rates are different (with the kinetic rate lower) when the dissociation front first moves into a cell, but practically coincide afterwards. However, at the very beginning of the simulation, a burst of very rapid gas release is observed in the case of kinetic dissociation. This pattern of behavior is consistent with expectations because the maximum deviation between kinetic and equilibrium predictions is anticipated to occur at the maximum deviation from equilibrium. This is followed by equilibrium dissociation along the L+G+W phase boundary. The coincidence of the kinetic and equilibrium rates indicates that equilibrium is established very rapidly, as dictated by the relatively fast intrinsic dissociation rate and the high temperature. In cases of thermal stimulation involving high temperatures, equilibrium and kinetic dissociation models are expected to give very similar results (in terms of overall gas release from the hydrate) because (a) the high intrinsic reaction rate does not pose a kinetic limitation on the reaction, and (b) the reaction rate is dominated by heat transfer issues.

In **Figure 6.4**, the cumulative gas volumes released from the hydrate in the two problems are very similar, and confirm the observations from the discussion on the rates. The discretization effects are evident in the distinctly "segmented" appearance of the curves, which exhibit "bumps" corresponding to the periodic rate patterns in **Figure 6.3**. Note that **Figures 6.3** and **6.4** were plotted using the data from the output files **`Hydrate_Status_1T`** and **`Hydrate_Status_1Tk`**.

In problems **`Test_1T`** and **`Test_1Tk`**, gas is produced as it escapes into the warm water across the $x = 0$ boundary. **Figures 6.5** and **6.6** (based on data from the **`Int_1_Series_1T`** and **`Int_1_Series_1Tk`** output files) show the volumetric production rate of CH_4 and the cumulative CH_4 production. In these two examples, all the CH_4 originates from the dissociation of the hydrate because no 'free' CH_4 was initially present in the system. **Figure 6.5** shows the same periodic pattern observed in **Figure 6.3**, denoting the effect of discretization. The CH_4 production rates (i.e., the fluxes across the $x = 0$ boundary) are initially the same, but then the kinetic rate decreases (relative to the equilibrium rate). This difference occurs as the hydrate dissociation front is about to move into an adjacent cell. The cumulative effect is reflected in the total gas production (shown in **Figure 6.4**, and measured as the total CH_4 volume that crosses the $x = 0$ boundary), which indicates lower gas production for kinetic dissociation. The effect of discretization is apparent in the "segmented appearance" of the gas production curves, which correspond directly to the periods in the production rates in **Figure 6.5**.

```
"Test_1Tk" ... Kinetic hydrate dissociation, thermal stimulation
MEMORY
'HYDRATE-KINETIC'
   3     4    4    .FALSE.                    ! NumCom, NumEqu, NumPhases, binary_diffusion
'Cartesian'   15   30    5  .FALSE.  .FALSE.
   2                                           ! MaxNum_SS
   2                                           ! MaxNum_Media
.FALSE.  .FALSE.  .FALSE.  'Saturation'
.FALSE.  'Continuous'                ! coupled_geochemistry, property_update [= 'Continuous', 'Iteration', 'Timestep']
.FALSE.  ' '  'Continuous'  0        ! coupled_geomechanics, geomechanical_code_name, property_update, num_geomech_par
ROCKS----1----*----2----*----3----*----4----*----5----*----6----*----7----*----8
DIRT1    1     2.6e3       .30  2.96E-13  2.96E-13  2.96E-13       3.1     1000.
     1.e-8              0.50e0                                   5.0e-2     3.0e0
BOUND    0     2.6e3     0.0e0  0.00E-13  0.00E-13  0.00E-13     1.0e2     1000.

HYDRATE--1----*-Modified Chlorobenzene data-*----5----*----6----*----7----*----8
     1                     ! HCom%NCom
'CH4'  6.0d0 1.00d00       ! Name, hydration number, mole fraction in composite hydrate
     1                     ! Number of coefficients in thermal conductivity polynomial
  4.5e-1                   ! Coefficients in the thermal conductivity polynomial
     1                     ! Number of coefficients in the specific heat polynomial
  2.1e03                   ! Coefficients in the specific heat polynomial
     1                     ! Number of coefficients in density polynomial
  9.2e02                   ! Coefficients in the density polynomial
.FALSE.                    ! inhibitor_present,T_MaxOff,C_MaxOff,MW_Inhib,D_Inhib,H_InhSol,DifCo_Inh
2                          ! F_EqOption
'KINETIC'                  ! Type of dissociation
8.1d4   3.6d4  1.0e-0      ! Activation energy, intrinsic rate constant, area factor
START----1----*----2----*----3----*----4----*----5----*----6----*----7----*----8
----*----1 MOP: 123456789*123456789*1234 ---*----5----*----6----*----7----*----8
PARAM----1----*----2----*----3----*----4----*----5----*----6----*----7----*----8
   3 080     01010003014002000040000311 1   0.00E-5
            2.200E+5    1.0e01   8.64E+4              9.8060
     1.E-5     1.E00                                  1.0e-8            AqH
            4.000e6               0.5e0                0.0e0                1.20
ELEME
A00 1              10.1000E+000.4000E+00          0.5100E-01-.5000E+00-.5000E+00
A00 2              10.1000E+000.4000E+00          0.1510E+00-.5000E+00-.5000E+00
A00 3              10.1000E+000.4000E+00          0.2510E+00-.5000E+00-.5000E+00
A00 4              10.1000E+000.4000E+00          0.3510E+00-.5000E+00-.5000E+00
A00 5              10.1000E+000.4000E+00          0.4510E+00-.5000E+00-.5000E+00
A00 6              10.1000E+000.4000E+00          0.5510E+00-.5000E+00-.5000E+00
A00 7              10.1000E+000.4000E+00          0.6510E+00-.5000E+00-.5000E+00
A00 8              10.1000E+000.4000E+00          0.7510E+00-.5000E+00-.5000E+00
A00 9              10.1000E+000.4000E+00          0.8510E+00-.5000E+00-.5000E+00
A0010              10.1000E+000.4000E+00          0.9510E+00-.5000E+00-.5000E+00
ina
A00 0              10.1000E-020.4000E-02          0.5000E-03-.5000E+00-.5000E+00

CONNE
A00 0A00 1                  10.5000E-030.5000E-010.1000E+01
A00 1A00 2                  10.5000E-010.5000E-010.1000E+01
A00 2A00 3                  10.5000E-010.5000E-010.1000E+01
A00 3A00 4                  10.5000E-010.5000E-010.1000E+01
A00 4A00 5                  10.5000E-010.5000E-010.1000E+01
A00 5A00 6                  10.5000E-010.5000E-010.1000E+01
A00 6A00 7                  10.5000E-010.5000E-010.1000E+01
A00 7A00 8                  10.5000E-010.5000E-010.1000E+01
A00 8A00 9                  10.5000E-010.5000E-010.1000E+01
A00 9A0010                  10.5000E-010.5000E-010.1000E+01
A0010A0011                  10.5000E-010.5000E-030.1000E+01

RPCAP----1----*----2----*----3----*----4----*----5----*----6----*----7----*----8
    9           .120       .02        3.
    7        0.45000   1.10e-1   8.0e-05      1.E6     1.0e0

INTERFACES----*----2----*----3----*----4----*----5----*----6----*----7----*----8
&Interface_General_Info  number_of_interfaces = 1 /
   &Individual_Interface_Specifics  interface_name         = 'Int_1',
                                    number_of_surfaces     = 1,
                                    sign_of_flow_direction = 'DIR'
                                    /
      &Surface_Specifics  definition_mode       = 'NameList',
                          number_of_connections = 1,
                          format_to_read_data = '*',
                          /
'A00 0A00 1'

GENER

INCON----1----*----2----*----3----*----4----*----5----*----6----*----7----*----8
A00 0           0.30000000E+00  Aqu
            4.000e6               0.0e0                0.0e0                45.00

ENDCY----1----*----2----*----3----*----4----*----5----*----6----*----7----*----8
```

Figure 6.2. Input file for example problem Test_1Tk (in Section 6.3) involving thermal stimulation, kinetic dissociation, and no inhibitor.

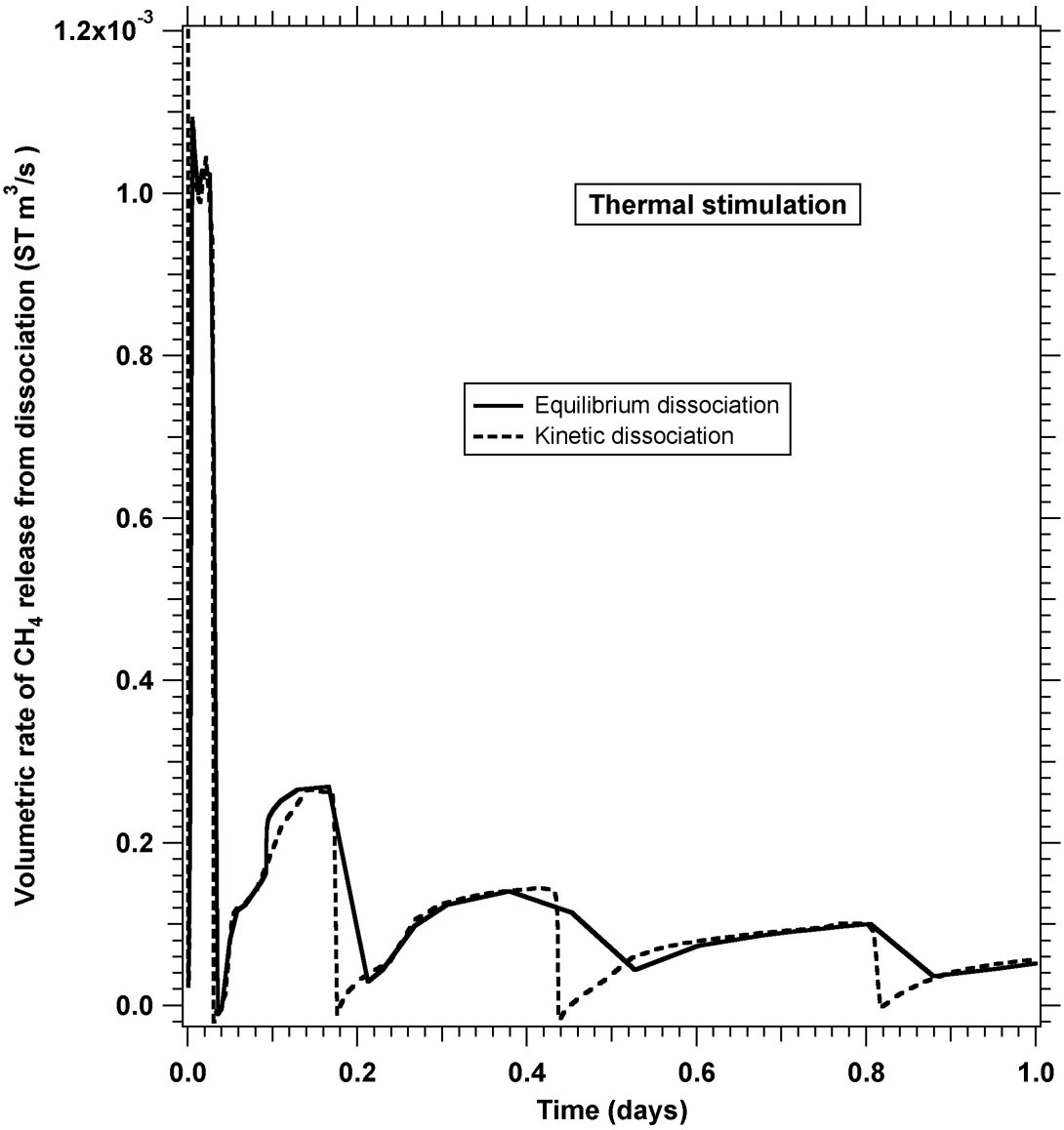

Figure 6.3. Comparison of the volumetric rates of CH_4 release from hydrate dissociation in problems `Test_1T` and `Test_1Tk`.

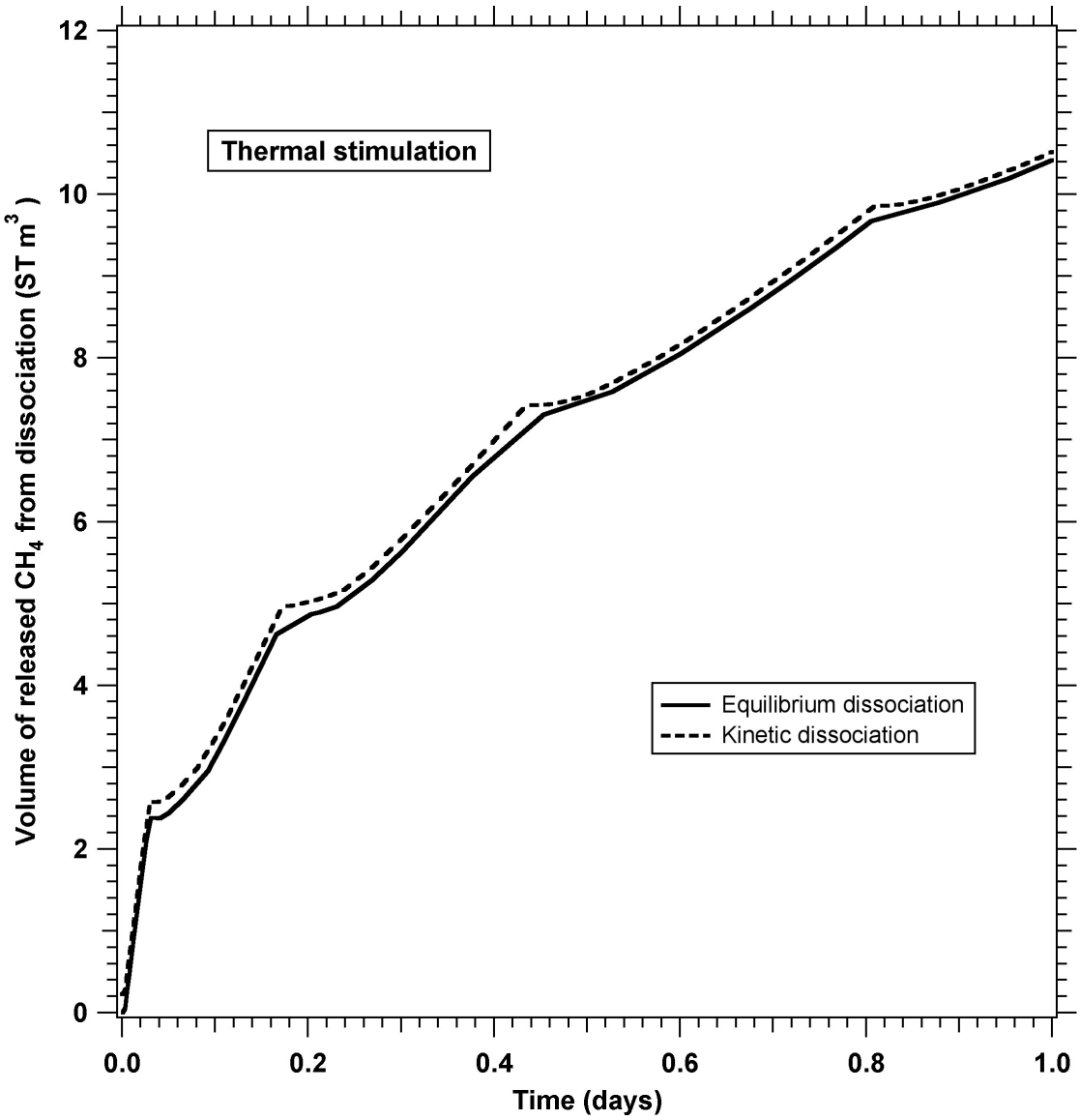

Figure 6.4. Comparison of the cumulative volumes of CH_4 released from hydrate dissociation in problems `Test_1T` and `Test_1Tk`.

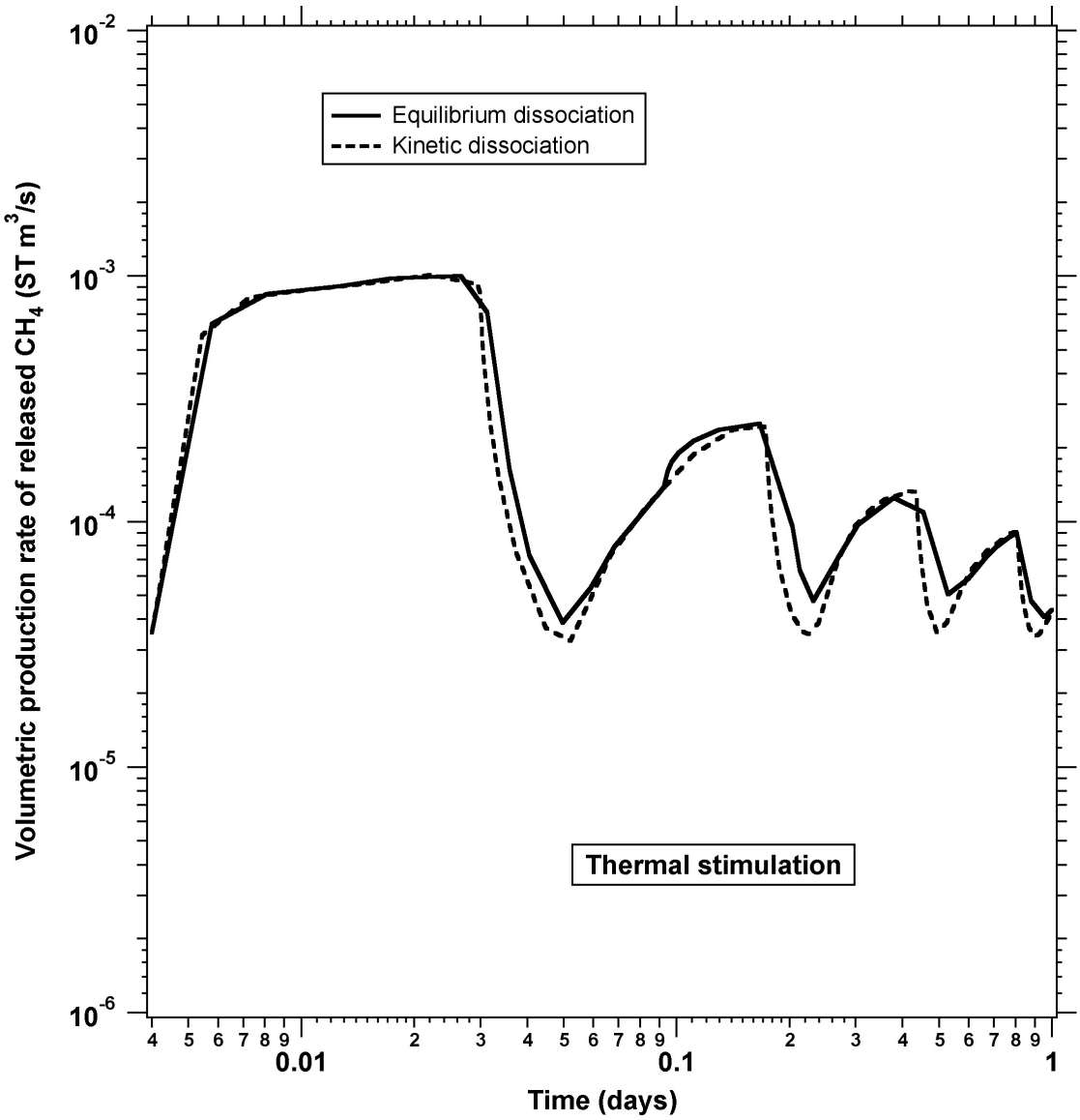

Figure 6.5. Comparison of the volumetric production rates of CH_4 (measured as the flux crossing the x = 0 boundary) in problems `Test_1T` and `Test_1Tk`.

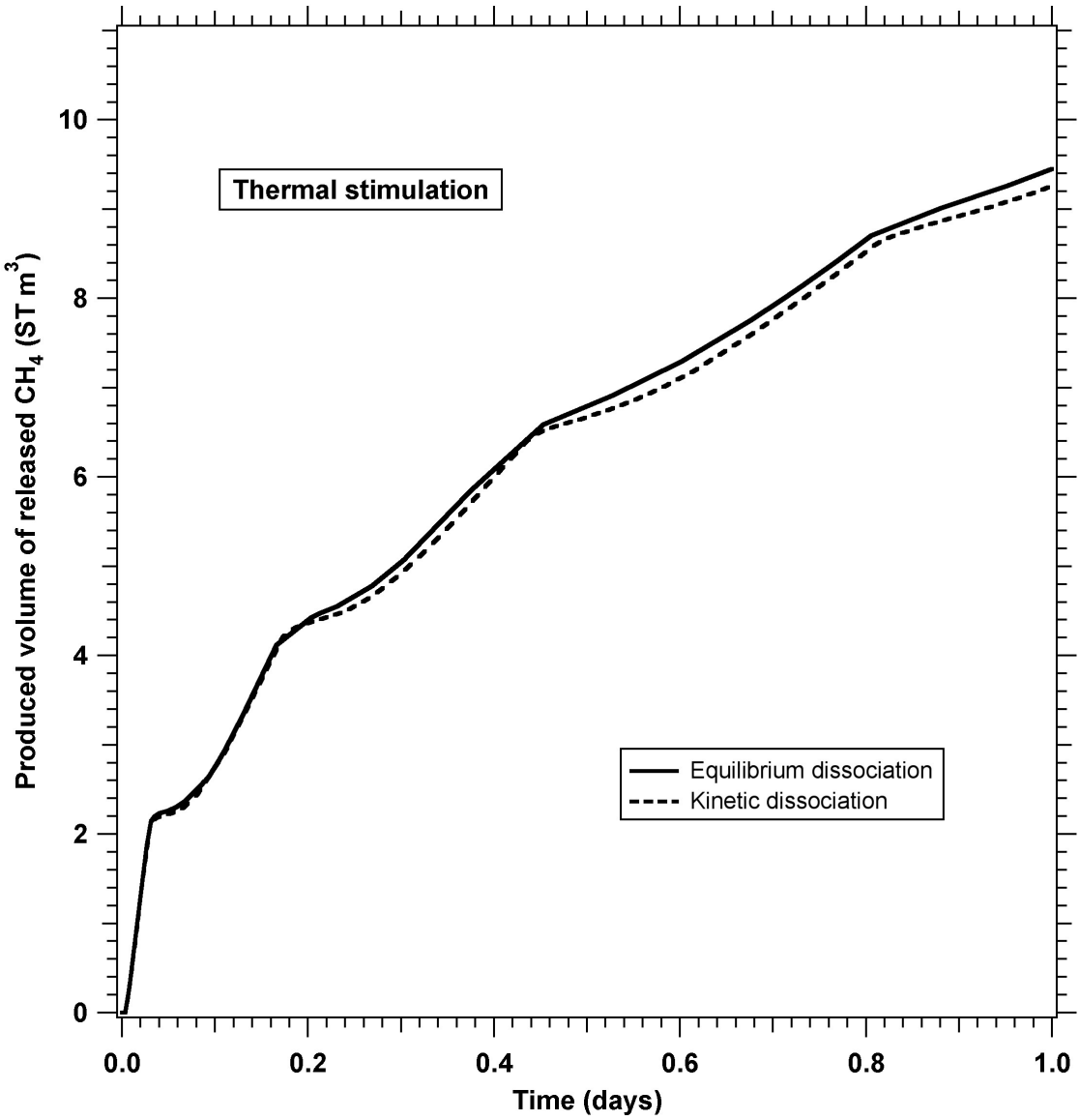

Figure 6.6. Comparison of the total production volumes of CH_4 (measured as the total volumes crossing the x = 0 boundary) in problems `Test_1T` and `Test_1Tk`.

6.4. Problems Test_1P: Depressurization, Equilibrium Dissociation, No Inhibitor

The only difference between the two-phase (hydrate and aqueous) 1-D problem in **`Test_1P`** and that discussed in **`Test_1T`** is in the boundary conditions at x = 0. Instead of a high-temperature permeable boundary (leading to thermal dissociation), the x = 0 boundary is now kept at a pressure of P_b = 2.7x10^6 Pa, which is lower than the initial pressure in the remainder of the column (P = 6x10^6 Pa). The pressure differential between the column and boundary and the non-zero permeability of the connection joining the two allow depressurization, which in turn induces dissociation. Note that the boundary pressure P_b is larger than the pressure at the quadruple point of CH_4-hydrate. This allows dissociation without reaching the quadruple point, which consequently keeps ice from forming. The constant boundary temperature of T_b = 1 ^{o}C is not expected to play a significant role in dissociation, despite its being above the melting point, because heat convection (fueled by fluid flow) is the main means of heat transfer, with conduction being a slow and inefficient process.

In the absence of an external heat source, the strongly endothermic reaction of hydrate dissociation is fueled by the heat provided by its surroundings. Consequently, temperature is expected to decline rapidly as dissociation proceeds.

The input file for the problem **`Test_1P`** appears in **Figure 6.7**. As an exercise, the novice user is asked to identify the differences between this file and the file **`Test_1T`**. The output files corresponding to this simulation (**`Test_1P.out`**, **`Hydrate_Status_1P`** and **`Int_1_Series_1P`**) can be found in the directory **`T+H_V1.5`** on the accompanying USB memory stick.

Review of the output files indicates that the evolution of temperature during dissociation conforms to expectations, exhibiting sharp and rapid declines. A very important observation is the much faster response of the hydrate to depressurization than to thermal stimulation. This difference in response was expected because of the very significant velocities at which the pressure and the temperature fronts propagate. The conclusion from these results (discussed more fully in Section 6.6) is that depressurization is a much more efficient hydrate dissociation process than thermal stimulation.

6.5. Problem Test_1Pk: Depressurization, Kinetic Dissociation, No Inhibitor

Hydrate dissociation is treated as a kinetic reaction in **`Test_1Pk`**. In all other respects, the problem is identical to that in `Test_1P`, as inspection of the input file in the directory **`T+H_V1.5`** readily reveals. The output files corresponding to this simulation(**`Test_1Pk.out`**, **`Hydrate_Status_1Pk`**, **`Int_1_Series_1Pk`**) can also be found in the same directory.

Review of the output files reveals a dissociation patterns with pressure, temperature and saturation distributions entirely analogous to those for the equilibrium dissociation problem. As in the case of thermal stimulation (see Section 6.3), kinetic hydrate dissociation results in substantially longer execution times and slower time advance in the simulations. This is caused by the more computationally intensive system, the larger (because of the additional degree of freedom) and more difficult-to-solve matrix, and by the parameters of kinetic dissociation that impose time step limitations. These results are more thoroughly discussed in Section 6.6.

```
 "Test_1P" ... Hydrate dissociation - depressurization
MEMORY
'HYDRATE-EQUILIBRIUM'
   2     3    4    .FALSE.           ! NumCom, NumEqu, NumPhases, binary_diffusion
'Cartesian' 15 30 5 .FALSE. .FALSE.  ! coordinate_system, Max_NumElem, Max_NumConx, ElemNameLength, active_conx_only,
   2                                 ! MaxNum_SS
   2                                 ! MaxNum_Media
.FALSE. .FALSE. .FALSE.            ! element_by_element_properties, porosity_perm_dependence, scaled_capillary_pressure
.FALSE.  'Continuous'              ! coupled_geochemistry, property_update [= 'Continuous', 'Iteration', 'Timestep']
.FALSE.  ' '  'Continuous'  0      ! coupled_geomechanics, geomechanical_code_name, property_update, num_geomech_param
ROCKS----1----*----2----*----3----*----4----*----5----*----6----*----7----*----8
DIRT1    1     2.6e3       .30  2.96E-13  2.96E-13  2.96E-13       3.1     1000.
     1.e-8              0.50e0                                  5.0e-2     3.0e0
BOUND    0     2.6e3     0.0e0  0.00E-13  0.00E-13  0.00E-13     1.0e2     1000.

HYDRATE--1----*----2----*----3----*----4----*----5----*----6----*----7----*----8
     1                       ! HCom%NCom
'CH4'  6.0d0 1.00d00         ! Name, hydration number, mole fraction in composite hydrate
     1                       ! Number of coefficients in thermal conductivity polynomial
  4.5e-1                     ! Coefficients in the thermal conductivity polynomial
     1                       ! Number of coefficients in the specific heat polynomial
  2.1e03                     ! Coefficients in the specific heat polynomial
     1                       ! Number of coefficients in density polynomial
  9.2e02                     ! Coefficients in the density polynomial
.FALSE.                      ! inhibitor_present,T_MaxOff,C_MaxOff,MW_Inhib,D_Inhib,H_InhSol,DifCo_Inh
2                            ! F_EqOption
'EQUILIBRIUM'                ! Type of dissociation
START----1----*----2----*----3----*----4----*----5----*----6----*----7----*----8
----*----1 MOP: 123456789*123456789*1234 ---*----5----*----6----*----7----*----8
PARAM----1----*----2----*----3----*----4----*----5----*----6----*----7----*----8
   3 080     00210003004002000400003000   0.00E-5
            8.640E+5    1.0e00   8.64E+6              9.8060
     1.E-5     1.E00                                  1.0e-8            AqH
            6.000e6              5.0e-1                7.20
ELEME
A00 1              10.1000E+000.4000E+00          0.5100E-01-.5000E+00-.5000E+00
A00 2              10.1000E+000.4000E+00          0.1510E+00-.5000E+00-.5000E+00
A00 3              10.1000E+000.4000E+00          0.2510E+00-.5000E+00-.5000E+00
A00 4              10.1000E+000.4000E+00          0.3510E+00-.5000E+00-.5000E+00
A00 5              10.1000E+000.4000E+00          0.4510E+00-.5000E+00-.5000E+00
A00 6              10.1000E+000.4000E+00          0.5510E+00-.5000E+00-.5000E+00
A00 7              10.1000E+000.4000E+00          0.6510E+00-.5000E+00-.5000E+00
A00 8              10.1000E+000.4000E+00          0.7510E+00-.5000E+00-.5000E+00
A00 9              10.1000E+000.4000E+00          0.8510E+00-.5000E+00-.5000E+00
A0010              10.1000E+000.4000E+00          0.9510E+00-.5000E+00-.5000E+00
ina                                                                          I
A00 0              10.1000E-020.4000E-02          0.5000E-03-.5000E+00-.5000E+00 I

CONNE
A00 0A00 1                   10.5000E-030.5000E-010.1000E+01
A00 1A00 2                   10.5000E-010.5000E-010.1000E+01
A00 2A00 3                   10.5000E-010.5000E-010.1000E+01
A00 3A00 4                   10.5000E-010.5000E-010.1000E+01
A00 4A00 5                   10.5000E-010.5000E-010.1000E+01
A00 5A00 6                   10.5000E-010.5000E-010.1000E+01
A00 6A00 7                   10.5000E-010.5000E-010.1000E+01
A00 7A00 8                   10.5000E-010.5000E-010.1000E+01
A00 8A00 9                   10.5000E-010.5000E-010.1000E+01
A00 9A0010                   10.5000E-010.5000E-010.1000E+01
A0010A0011                   10.5000E-010.5000E-030.1000E+01

RPCAP----1----*----2----*----3----*----4----*----5----*----6----*----7----*----8
    9           .120       .02        3.
    7        0.45000   1.10e-1   8.0E-05      1.E6     1.0e0
COFT -----1----*----2----*----3----*----4----*----5----*----6----*----7----*----8
A00 0A00 1


GENER


INCON----1----*----2----*----3----*----4----*----5----*----6----*----7----*----8
A00 0           0.30000000E+00  Aqu
            2.700e6              00.0e0                1.00


ENDCY----1----*----2----*----3----*----4----*----5----*----6----*----7----*----8
```

Figure 6.7. Input file for example problem Test_1Pk (in Section 6.4) involving depressurization, equilibrium dissociation, and no inhibitor.

6.6. Problem Test_1P_Ice: Thermal Stimulation, Kinetic Dissociation, No Inhibitor, Ice Evolution

The only difference between this problem and that in **`Test_1P`** is in the boundary pressure at x = 0. By setting P_b = 5x10^5 Pa, the boundary is kept at a pressure significantly lower than that at the quadruple point of CH_4-hydrate. The lower pressure is expected to lead to faster and larger CH_4 release because of the significantly larger pressure differential that drives dissociation, as well as to the emergence of ice as the system tends to the boundary pressure. Of particular interest are the consequences of ice on the relative permeability of gas. Unless properly managed, the emergence of ice can significantly reduce the pore space available to gas flow because ice has a lower density than the liquid water it replaces, and can adversely affect flow and gas production.

All the input and output files corresponding to the problem **`Test_1P_ice`** can be found in the directory **`T+H_V1.5,`** where the standard TOUGH+ output **`Test_1P_ice.out`** (showing the changes in the phase regimes during the simulation) is also located. From its original state on the L+H phase regime, the rapid depressurization induces CH_4-hydrate dissociation, gas emergence, and the appearance of the L+G+H regime. As depressurization and dissociation continue, ice evolves as the system reaches the quadruple point, where it remains at a constant pressure and temperature until the hydrate is exhausted. Afterwards, the A+I+G phase regime appears, during which pressure changes but the temperature remains constant because of the liquid water-ice coexistence, and equal to that of the triple point of water. Because the x=0 boundary is kept at a temperature above freezing, ice melts eventually, and an aqueous and gas system remains.

The results of the illustrative problems in problems **Test_1P**, **Test_1Pk** and **Test_1P_ice** are compared in **Figures 6.8** to **6.11**. It should be noted that relatively coarse discretization has an effect on the results, but appears less pronounced than in the case of thermal stimulation.

Figure 6.8 shows the cumulative rates of CH_4 release from the dissociation of hydrate. Unlike the case of thermal dissociation, both kinetic and heat transfer limitations can affect dissociation in depressurization-induced gas release from hydrates. This is demonstrated in **Figure 6.8**, which shows very different initial rate patterns for the equilibrium and the kinetic problems. After the initial a burst of very rapid gas release at the very beginning of the population (corresponding to the maximum deviation from equilibrium), the rate for kinetic dissociation at early times is substantially lower than that for equilibrium dissociation. The relationship is inversed at later times, and eventually the CH_4 release rates for kinetic and equilibrium dissociation become about the same as the entire system approaches equilibrium. As expected, the release rate of CH_4 from hydrate dissociation is substantially higher in problem **Test_1P_ice** because of the larger pressure differential. The higher dissociation rate leads to exhaustion of the hydrate at a much earlier time than in the other two problems, leading to zero release and denoted by the vertical segment of the curve at about t = 0.01 days.

In **Figure 6.9**, the cumulative gas volumes released from the hydrate in problems **Test_1P** and **Test_1Pk** are different at very early times, but become similar later. The cumulative gas rate for problem **Test_1P_ice** offers stark differences, and shows much larger volumes and exhaustion of the hydrate (marked by the flat part of the curve). The obvious implication is that, as long as potentially adverse relative permeability

effects can be avoided, enhanced depressurization provides faster rates and early gas recovery. Compared to the **Figures 6.3** and **6.4**, **Figures 6.5** and **6.6** convincingly demonstrate the superiority and efficiency of depressurization as a method of gas production from gas hydrates. Note that **Figures 6.8 and 6.9** were plotted using the data from the output files **`Hydrate_Status_XXX`**.

In these problems, gas is produced as it escapes into the low-pressure boundary at $x = 0$. **Figures 6.10** and **6.11** (based on data from the **`Int_1_Series_XXX`** output files) show the volumetric production rate of CH_4 and the cumulative CH_4 production. Because of the L+H initial regime, all the CH_4 originates from the dissociation of the hydrate. **Figure 6.10** shows that the CH_4 production rate (i.e., the fluxes across the $x = 0$ boundary) for kinetic dissociation lags behind that for equilibrium dissociation at a very early time, then exceeds it, and finally the two become roughly equal at later times. The production rate for the **`Test_1P_ice`** problem is significantly larger, and becomes zero at a very early time because no hydrate is left in the system (see the **`Int_1_Series_1P_ice`** file in the directory **`T+H_V1.5`**).

In **Figure 6.11**, the total gas production (measured as the CH_4 volume that crosses the $x = 0$ boundary) from the kinetic dissociation problem remains consistently lower than that for the equilibrium dissociation case, and the maximum deviation occurs at a very early time. Similarly to the pattern observed in **Figure 6.9**, gas production in the **`Test_1P_ice`** problem is significantly larger and leads to very early disappearance of the hydrate. A comparison of Figures **6.10** and **6.11** to the analogous ones for thermal stimulation (**Figures 6.5** and **6.6**) further confirm the superiority of depressurization as a dissociation strategy.

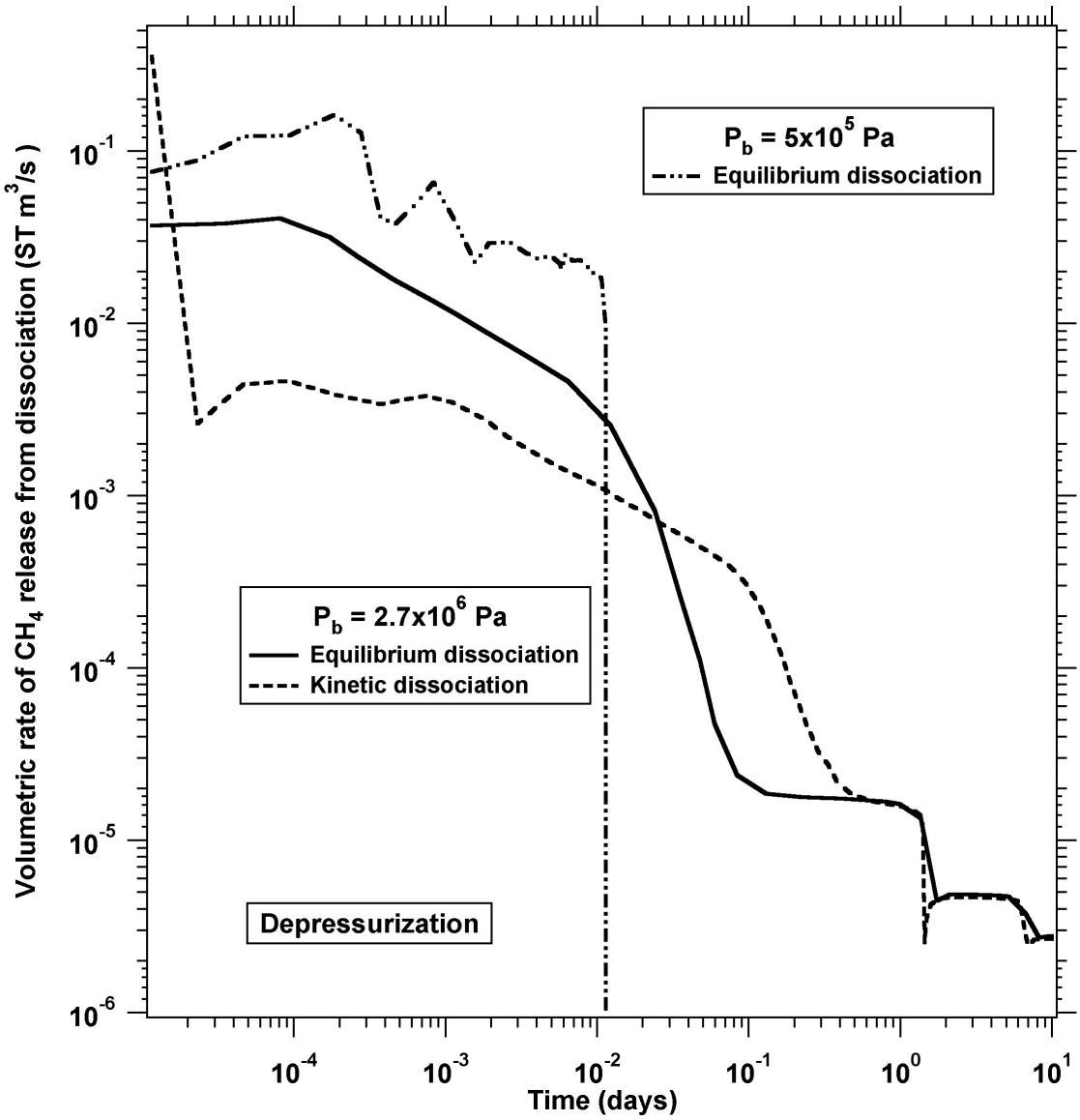

Figure 6.8. Comparison of the volumetric rates of CH_4 release from depressurization-induced hydrate dissociation in problems `Test_1P`, `Test_1Pk` and `Test_1P_ice`.

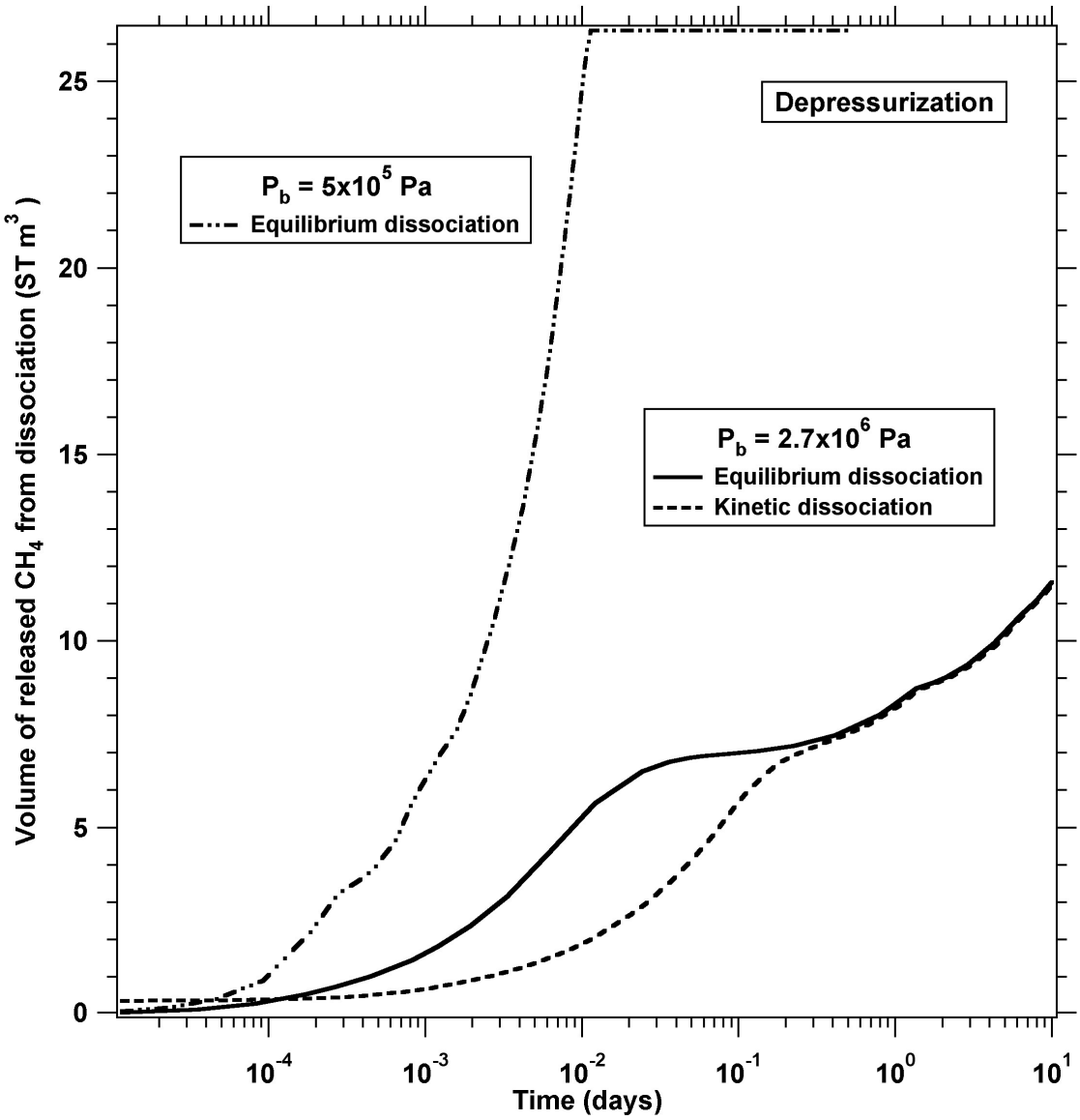

Figure 6.9. Comparison of the cumulative volumes of CH_4 released from depressurization-induced hydrate dissociation in problems `Test_1P, Test_1Pk` and `Test_1P_ice`.

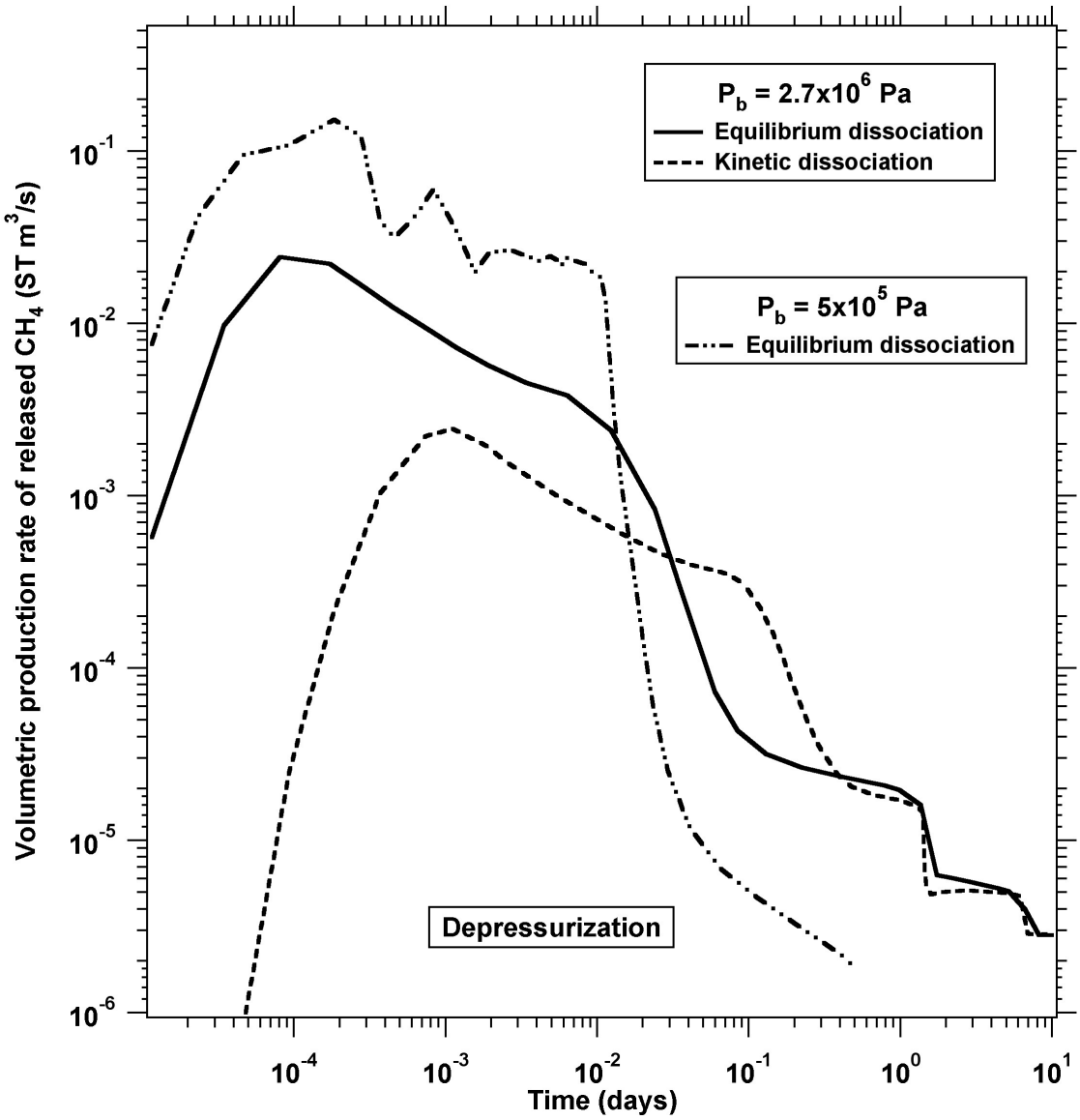

Figure 6.10. Comparison of the volumetric production rates of CH_4 (measured as the flux crossing the x = 0 boundary) in problems `Test_1P`, `Test_1Pk` and `Test_1P_ice`.

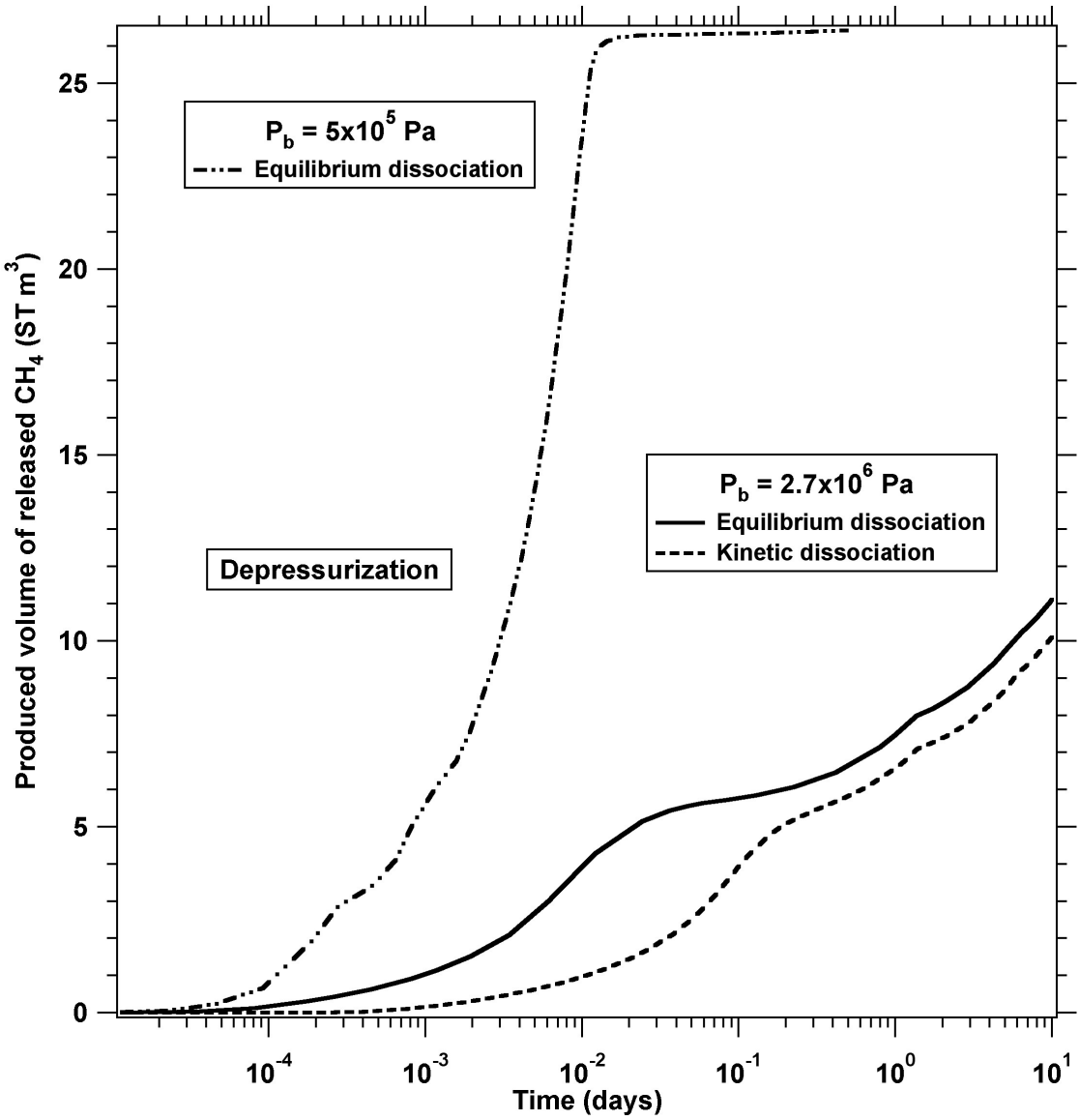

Figure 6.11. Comparison of the total production volumes of CH_4 (measured as the total volumes crossing the x = 0 boundary) in problems `Test_1P`, `Test_1Pk` and `Test_1P_ice`.

6.7. Problem Test_1TbS and Test_1TbSk: Hydrate Formation, Equilibrium and Kinetic Hydration Reaction, Inhibitor

The porous medium in 1-D columns in problems **`Test_1TbS`** and **`Test_1TbSk`** has the same properties as those reported in problem **`Test_1P`** (see Section 6.2), but the systems have different initial and boundary conditions. Because the pressure $P = 4\text{x}10^6$ Pa and temperature $T = 8.5$ ^{o}C are outside the stability zone of hydrate, the pore space is filled by a two-phase system involving a gas and an aqueous phase. The aqueous phase is a NaCl solution, in which the initial mass fraction of the salt is $X = 10^{-3}$. The column is attached to a constant pressure boundary at $x = L_{max}$ that can provide fluids to the active domain. The $x = 0$ boundary is impermeable, thermally conductive, and at a constant temperature of $T_b = 1.2$ ^{o}C. Because of conduction, the temperature in the column is expected to drop below the hydration temperature at the prevailing pressure, leading to the formation of hydrate. The temperature decline is somewhat buffered by the exothermic reaction of hydrate formation, and the formation process is affected by the presence of an inhibitor. In addition to the original equilibrium problem, a second case was investigated, in which the initial temperature was higher, with $T = 4.5$ ^{o}C. The lower initial T is expected to lead to earlier and faster hydrate formation.

An equilibrium hydrate reaction is assumed in problem **`Test_1TbS`**, while a kinetic hydrate reaction is assumed in **`Test_1TbSk`**. The input files and all the corresponding output files are available in the directory **`T+H_V1.5`**. The outputs corresponding to the lower initial T have the identifier '**`_1TbS2`**'. A review of the standard TOUGH+ output files clearly shows the evolution of hydrate. Of particular

interest is the increase in the inhibitor concentration as hydrate is formed. This is consistent with expectations because inhibitors cannot be partitioned into the solid hydrates. As in all previous kinetic cases, the kinetic treatment of the hydration equation results in longer execution times and slower advancement of the simulation time.

Figure 6.12 shows the cumulative rates of CH_4 consumption during hydrate formation. With the exception of results at very early times (when the rate corresponding to hydrate formation is larger because of maximum deviation from equilibrium), the CH_4 consumption rate for $T = 8.5\ ^{o}C$ are practically identical for both kinetic and equilibrium hydrate reaction. This was expected because the heat removal occurs through conduction, which is a very slow process and dominates the reaction. Additionally, the onset of hydrate evolution occurs at the same time for both cases.

The CH_4 consumption rate for the $T = 4.5\ ^{o}C$ equilibrium reaction case is significantly larger, and hydrate evolves at an earlier time. These results are reflected in **Figure 6.13**, which shows the cumulative CH_4 consumption during the formation process. The total volume of reacted CH_4 is the same for both the $T = 8.5\ ^{o}C$ kinetic and equilibrium reaction, while it is much larger for the $T = 4.5\ ^{o}C$ equilibrium reaction (i.e., the amount consumed is much lower).

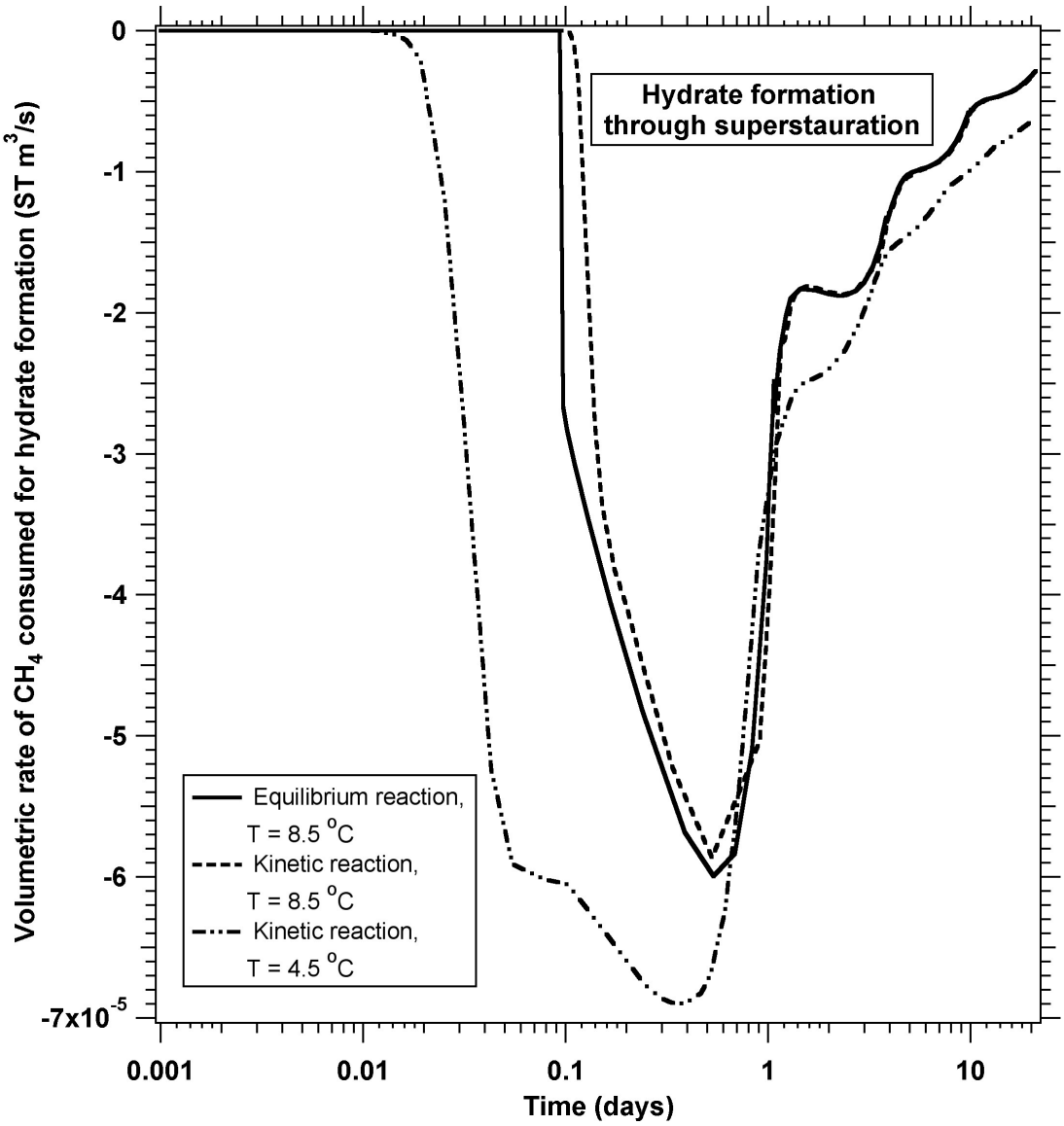

Figure 6.6. Comparison of the volumetric rates of CH_4 consumption during hydrate formation in problems `Test_1TbS`, `Test_1TbSk` and `Test_1TbS2`.

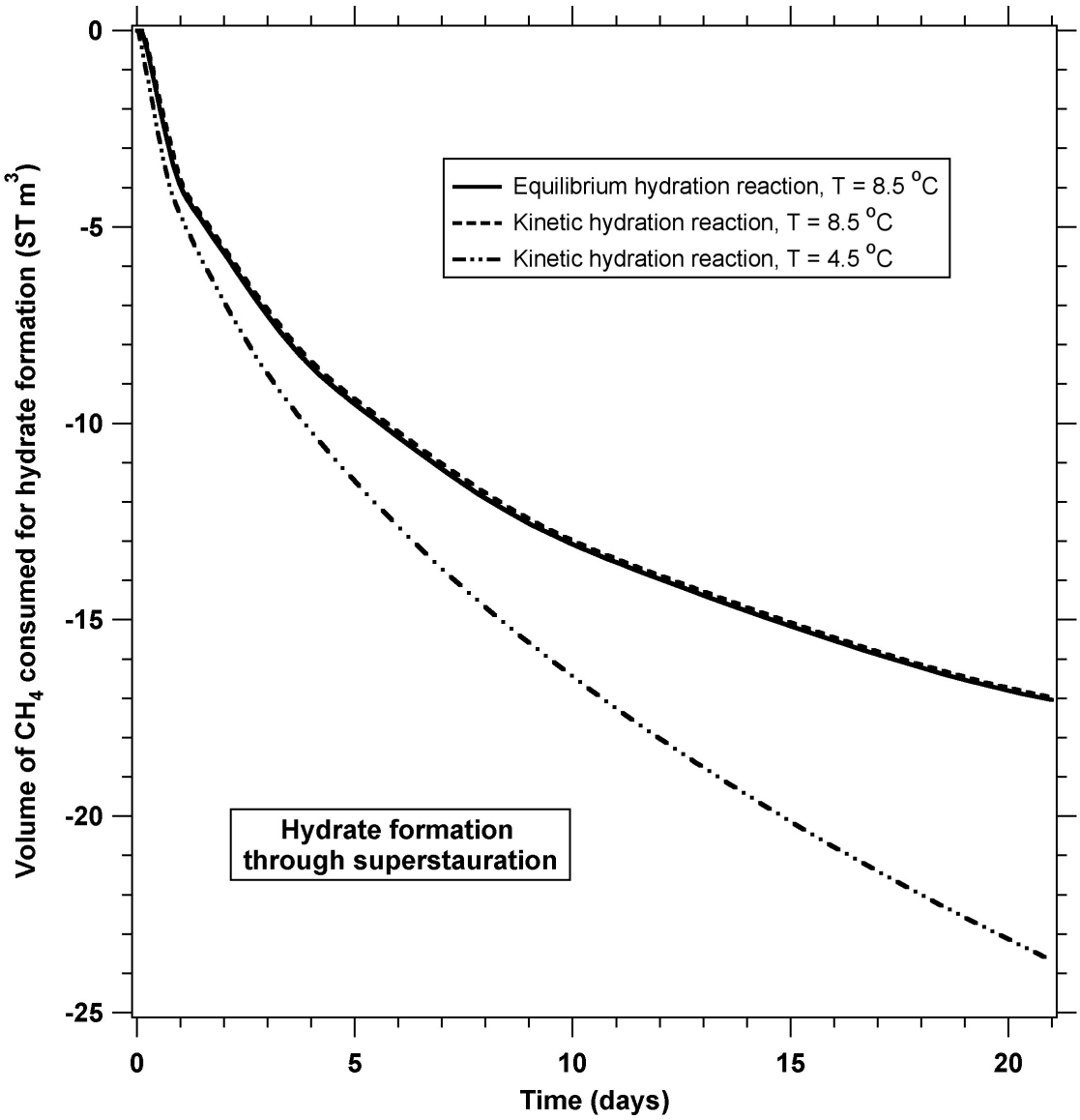

Figure 6.13. Comparison of the cumulative volumes of CH_4 consumed during hydrate formation in problems `Test_1TbS`, `Test_1TbSk` and `Test_1TbS2`.

6.8. Problem Test_2Qp: Equilibrium Hydrate Dissociation, Depressurization, Radial Grid - Single Well

Problem **`Test_2Qp`** represents a more realistic scenario of gas production from a Class 3 (Moridis and Collett, 2004) hydrate deposit in which water and hydrate are initially at equilibrium. In the deposit, $P = 9.8\text{x}10^6$ Pa, $T = 6.5$ ^{o}C, and the initial hydrate saturation is $S_H = 0.5$. Such conditions can be encountered at the bottom of the stability zone in permafrost accumulations (Moridis et al., 2003). The input file and all the corresponding output files are available in the directory **`T+H_V1.5`** on the accompanying USB memory stick.

This problem involves production from a 10-m thick cylindrical reservoir that extends to $R_{max} = 224$ m. The properties of the formation are the same with those in all previous problems (see Section 6.1). A Dirichlet-type (constant conditions equal to the initial conditions) boundary is assumed at R_{max}, i.e., the outer rim of the grid. Fluids are withdrawn at a mass flow rate of $Q = 1$ kg/s through a well at the center of the grid, and are distributed in the production stream according to their mobilities. The fluid withdrawal causes a pressure decline that leads to the depressurization-induced release of CH_4.

The grid in the problem is much larger than in the previous examples, but still insufficient to provide the resolution needed for the representation of an infinite-acting system. Because of this, the proximity of the boundary to the well, the near incompressibility of the aqueous phase, and the quantum-type system behavior in

equilibrium dissociation, discretization effects are expected to appear in the estimation of the dissociation rates (see earlier discussions).

The evolution of (a) the cumulative rate of CH_4 release from dissociation and (b) the cumulative volume of CH4 released from dissociation in the repository are shown in **Figures 6.14** and **6.15**, respectively. As expected, the curve of the cumulative rate of CH4 release exhibits early oscillations attributed to both the rather coarse discretization and the quantum nature of hydrate dissociation. As expected, the release rate increases initially because of advancing depressurization, but begins to decline after a maximum is reached. This decline is caused by the rapid cooling of the hydrate because of advancing dissociation, which affects the rate of dissociation (and the consequent CH_4 release) of the remaining hydrate. As discussed earlier, the jagged appearance of the rate curve in **Figure 6.14** is caused by the coarse discretization. Conversely, the curve of the cumulative volume of released CH_4 is smooth, with the maximum release rate marked by the inflection point at about t = 16 days.

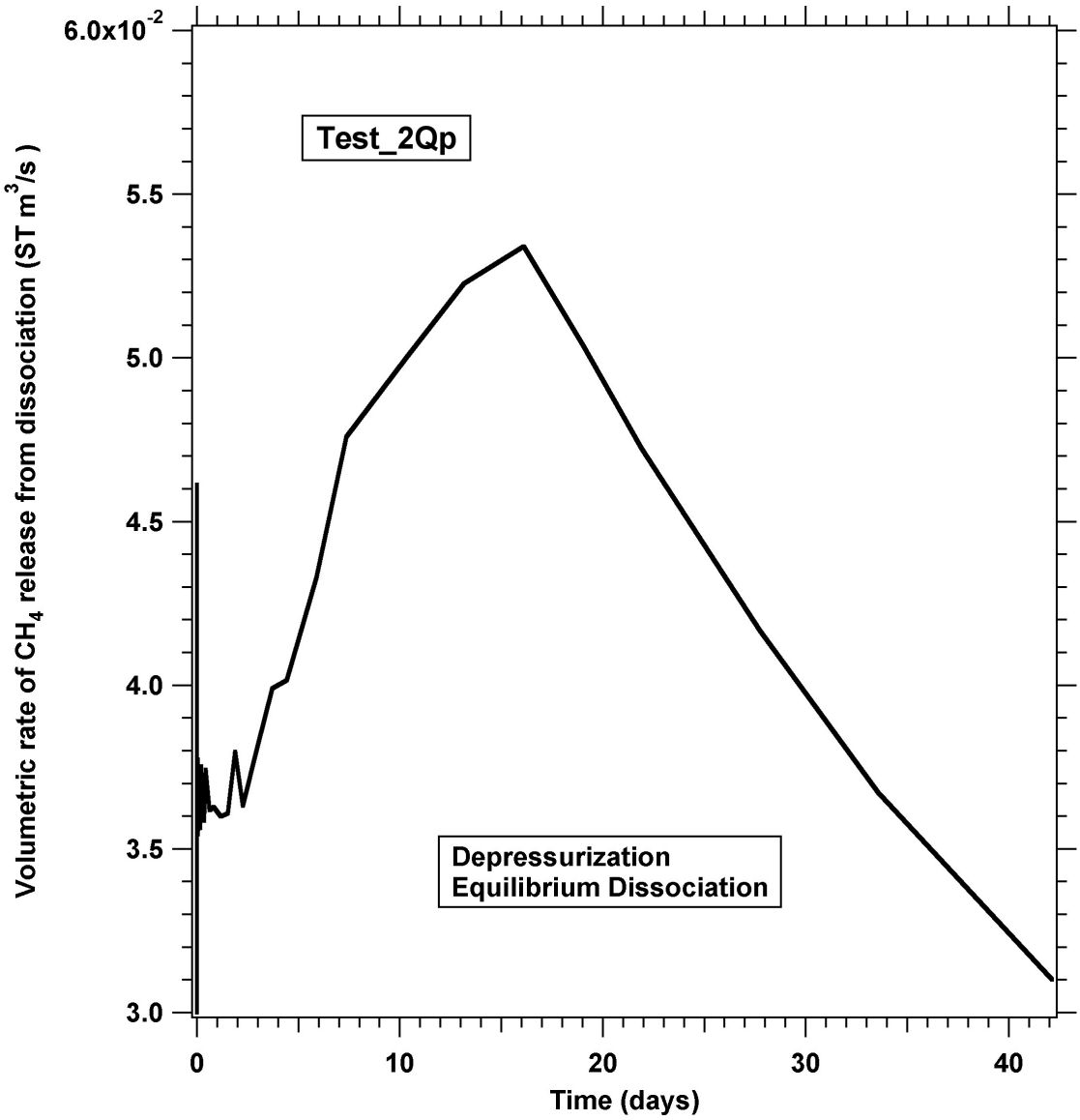

Figure 6.14. Volumetric rate of CH_4 release during hydrate dissociation in problem `Test_2Qp`.

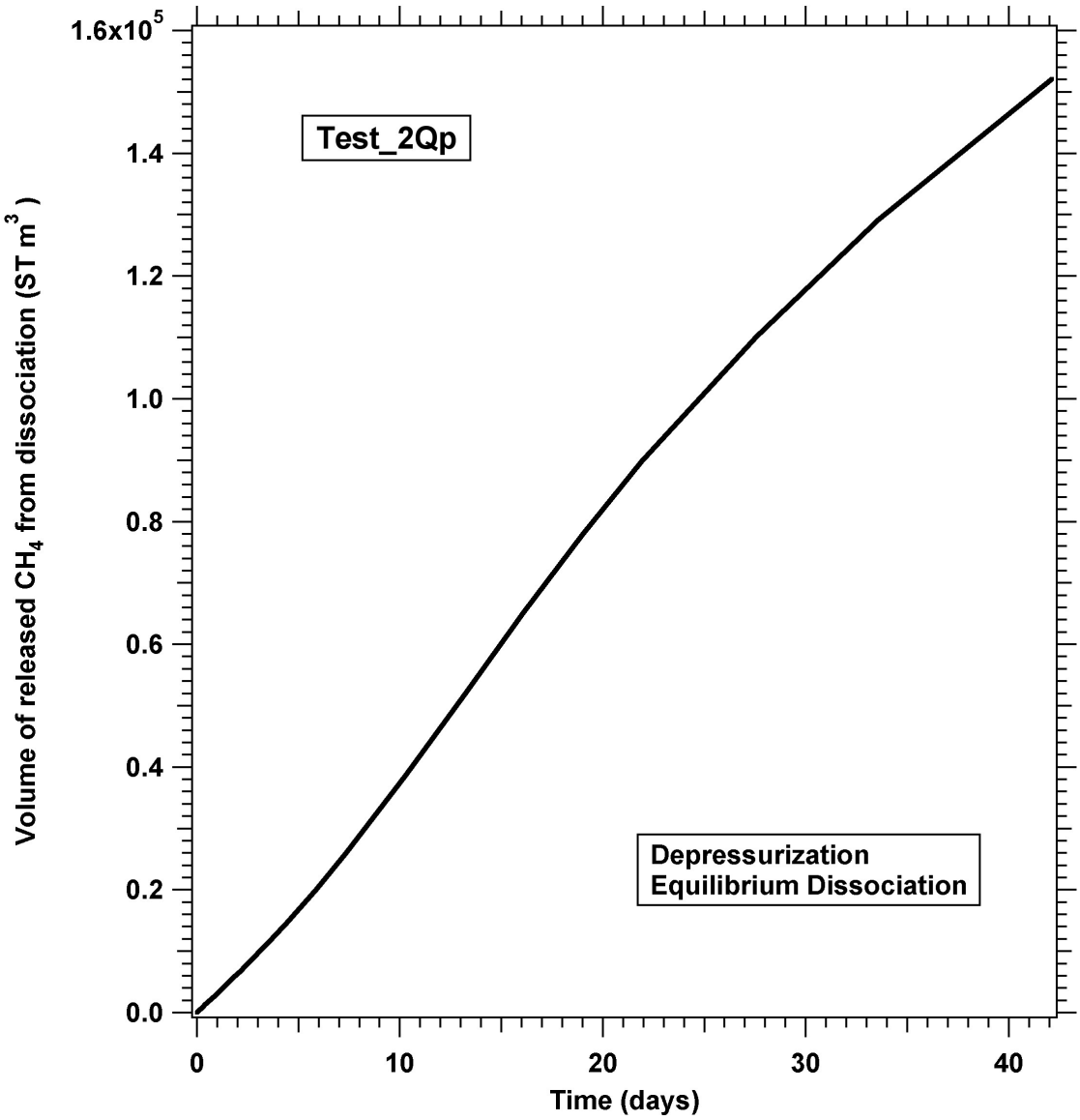

Figure 6.15. Cumulative volume of CH_4 released during hydrate dissociation in problem `Test_2Qp`.

6.9. Problem Test_3Qpk: Kinetic Hydrate Dissociation, Depressurization, Radial Grid - Single Well with Wellbore Heating

Problem **`Test_3Qpk`** uses the same grid, and porous medium and boundary conditions as problem **`Test_2Qp`**. This deposit, for which P = 9.51×10^6 Pa and T = 6.5 ^oC, involves a deposit in which water, gas and hydrate are initially at equilibrium. The initial gas and hydrate saturations are S_G = 0.5 and S_H = 0.4, respectively. A Dirichlet-type boundary (constant conditions equal to the initial conditions) is assumed at R_{max}, i.e., the outer rim of the grid. Fluids are withdrawn at a mass flow rate of Q = 0.3 kg/s through a well at the center of the grid, and are distributed in the production stream according to their mobilities. The fluid withdrawal causes a pressure decline that leads to the depressurization-induced release of CH_4. To alleviate potential hydrate buildup problems that can severely restrict flow to the well (possibly because of temperature drop and availability of gas and water in the vicinity of the well), the wellbore is heated at a rate of Q_H = 1.2 KW. The input file and all the corresponding output files are available in the directory **`T+H_V1.5`**.

The evolution of the rates of (a) cumulative CH_4 release in the deposit, and (b) gas production at the well are shown in **Figure 6.16**. Because of the coexistence of the three phases in the initial system, the curve of the CH_4 release rate is smooth. A comparison of these two curves reveals that the contribution of gas from hydrate dissociation to the rate of gas production decreases progressively with time, and becomes minor at the end of the simulation period. The reason for this performance is the continuing cooling of the hydrate as it dissociates, in addition to the proximity of the well to the (constant-

conditions) boundary and the relatively large permeability, which do not allow efficient depressurization of the system. Consequently, the quasi steady-state condition that is reached rather early is not conducive to increased gas production because the system adjusts to a new state of equilibrium. The novice user is encouraged to investigate the system behavior if the Dirichlet-type boundary is replaced by a no-flow Neuman boundary.

The cumulative volumes of (a) CH_4 released from dissociation in the repository and (b) produced from the wells are shown in **Figure 6.17**. The declining contribution of CH_4 from dissociation is reflected in the practically flat portion of the released CH_4 curve.

Figure 6.16. Volumetric rates of CH_4 (a) release in the reservoir during hydrate dissociation and (b) production from the well in problem `Test_3Qpk`.

Figure 6.17. Cumulative volumes of CH_4 (a) released in the reservoir during hydrate dissociation and (b) produced from the well in problem `Test_3Qpk`.

6.10. Problem Test_2D: Equilibrium Hydrate Dissociation, 2-D Areal System

Problem **`Test_2D`** describes gas production from a realistic areal 2-D hydrate-bearing formation that has the same porous medium properties as all the previous examples. The simulation domain consists of a square system with a side of 50 m and a formation thickness of 10 m. The domain is subdivided in 50 x 50 = 2500 cells in (x,y), with the well located in the cell at (x,y) = (0.5 m, 0.5 m). This is considered a part of a large-scale production system that involves a deposit of considerable areal extent and a large number of producing wells. Under these conditions, the simulation domain represents one quarter of the basic production stencil, and its outer boundaries are no-flow Neuman-type boundaries because of symmetry. The 2-D geometry of the system automatically implies no flow in the third direction, i.e., the system is treated as insulated along its top and bottom boundaries. While this is not strictly true in porous media, such heat transfer through impermeable boundaries can only occur through conduction, which is a very slow process and is not expected to appreciably affect the results. Additionally, by ignoring heat contribution from its boundaries, this simulation provides the worst-case scenario of gas production from such a hydrate accumulation.

In this deposit, water, gas and hydrate are initially at equilibrium, and the pressure is the hydration pressure corresponding to T = 12.5 ^{o}C. The initial gas, aqueous and hydrate phase saturations are S_G = 0.1, S_A = 0.3 and S_H = 0.6, respectively. Fluids are withdrawn at a mass flow rate of Q = 0.5 kg/s through the production well, and are distributed in the production stream according to their mobilities. The fluid withdrawal causes a pressure decline that leads to the depressurization-induced release of CH_4. The

production flow rate remains constant, and is certain to lead to temperature decline and ice appearance because of the endothermic nature of dissociation. The input file and all the corresponding output files are available in the directory **`T+H_V1.5`**. Because of the computationally intensive nature of this realistic problem, the simulation period was limited to two days. Interested users are encouraged to run this problem (modified per their desires) for longer periods.

Figure 6.18 shows the evolution of the cumulative volume of CH4 released from dissociation in the repository in the first two days of production. Note that the released volume increases practically linearly with time. In this short period, a daily release of about 10000 ST m^3 from the hydrate is observed. This is expected to change at later times, when exhaustion of the 'free' gas and hydrate resources in the reservoir will inevitably lead to a sublinear performance.

The pressure distribution in the reservoir at t = 2 days in **Figure 6.19** indicates substantial pressure declines over an extended portion of the domain, indicating significant hydrate dissociation (as supported by the results in **Figure 6.18**). The corresponding temperature distribution in **Figure 6.20** shows an extended cool region even at that early time, providing additional indirect evidence of dissociation.

Direct evidence of dissociation is provided by the corresponding hydrate distribution at the same time in **Figure 6.21**, which clearly indicates severe hydrate dissociation within 5 m from the well, and measurable dissociation as far as 15 m away from the well. While these are very positive and encouraging results, they are not indicative of the production potential if there is no information on the relative permeability regime in the vicinity of the wellbore. The production potential of the

hydrate accumulation can be seriously diminished if the water (released from the hydrate dissociation) or the ice (that can be formed in the course of the endothermic reaction) inhibit the flow of gas toward the well.

The answer to this question is provided by the distributions of the aqueous and gas phase saturations at t = 2 days in **Figures 6.22** and **6.23**. While the water saturation increases in the vicinity of the well in the process of dissociation, the gas saturation increases also. Such a desirable regime then becomes a production management and design issue in the design of appropriate production strategies from the hydrate deposit.

Figure 6.18. Volumetric rates of CH_4 release from the hydrate in the reservoir during gas production in problem `Test_2D`.

Figure 6.19. Pressure distribution in the reservoir at t = 2 days in problem `Test_2D`.

Figure 6.20. Temperature distribution in the reservoir at t = 2 days in problem `Test_2D`.

Figure 6.21. Hydrate saturation distribution in the reservoir at t = 2 days in problem `Test_2D`.

Figure 6.22. Aqueous phase saturation distribution in the reservoir at t = 2 days in problem `Test_2D`.

Figure 6.23. Gas saturation distribution in the reservoir at t = 2 days in problem `Test_2D`.

7.0 Acknowledgements

This work was supported by the Assistant Secretary for Fossil Energy, Office of Natural Gas and Petroleum Technology, through the National Energy Technology Laboratory, under the U.S. Department of Energy, Contract No. DE-AC02-05CH11231.

PAGE LEFT INTENTIONALLY BLANK

8.0 References

Atkinson, P.G., R. Celati, R. Corsi and F. Kucuk. Behavior of the Bagnore Steam/CO_2 Geothermal Reservoir, Italy, *Soc. Pet. Eng. J.*, 228 - 238, 1980.

Aunzo, Z.P., G. Bjornsson and G.S. Bodvarsson. Wellbore Models GWELL, GWNACL, and HOLA, Lawrence Berkeley National Laboratory Report LBL-31428, Berkeley, CA, October 1991.

Aziz, K. and A. Settari. *Petroleum Reservoir Simulation*, Elsevier, London and New York, 1979.

Ballard, A.L. A Non-Ideal Hydrate Solid Solution Model for a Multi-Phase Equilibria Program, Ph.D. Thesis, Colorado School of Mines, 2002

Battistelli, A., C. Calore and K. Pruess. The Simulator TOUGH2/EWASG for Modeling Geothermal Reservoirs with Brines and Non-Condensible Gas, *Geothermics*, Vol. 26, No. 4, pp. 437 - 464, 1997.

Bird, R., W.E. Stewart and E.N. Lightfoot. *Transport Phenomena*, John Wiley & Sons, New York, NY, 1960.

Brand, C.W., J.E. Heinemann and K. Aziz. The Grid Orientation Effect in Reservoir Simulation, Paper SPE-21228, presented at Society of Petroleum Engineers Eleventh Symposium on Reservoir Simulation, Anaheim, CA, February 1991.

Cass, A., G.S. Campbell and T.L. Jones. Enhancement of Thermal Water Vapor

Diffusion in Soil. *Soil Sci. Soc. Am. J.,* Vol. 48, no. 1, pp. 25 - 32, 1984.

Clarke, M., and P.R. Bishnoi. Determination of activation energy and intrinsic rate constant of methane gas hydrate decomposition; Canadian Journal of Chemical Engineering, v. 79, no.1, p. 143-147, 2001.

Coats, K.H. Geothermal Reservoir Modeling, paper SPE-6892, presented at the 52nd Annual Fall Technical Conference and Exhibition of the SPE, Denver, Colorado, October 1977.

Coats, K.H. and A.B. Ramesh. Effects of Grid Type and Difference Scheme on Pattern Steamflood Simulation Results, paper SPE-11079, presented at the 57th Annual Fall Technical Conference and Exhibition of the Society of Petroleum Engineers, New Orleans, LA, September 1982.

Corey, A.T. The Interrelation Between Gas and Oil Relative Permeabilities, *Producers Monthly*, 38-41, November 1954.

Cygan, R.T. The Solubility of Gases in NaCl Brine and a Critical Evaluation of Available Data, SAND90-2848, Sandia National Laboratories, Albuquerque, New Mexico, 1991.

Dean, J.A. (ed.). *Lange's Handbook of Chemistry*, McGraw Hill, Thirteenth Edition, New York, 1985.

de Marsily, G. *Quantitative Hydrogeology*, Academic Press, Orlando, FL, 1986.

Doughty, C. and K. Pruess. A Similarity Solution for Two-Phase Water, Air and Heat Flow Near a Linear Heat Source in a Porous Medium, *J. of Geophys. Res.*, 97 (B2), 1821-1838, 1992.

Duff, I.S. MA28—A Set of FORTRAN Subroutines for Sparse Unsymmetric Linear Equations, AERE Harwell Report R 8730, 1977.

Edlefsen, N.E. and A.B.C. Anderson. Thermodynamics of Soil Moisture, *Hilgardia*, 15 (2), 31–298, 1943.

Edwards, A.L. TRUMP: A Computer Program for Transient and Steady State Temperature Distributions in Multidimensional Systems, National Technical Information Service, National Bureau of Standards, Springfield, VA, 1972.

Falta, R.W., K. Pruess, I. Javandel and P.A. Witherspoon. Density - Driven Flow of Gas in the Unsaturated Zone Due to the Evaporation of Volatile Organic Compounds, *Water. Resour. Res.*, Vol. 25, No. 10, pp. 2159 - 2169, 1989.

Falta, R.W., K. Pruess, S. Finsterle, and A. Battistelli. T2VOC User's Guide, Lawrence Berkeley Laboratory Report LBL-36400, Berkeley, CA, March 1995.

Fatt, I. and W.A. Klikoff. Effect of Fractional Wettability on Multiphase Flow Through Porous Media, *AIME Transactions*, 216, 246, 1959.

Faust, C.R. and J.W. Mercer. Summary of Our Research in Geothermal Reservoir Simulation, Proc. Workshop on Geothermal Reservoir Engineering, Stanford University, Stanford, CA, SGP-TR-12, 1975.

Finley, N.C. and M. Reeves. Swift Self-Teaching Curriculum, Report SAND81-0410, Sandia National Laboratory, Albuquerque, NM, 1982.

Gupta, A. Methane Hydrate Dissociation Measurements and Modeling:The Role of Heat Transfer and Reaction Kinetics, Ph.D. Thesis, Colorado School of Mines, 2007

Grant, M.A. Permeability Reduction Factors at Wairakei, paper 77-HT-52, presented at AICHE-ASME Heat Transfer Conference, Salt Lake City, Utah, August 1977.

Hadgu, T. and D.H. Freeston. A Multi-Purpose Wellbore Simulator. *Geothermal Resources Council Transactions*, Vol. 14, pp. 1279 - 1286, 1990.

Hadgu, T., R.W. Zimmerman and G.S. Bodvarsson. Coupled Reservoir-Wellbore Simulation of Geothermal Reservoir Behavior. *Geothermics*, Vol. 24, No. 2, pp. 145-166, 1995.

Herbert, A.W., C.P. Jackson and D.A. Lever. Coupled Groundwater Flow and Solute Transport with Fluid Density Strongly Dependent on Concentration, *Water Resour. Res.*, Vol. 24, No. 10, pp. 1781 - 1795, 1988.

Hirschfelder, J.O., C.F. Curtiss and R.B. Bird. *Molecular Theory of Gases and Liquids*, John Wiley & Sons, New York, NY, 1954.

International Formulation Committee. *A Formulation of the Thermodynamic Properties of Ordinary Water Substance,* IFC Secretariat, Düsseldorf, Germany, 1967.

Itasca Consulting Group. *FLAC3D: Fast Lagrangian Analysis of Continua in 3 Dimensions*, Minneapolis, Minnesota, 2002.

Jury, W.A., W.F. Spencer and W.J. Farmer. Behavior Assessment Model for Trace Organics in Soil: I. Model Description, *J. Environ. Qual.,* Vol. 12, No. 4, pp. 558 - 564, 1983.

Kim, H.C., Bishnoi, P.R., Heideman, R.A., and Rizvi, S.S.H, *Chem. Eng. Sci.*, *42*, 1645-1653, 1987.

Klinkenberg, L.J. The Permeability of Porous Media to Liquids and Gases, in *API Drilling and Production Practice,* pp. 200–213, 1941.

Kruger, P. and H.J. Ramey, Jr. Stimulation and Reservoir Engineering of Geothermal Resources, Stanford Geothermal Program Report SGR-TR-1, Stanford University,

Stanford, CA, 1974.

Lam, S.T., A. Hunsbedt, P. Kruger and K. Pruess. Analysis of the Stanford Geothermal Reservoir Model Experiments Using the LBL Reservoir Simulator, *Geothermics*, 17 (4), 595 - 605, LBL-25957, 1988.

Leverett, M.C. Capillary Behavior in Porous Solids, *Trans. Soc. Pet. Eng. AIME*, 142, 152-169, 1941.

Loomis, A.G. Solubilities of Gases in Water, in: *International Critical Tables, Vol. III*, E. W. Washburn, (ed.), McGraw-Hill, New York, NY, pp. 255–257, 1928.

Marion, G.M., Jakubowski, S.D., The compressibility of ice to 2.0 kbar, Cold Regions Science and Technology, Volume 38, Issues 2-3, p. 211-218, 2004.

de Marsily, G. *Quantitative Hydrogeology*, Academic Press, Orlando, FL, 1986.

Mason, E.A. and A.P. Malinauskas. *Gas Transport in Porous Media: The Dusty Gas Model,* Elsevier, Amsterdam, The Netherlands, 1983.

Michaelides, E.E. Thermodynamic Properties of Geothermal Fluids, Geothermal Resources Council Transactions, Vol. 5, pp. 361 - 364, 1981.

Miller, A.B. A Brine-Steam Properties Computer Program for Geothermal Energy Calculations, Lawrence Livermore National Laboratory Report UCRL-52495, Livermore, CA, June 1978.

Millington, R.J. and J.P. Quirk. Permeability of Porous Solids, *Trans. Faraday Soc.*, 57, 1200-1207, 1961.

Milly, P.C.D. Moisture and Heat Transport in Hysteretic, Inhomogeneous Porous Media: A Matric-Head Based Formulation and a Numerical Model, *Water Resour. Res.*, Vol. 18, No. 3, pp. 489 - 498, 1982.

Moridis, G.J. Numerical studies of gas production from methane hydrates; Society of Petroleum Engineers Journal, Vol. 32, No.8, pp. 359-370, 2003.

Moridis, G.J., Numerical studies of gas production from methane hydrates; Society of Petroleum Engineers Reservoir Evaluation and Engineering, Vol. 27, No.3, pp. 175-183, 2004.

Moridis, G.J. and T. Collett, Gas Production from Class 1 Hydrate Accumulations, in Recent Advances in the Study of Gas Hydrates, C. Taylor and J. Qwan, Editors, Kluwer Academic/Plenum Publishers (Section I, Chapter 6, pp. 75-88), 2004.

Moridis, G. and K. Pruess. TOUGH Simulations of Updegraff's Set of Fluid and Heat Flow Problems, Lawrence Berkeley Laboratory Report LBL-32611, Berkeley, CA, November 1992.

Moridis, G. and K. Pruess. Flow and Transport Simulations Using T2CG1, a Package of Conjugate Gradient Solvers for the TOUGH2 Family of Codes, Lawrence Berkeley Laboratory Report LBL-36235, Berkeley, CA, 1995.

Moridis, G. and K. Pruess. T2SOLV: An Enhanced Package of Solvers for the TOUGH2 Family of Reservoir Simulation Codes, *Geothermics*, Vol. 27, No. 4, pp. 415 - 444, 1998.

Moridis, G.J., Collett, T. S., Dallimore, S.R., Satoh, T., Hancock, S., and Weatherhill, B. Numerical studies of gas production from several methane hydrate zones at the Mallik site, Mackenzie Delta, Canada; Journal of Petroleum Science and Engineering, v. 43, p. 219-239, 2004 (also Report LBNL-50257, Lawrence Berkeley National Laboratory, Berkeley, California, 2002).

Moridis, G.J., Kowalsky, M.B., Pruess, K., TOUGH-Fx/HYDRATE v1.1 User's Manual: A Code for the Simulation of System Behavior in Hydrate-Bearing Geologic Media, Report LBNL-58950, Lawrence Berkeley National Laboratory, Berkeley, CA (2005).

Moridis, G.J., Kowalsky, M.B., Pruess, K., TOUGH+HYDRATE v1.0 User's Manual: A Code for the Simulation of System Behavior in Hydrate-Bearing Geologic Media, Report LBNL-0149E, Lawrence Berkeley National Laboratory, Berkeley, CA (2008).

Moridis, G.J., Kowalsky, M.B., Pruess, K., TOUGH+HYDRATE v1.1 User's Manual: A Code for the Simulation of System Behavior in Hydrate-Bearing Geologic Media, Report LBNL-0149E, Lawrence Berkeley National Laboratory, Berkeley, CA (2009).

Moridis, G.J., Kowalsky, M.B., Pruess, K., TOUGH+HYDRATE v1.2 User's Manual: A Code for the Simulation of System Behavior in Hydrate-Bearing Geologic Media, Report LBNL-0149E, Lawrence Berkeley National Laboratory, Berkeley, CA (2012).

Morrow, C., D. Lockner, D. Moore and J. Byerlee. Permeability of Granite in a Temperature Gradient, *Journal of Geophysical Research*, 86 (84), 3002-3008, April 1981.

Mualem, Y. A New Model for Predicting the Hydraulic Conductivity of Unsaturated Porous Media, *Water Resour. Res.*, Vol. 12, No. 3, pp. 513 - 522, 1976.

Murray, L. and C. Gunn. Toward Integrating Geothermal Reservoir and Wellbore Simulation: TETRAD and WELLSIM, Proc. 15th NZ Geothermal Workshop, Auckland, New Zealand, 1993.

Narasimhan, T.N. and P.A. Witherspoon. An Integrated Finite Difference Method for Analyzing Fluid Flow in Porous Media, *Water Resour. Res.*, Vol. 12, No. 1, pp. 57 – 64, 1976.

Narasimhan, T.N., P.A. Witherspoon and A.L. Edwards. Numerical Model for Saturated-Unsaturated Flow in Deformable Porous Media, Part 2: The Algorithm, *Water Resour. Res.*, 14 (2), 255-261, 1978.

Oldenburg, C.M. and K. Pruess. A Two-Dimensional Dispersion Module for the TOUGH2 Simulator, Lawrence Berkeley Laboratory Report LBL-32505, Berkeley, CA, September 1993.

Oldenburg, C.M. and K. Pruess. EOS7R: Radionuclide Transport for TOUGH2, Lawrence Berkeley Laboratory Report LBL-34868, Berkeley, CA, November 1995.

Oldenburg, C.M. and K. Pruess. Higher-Order Differencing for Phase Front Propagation in Geothermal Systems, Proc., Twenty-Third Workshop on Geothermal Reservoir Engineering, Stanford University, January 1998.

O'Sullivan, M.J. A Similarity Method for Geothermal Well Test Analysis, *Water Resour. Res.*, Vol. 17, No. 2, pp. 390 – 398, 1981.

O'Sullivan, M.J., G.S. Bodvarsson, K. Pruess and M.R. Blakeley. Fluid and Heat Flow in Gas-Rich Geothermal Reservoirs, *Society of Petroleum Engineers Journal*, Vol. 25, No. 2, pp. 215 - 226, April 1985.

Pape, H., C. Clauser and J. Iffland. Permeability Prediction Based on Fractal Pore-Space Geometry, *Geophysics,* Vol. 64, No. 5, pp. 1447 - 1460, 1999.

Peaceman, D.W. *Fundamentals of Numerical Reservoir Simulation*, Elsevier, Amsterdam, The Netherlands, 1977.

Peaceman, D.W. Interpretation of Well-Block Pressures in Numerical Reservoir Simulation with Nonsquare Grid Blocks and Anisotropic Permeability, paper SPE-10528, presented at the Sixth SPE Symposium on Reservoir Simulation of the Society of Petroleum Engineers, New Orleans, LA, January 1982.

Phillips, O.M. *Flow and Reactions in Permeable Rocks,* Cambridge University Press, Cambridge, New York, Melbourne, 1991.

Pickens, J.F., R.W. Gillham and D.R. Cameron. Finite Element Analysis of the Transport of Water and Solutes in Tile-Drained Soils, *J. of Hydrology*, 40, 243-264, 1979.

Potter, J.M. and D.L. Brown. The Volumetric Properties of Aqueous Sodium Chloride Solutions, U. S. Geological Survey, Bulletin 1421-C, 1977.

Pritchett, J.W. Numerical Calculation of Multiphase Fluid and Heat Flow in Hydrothermal Reservoirs, Proc. Workshop on Geothermal Reservoir Engineering, Stanford University, Stanford, CA, pp. 201–205, SGP-TR-12, 1975.

Pritchett, J.W., M.H. Rice and T.D. Riney. Equation-of-State for Water-Carbon Dioxide

Mixtures: Implications for Baca Reservoir, Report DOE/ET/27163-8, Systems, Science and Software, La Jolla, CA, February 1981.

Pruess, K. GMINC - A Mesh Generator for Flow Simulations in Fractured Reservoirs, Lawrence Berkeley Laboratory Report LBL-15227, Berkeley, CA, March 1983.

Pruess, K. TOUGH User's Guide, Nuclear Regulatory Commission Report NUREG/CR-4645; also Lawrence Berkeley Laboratory Report LBL-20700, 1987.

Pruess, K. TOUGH2 - A General Purpose Numerical Simulator for Multiphase Fluid and Heat Flow, Lawrence Berkeley Laboratory Report LBL-29400, Berkeley, CA, 1991a.

Pruess, K. EOS7, An Equation-of-State Module for the TOUGH2 Simulator for Two-Phase Flow of Saline Water and Air, Lawrence Berkeley Laboratory Report LBL-31114, Berkeley, CA, 1991b.

Pruess, K. Grid Orientation and Capillary Pressure Effects in the Simulation of Water Injection into Depleted Vapor Zones, *Geothermics*, Vol. 20, No. 5/6, pp. 257 - 277, 1991c.

Pruess, K., J.M. Zerzan, R.C. Schroeder and P.A. Witherspoon. Description of the Three-Dimensional Two-Phase Simulator SHAFT78 for Use in Geothermal Reservoir Studies, paper SPE-7699, presented at the Fifth SPE Symposium on Reservoir Simulation, Denver, CO, February 1979.

Pruess, K. and R.C. Schroeder. SHAFT 79 User's Manual, Lawrence Berkeley Laboratory Report LBL-10861, Berkeley, CA, March 1980.

Pruess, K., and T.N. Narasimhan. On Fluid Reserves and the Production of Superheated Steam from Fractured, Vapor-Dominated Geothermal Reservoirs, *J. Geophys. Res.*, Vol. 87, No. B11, pp. 9329 - 9339, 1982.

Pruess, K. and G.S. Bodvarsson. A Seven-Point Finite Difference Method for Improved Grid Orientation Performance in Pattern Steam Floods, *Proceedings*, Seventh Society of Petroleum Engineers Symposium on Reservoir Simulation, Paper SPE-12252, pp. 175 - 184, San Francisco, CA, 1983.

Pruess, K. and G.S. Bodvarsson. Thermal Effects of Reinjection in Geothermal Reservoirs with Major Vertical Fractures, *J. Pet. Tech.*, Vol. 36, No. 10, pp. 1567 – 1578, 1984.

Pruess, K. and T.N. Narasimhan. A Practical Method for Modeling Fluid and Heat Flow in Fractured Porous Media, *Soc. Pet. Eng. J.*, Vol. 25, No. 1, pp. 14-26, February 1985.

Pruess, K., J.S.Y. Wang and Y.W. Tsang. On Thermohydrological Conditions Near High-Level Nuclear Wastes Emplaced in Partially Saturated Fractured Tuff. Part 2.

Effective Continuum Approximation, *Water Resour. Res.*, Vol. 26, No. 6, pp. 1249 - 1261, 1990.

Pruess, K., A. Simmons, Y.S. Wu and G. Moridis. TOUGH2 Software Qualification, Lawrence Berkeley National Laboratory Report LBL-38383, Berkeley, CA, February 1996.

Pruess, K., C. Oldenburg, and G.Moridis. TOUGH2 User's Guide – Version 2.0, Lawrence Berkeley Laboratory Report LBL-43134, Berkeley, CA, 1999.

Reagan, M.T., G.J. Moridis, J.N. Johnson, L. Pan, C.M. Freeman, K.L. Boyle, N.D. Keen and J. Husebo. Field-Scale Simulation of Production from Oceanic Gas Hydrate Deposits, Transport In Porous Media, In Press (doi: 10.1007/s11242-014-0330-7), 2014.

Reeves, M., D. S. Ward, N. D. Johns and R. M. Cranwell. Theory and Implementation of Swift II, The Sandia Waste-Isolation Flow and Transport Model for Fractured Media, Report No. SAND83-1159, Sandia National Laboratory, Albuquerque, NM, 1986.

Richards, L.A. Capillary Conduction of Liquids Through Porous Mediums, *Physics*, Vol. 1, pp. 318 - 333, 1931.

Rutqvist J. and C.-F Tsang. A Study of Caprock Hydromechanical Changes Associated with CO_2 Injection into a Brine Aquifer. *Environmental Geology*, Vol. 42, pp. 296-305, 2002.

Scheidegger, A. E. *The Physics of Flow Through Porous Media*, University of Toronto Press, Toronto and Buffalo, Third Edition, 1974.

Sleijpen, G.L.G. and D. Fokkema. BiCGSTAB(m) for Linear Equations Involving Unsymmetric Matrices with Complex Spectrum, *Electronic Transactions on Numerical Analysis*, Vol. 1, pp. 11 - 32, 1993.

Sloan, E.D., *Clathrate Hydrates of Natural Gases*, Marcel Dekker, Inc.: New York, NY, 1998.

Stone, H.L., Probability Model for Estimating Three-Phase Relative Permeability. *Trans. SPE of AIME,* Vol. 249, 214-218, 1970.

Sutton, F.M. and A. McNabb. Boiling Curves at Broadlands Field, New Zealand, *N. Z. J. Sci.*, Vol. 20, pp. 333 - 337, 1977.

Tanaka, H., Thermal expansivities of cubic ice I and ice VII, Journal of Molecular Structure: THEOCHEM, Volumes 461-462, Pages 561-567, 1999.

TecPlot, Inc., *Tecplot 10 User's Manual*, Bellevue, Washington, 2003.

Thomas, G.W. *Principles of Hydrocarbon Reservoir Simulation*. International Human Resources Development Corporation, Boston, 1982.

Tsang, Y.W. and K. Pruess. Further Modeling Studies of Gas Movement and Moisture Migration at Yucca Mountain, Nevada, Lawrence Berkeley Laboratory Report LBL-29127, Berkeley, CA, 1990.

Udell, K.S. and J.S. Fitch. Heat and Mass Transfer in Capillary Porous Media Considering Evaporation, Condensation, and Non-Condensible Gas Effects, paper presented at 23rd ASME/AIChE National Heat Transfer Conference, Denver, CO, 1985.

van der Vorst, H.A. Bi-CGSTAB: A Fast and Smoothly Converging Variant of BiCG in the Presence of Rounding Errors, *SIAM J. Sci. Statist. Comput.*, Vol. 13, pp. 631 - 644, 1992.

van Genuchten, M.Th. A Closed-Form Equation for Predicting the Hydraulic Conductivity of Unsaturated Soils, *Soil Sci. Soc.*, Vol. 44, pp. 892 - 898, 1980.

Vargaftik, N.B. *Tables on the Thermophysical Properties of Liquids and Gases*, 2nd Ed., John Wiley & Sons, New York, NY, 1975.

Vaughan, P.J. Analysis of Permeability Reduction During Flow of Heated, Aqueous Fluid Through Westerly Granite, in C.F. Tsang (ed.), *Coupled Processes Associated with Nuclear Waste Repositories*, pp. 529 - 539, Academic Press, New York, 1987.

Verma, A.K., K. Pruess, C.F. Tsang and P.A. Witherspoon. A Study of Two-Phase Concurrent Flow of Steam and Water in an Unconsolidated Porous Medium, Proc. 23rd National Heat Transfer Conference, Am. Society of Mechanical Engineers, Denver, CO, 135–143, 1985.

Verma, A. and K. Pruess. Thermohydrologic Conditions and Silica Redistribution Near High-Level Nuclear Wastes Emplaced in Saturated Geological Formations, *J. of Geophys. Res.*, Vol. 93, No. B2, pp. 1159-1173, 1988.

Vinsome, P.K.W. and J. Westerveld. A Simple Method for Predicting Cap and Base Rock Heat Losses in Thermal Reservoir Simulators, *J. Canadian Pet. Tech.*, Vol. 19, No. 3, pp. 87 – 90, July-September 1980.

Walker, W.R., J.D. Sabey, and D.R. Hampton. Studies of Heat Transfer and Water Migration in Soils, Final Report, Department of Agricultural and Chemical Engineering, Colorado State University, Fort Collins, CO, 80523, April 1981.

Warren, J.E. and P.J. Root. The Behavior of Naturally Fractured Reservoirs, *Soc. Pet. Eng. J., Transactions, AIME, 228*, 245-255, September 1963.

Webb, S.W. Gas-Phase Diffusion in Porous Media - Evaluation of an Advective-Dispersive Formulation and the Dusty Gas Model for Binary Mixtures, *J. Por.*

Media, Vol. 1, No. 2, pp. 187 - 199, 1998.

Webb, S.W. and C.K. Ho. Review of Enhanced Vapor Diffusion in Porous Media, in: K. Pruess (ed.), *Proceedings of the TOUGH Workshop '98,* Lawrence Berkeley National Laboratory Report LBNL-41995, pp. 257 - 262, Berkeley, CA, 1998a.

Webb, S.W. and C.K. Ho. Enhanced Vapor Diffusion in Porous Media - LDRD Final Report, Sandia National Laboratories Report SAND98-2772, Albuquerque, NM, 1998b.

Wu, Y.S., K. Pruess and Z.X. Chen. Buckley-Leverett Flow in Composite Media, *SPE Advanced Technology Series,* Vol. 1, No. 2, pp. 36 - 42, 1993.

Xu, T., Y. Ontoy, P. Molling, N. Spycher, M. Parini and K. Pruess. Reactive Transport Modeling of Injection Well Scaling and Acidizing at Tiwi Field, Philippines, *Geothermics,* Vol. 33, No. 4, pp. 477 - 491, 2004.

Yanosik, J.L. and T.A. McCracken. A Nine-Point, Finite Difference Reservoir Simulator for Realistic Prediction of Adverse Mobility Ratio Displacements, *Soc. Pet. Eng. J.*, 253 – 262, 1979.

DISCLAIMER

This document was prepared as an account of work sponsored by the United States Government. While this document is believed to contain correct information, neither the United States Government nor any agency thereof, nor The Regents of the University of California, nor any of their employees, makes any warranty, express or implied, or assumes any legal responsibility for the accuracy, completeness, or usefulness of any information, apparatus, product, or process disclosed, or represents that its use would not infringe privately owned rights. Reference herein to any specific commercial product, process, or service by its trade name, trademark, manufacturer, or otherwise, does not necessarily constitute or imply its endorsement, recommendation, or favoring by the United States Government or any agency thereof, or The Regents of the University of California. The views and opinions of authors expressed herein do not necessarily state or reflect those of the United States Government or any agency thereof or The Regents of the University of California.

Ernest Orlando Lawrence Berkeley National Laboratory is an equal opportunity employer.